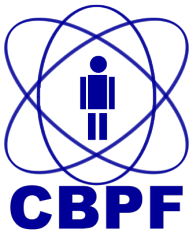

Centro Brasileiro de Pesquisas Físicas

COSMO

An Analysis of Linear Perturbations and Quasi-Normal Modes of Kerr Black Holes

Luís Felipe Longo Micchi

A Thesis submitted in partial fulfillment of the requirements for the degree of Master of Science in Physics.

Supervisor: Marc Casals

Rio de Janeiro

March 2018

Micchi, Luís Felipe Longo

An Analysis of Linear Perturbations and Quasi-Normal Modes of Kerr Black Holes / Luís Felipe Longo Micchi - Rio de Janeiro: CBPF, 2018.

Supervisor: Marc Casals

Thesis (M.Sc.) - CBPF / Programa de Pós-graduação Acadêmico em Física, 2018.

1. General Relativity. 2. Rotating Black Holes. 3. Teukolsky equation. 4. MST method 5. Perturbation Theory. 6.Quasi-normal modes I. Casals, Marc, Supervisor. II. CBPF, COSMO, Programa de Pós-graduação Acadêmico em Física. III. An Analysis of QNM's of Kerr Black Holes through the MST method.

Abstract

An Analysis of Linear Perturbations and Quasi-Normal Modes of Kerr Black Holes

Luís Felipe Longo Micchi

Supervisor: Marc Casals

This work is a thesis about linear perturbation theory of rotating black holes, so-called Kerr black holes (Kerr BH's). As such we start with a review of several analytical methods that have been developed in the last few decades. We use these methods to investigate the analytical properties of the retarded Green Function (GF) of the wave equation in this space-time. The properties of the GF that we are concerned with in this work are the branch cuts (BC's) and the poles of its Fourier modes in the complex-frequency plane. Each one of them is related to specific features of the BH, for instance the poles in the GF are related to its characteristic modes of vibration (the *quasi-normal modes*, QNM). Another interesting subject of study is the BH (in)stability. When discussing mode stability of BH's, QNM's and BC's play a major role, since they can lead to instabilities depending on their localization on the complex-frequency plane

The novelty of our work is that our search for QNM modes is performed using the semi-analytical method called MST method, which allow us to construct solutions to the homogeneous wave equation and the retarded GF in term of series of hypergeometric functions. This method is explained in our review. We also used this method to search

for BC's and to study the superradiance phenomenon. These topics were investigated first in the sub-extremal rotating case for which we were able to reproduce results found in the literature. The MST method was also applied to the extremal rotating BH and its use allowed us to access QNM frequencies in the extremal Kerr case. Since it is known that there is a new BC in the extremal case, we studied the formation of this new feature as extremality is approached.

We hope that our work will contain some of the first few steps towards the understanding of wave propagation around extremal Kerr BH's.

Keywords: General Relativity, Rotating Black Holes, Teukolsky equation, MST method, Perturbation Theory, Quasi-normal modes

Acknowledgments

Primeiramente, agradeço a todos da minha família, tanto a de sangue quanto as que pude escolher. Irinea, Ana, Heberth, Sônia, Lúcio, Ângela, Rosimere, Luisa, Ricardo, Pedro , Duda, João, Paola, Gabi e tantos outros. Cada um de vocês me foi de grande valia no percurso que me trouxe até aqui. Sem vocês nada disso teria sido possível.

Agradeço ao meu orientador, professor Marc Casals, por todas as horas dedicadas a minha capacitação para a realização deste trabalho. Os créditos deste trabalho são tão seus quanto meus.

Agradeço a todos os professores que tive no percurso do meu Mestrado aqui no CBPF. Em especial, agradeço ao professor José Helayel-Neto, por tantos cursos, conselhos e conversas que me foram úteis durante esses 2 anos.

Aos amigos de graduação, em especial 3, sem os quais as intermináveis horas de estudos seriam ainda mais longas : Yara, Foster e Zé Hugo. Foster ajudando com as zueiras e com a gourmetização da vida. Zé Hugo sendo um amigo sempre presente. Yara me ajudou demais. Pelas discussões gravitacionais e ajudas institucionais, agradeço aos colegas de sala Gabriel, Arthur e David.

Por todo o suporte que você me deu, ajudando a me entender e me superar a cada obstáculo nesse árduo percurso, agradeço também a você, Ana Laura.

Finalmente, agradeço a todo suporte da equipe do CBPF e da CAPES no financiamento dos meus estudos pelos últimos anos.

Dedicated to My grandfather, Altamiro Longo.

To Sir with love.

Mais longe minha vista chegou.
A razão foi você me amparar,
Me acolher e me apadrinhar.
Em seu ombro me posicionou.

Dedico este ao meu Gigante
Que da Aviação foi amante.
Mas foi o newtoniano amor,
Que emitiu a mim com primor.

Sempre com a preciosa lição
Cheia de maestria e paixão,
Ensinou sobre vida e função.

Mesmo sabendo que não voltará
Meu amor pra sempre existirá
Por você, meu eterno vô Tatá.

Soneto do Gigante,

autoria própria.

Contents

List of Figures

List of Tables

Notations and Conventions

Throughout this work, we used geometrized units where $G = c = 1$. We also adopt the (-,+,+,+) convention for the metric signature. The coordinate system is chosen such that the position vector is $x^\mu = (t, r, \theta, \varphi)$, which are the Boyer-Lindquist coordinates. For reference, the following is a list of symbols and acronyms that are used often throughout the text.

GF	Green Function
BH	Black Hole
NEK	Near Extremal Kerr
QNM	Quasi Normal Modes
CF	Continued Fraction
BC	Branch Cut
LIGO	Laser Interferometer Gravitational-wave Observatory
M	Black hole's mass
a	Black hole's angular momentum
ZDM	Zero Damped Modes
DM	Damped Modes
NM	Normal Modes
TRM	Totally Reflected Modes
ZAMO	Zero Angular Momentum Observer
PDE	Partial Differential Equation
ODE	Ordinary Differential Equation
MST	Mano, Suzuki, and Takasugi (method)
AS	Algebraically Special
ω_{lmn}	QNM frequency
ω_{SR}	Superrandiance Bound Frequency
ω_{HW}	Hartle Wilkins frequency

Chapter 1

Introduction

When dealing with a vibrating system, one of the aspects that plays a significant role is the existence of its characteristic modes of vibration or normal modes (NM's). A well-known case where we deal with NM's is in the context of vibrating strings, where they represent standing waves traveling across the string. In these systems, it is shown that there is an infinite number of NM's [1]. It is also shown that these characteristic modes have real frequencies, which are related to the length of the string [1]. This means that, if one has a prior knowledge of the NM's of a string, one can infer its size. In the context of black hole (BH) physics, similar characteristic modes of vibration also appear, but with some significant changes. By contrast with the previous example, BH's are not conservative systems: they are dissipative due to the presence of an event horizon. This has the consequence that perturbations of a BH are not standing waves but damped waves, meaning that their characteristic frequencies have a non-zero imaginary part. Due to this dissipative property, these modes are now called *quasi*-normal modes (QNM's). A question that follows immediately is whether it is possible to work out the inverse problem, like it was done in the string case. The answer is that QNM's are related to the mass, spin, net electrical charge and the (in)stability of the "vibrating" BH [2]. In this work we are interested in studying BH's with spin and zero net electrical charge, Kerr BH's as they are known in the literature.

Since LIGO (Laser Interferometer Gravitational-wave Observatory)'s first detections of gravitational waves [3–8], it has been possible to measure for the first time in history the main QNM's of BH's resulting from collisions of two black holes [9]. In these measurements, the QNM's appear as the leading frequencies of the late-time phase (ringdown) of the gravitational waveform, helping to estimate the mass and spin of the final BH's. In the light of this historical achievement, a better understanding of the QNM's of BH's is of great interest. Many authors have calculated QNM's for different space-times in the last decade (several examples can be found in the review [10] and in references therein), but a case where little is known is that of a maximally-rotating (extremal) BH. There is only one paper where this problem has been tackled directly [11], to the best of our knowledge.

At first sight, it might seem like a purely academical question because it is widely believed that there exists an astrophysical upper limit to the BH spin [12], which would keep the BH away from extremality. However, observations in the electromagnetic spectrum do not completely eliminate the existence of extremal Kerr BH's [13–15]. Another reason that makes extreme Kerr a case of interest is the fact that the transition from the sub-extremal to the extremal case of certain physical quantities might not necessarily be smooth, as seen in [16]. In the context of QNM's, it has been shown that some of them "pile up" when the BH is arbitrarily close to extremality [17–20]. In this work we will investigate QNM's in extreme Kerr by means of a novel way that differs from the one used in [11]. This will serve both as a check of the results in [11] and as means to obtain new QNM frequencies and as a way to investigate what happens to the modes that "pile up". We also check the applicability of this new way of searching for QNM's by reproducing results for sub-extremal Kerr BH's.

Chapter 2

Rotating Black Holes: The Kerr Metric

For astrophysical reasons, the most realistic BH study case is that of a rotating BH with zero net eletrical charge [2, 21]. A BH that has mass M and angular momentum per unit mass a is described by the Kerr metric. In Boyer-Lindquist coordinates, this metric is expressed as [2, 21]

$$ds^2 = -\frac{\Delta}{\Sigma}\left(dt - a\sin^2(\theta)d\varphi\right)^2 + \frac{\sin^2(\theta)}{\Sigma}\left((r^2+a^2)d\varphi - adt\right)^2 + \frac{\Sigma}{\Delta}dr^2 + \Sigma d\theta^2, \quad (2.1)$$

where $\Sigma \equiv r^2 + a^2\cos^2(\theta)$, $\Delta \equiv r^2 - 2Mr + a^2$, and the range of coordinates are $0 \leq \theta \leq \pi$, $0 < \varphi \leq 2\pi$, $0 < r < \infty$ and $-\infty < t < \infty$. This space-time has two symmetries: it is time-independent and axisymmetric. These two isometries are generated by the vectors:

$$\xi_{(t)} \equiv \frac{\partial}{\partial t}, \quad \text{and} \quad \xi_{(\varphi)} \equiv \frac{\partial}{\partial \varphi}, \quad (2.2)$$

which are Killing vectors of this space-time [22].

It is obvious from equation (2.1) that this metric is divergent for $\Sigma = 0$ and for $\Delta = 0$. If we trace the curvature scalars, we can check that for $\Delta = 0$ they are finite, but at $\Sigma = 0$ the Kretschmann scalar diverges [23]. This indicates that there is a region of this space-time that constitutes a physical singularity. This singularity takes place at $r = 0$

and $\theta = \pi/2$. One can perform a slicing of this space-time, generating 3D hypersurfaces of constant t. Focusing on one of these surfaces, one may be inclined to believe that the singularity has a point-like projection on this surface, but this belief is not correct. The reason for this is that Boyer-Lindquist coordinates are a form of spheroidal coordinates that is related to Cartesian coordinates as

$$x = \sqrt{r^2 + a^2}\sin(\theta)\cos(\varphi), \quad y = \sqrt{r^2 + a^2}\sin(\theta)\sin(\varphi), \quad z = r\cos(\theta). \tag{2.3}$$

Bearing this coordinate change in mind, it is possible to check that the projection of the singularity on constant t hypersurfaces is actually a ring.

One might be interested in finding a hypersurface that is a one-way membrane. Such goal can be achieved requiring a surface of constant r to be null, i.e.:

$$g^{\mu\nu}\partial_\mu r \partial_\nu r = g^{rr} = 0, \tag{2.4}$$

which implies $\Delta = 0$, which is the same condition that describes the unphysical singularities. This condition is met at $r = r_\pm \equiv M \pm \sqrt{M^2 - a^2}$, where r_+ is the outer event horizon and r_- is the inner horizon. The hypersurface defined for $r = r_+$ is an event horizon, meaning that for $r < r_+$ the light cones are entirely pointing inwards consequently this region will be inaccessible for an observer that is located outside this region [2,24]. As one can see, the roots of $\Delta = 0$ are only real if $a \leq M$. This means that for $a > M$ a event horizon does not exist and it is said to be a "naked" singularity. Due to the weak cosmic censorship hypothesis [22,25], it is widely believed that there should not exist singularities that are not surrounded by an event horizon, i.e., a naked singularity. The weak cosmic censorship hypothesis then imposes a natural upper limit to the BH angular momentum that is $a = M$. At extremality we have that horizon radius is $r_H = r_+ = r_- = M$. A BH that has the maximum value of a is said to be an extremal Kerr BH.

Another interesting feature of rotating BH's appears when one looks at stationary observers. By definition, a static observer is one whose four-velocity is proportional to the vector $\xi_{(t)}$. When $g_{tt} > 0$ this vector is space-like, and so no static observer can exist in this region. This condition is met if $M - \sqrt{M^2 - a^2\cos^2(\theta)} < r < r_{\rm ergo} \equiv M + \sqrt{M^2 - a^2\cos^2(\theta)}$. The region $r_+ < r < r_{\rm ergo}$ is named the ergoregion or ergosphere. The boundary surface of the ergosphere can be shown to be a surface of infinite redshift [21]. It is important to notice that the surface that delimits the ergosphere externally ($r = r_{\rm ergo}$) is not a one-way membrane. So a particle can, in principle, enter the ergoregion and later on escape from it, if it does not cross the event horizon.

Another important class of observers is that of stationary observers. By definition, a stationary observer is one whose four-velocity is a linear combination of the Killing vectors associated with time translation invariance ($\xi_{(t)}$) and axial symmetry ($\xi_{(\varphi)}$) of this space-time [24]. An observer that has angular velocity Ω, it will have a four velocity of

$$v^\mu = v^t(\xi^\mu_{(t)} + \Omega\xi^\mu_{(\varphi)}). \tag{2.5}$$

This observer only exists if $v^\mu v_\mu < 0$, which is equivalent to:

$$g_{tt} + 2\Omega g_{t\varphi} + \Omega^2 g_{\varphi\varphi} < 0. \tag{2.6}$$

This is only true if Ω is inside the interval $[\Omega_-, \Omega_+]$, where

$$\Omega_\pm = \frac{-g_{t\varphi} \pm \sqrt{\Delta}\sin(\theta)}{g_{\varphi\varphi}}. \tag{2.7}$$

This means that this class of observers only exists for $r > r_+$. It is straightfoward to check that $\Omega_+ = \Omega_-$ when $r = r_+$. At this surface it is possible to find

$$\Omega_H \equiv \Omega_\pm|_{r_+} = \frac{a}{2Mr_+} = \frac{a}{r_+^2 + a^2}, \tag{2.8}$$

which is the only possible angular velocity for a stationary "observer" at the horizon [1]. To Ω_H we give the name horizon frequency. In the extremal limit this quantity is simply ${}^{x}\Omega_H = (2M)^{-1}$.

A sub-class of stationary observers is the Zero Angular Momentum Observer (ZAMO) class. As the name suggests, this sub-class of observer will follow a trajectory with L=0, where

$$L = \xi^{\mu}_{(\varphi)} v_{\mu}, \tag{2.9}$$

is the angular momentum. This condition constrains the four-velocity of these observers to be [26]

$$v^{\mu}_{ZAMO} = \left(\frac{-g_{\varphi\varphi}}{\Delta \sin^2(\theta)}\right)^{1/2} \left(1, 0, 0, \frac{-g_{t\varphi}}{g_{\varphi\varphi}}\right). \tag{2.10}$$

From this we can calculate the proper four-acceleration at a radius r as

$$a^{\mu}_{ZAMO} = v^{\nu}_{ZAMO} \nabla_{\nu} v^{\mu}_{ZAMO}. \tag{2.11}$$

The $a_{ZAMO}(r) = \sqrt{-a^{\mu}_{ZAMO} a_{\mu ZAMO}}$ is the proper four-acceleration as measured at a radius r. In order to obtain the four-acceleration of an observer at a radial distance r as measured from infinity, one needs to multiply $a_{ZAMO}(r)$ by the redshift factor thus obtaining

$$a^{\infty}_{ZAMO}(r) = a_{ZAMO}(r) \frac{\left(-\xi^{\mu}_{(t)} p_{\mu}\right)_{\infty}}{\left(-\xi^{\mu}_{(t)} p_{\mu}\right)_{r}}, \tag{2.12}$$

where p_{μ} is the observer's four-momentum. When evaluating (2.12) at $r = r_+$, one obtains:

$$a^{\infty}_{ZAMO}(r_+) = \frac{(M^2 - a^2)^{1/2}}{2M r_+}. \tag{2.13}$$

[1] Strictly speaking, there is no stationary observer at the horizon, because in this boundary $v^{\mu} v_{\mu} = 0$. These would imply that the observer is traveling at the light speed. As no observer can travel with this speed there is no observer at the horizon.

To $a^{\infty}_{ZAMO}(r_+)$ it is given the name of surface gravity, since it can be understood as the gravitational acceleration at the horizon. It can be proven that this quantity is constant over the horizon and relates to the BH temperature as [22]

$$T_H = \frac{a^{\infty}_{ZAMO}(r_+)}{2\pi}. \tag{2.14}$$

Chapter 3

Linear Perturbation of Rotating Black Holes

In this chapter we summarize most of the results of linear perturbation theory of rotating BH's. In the first section, we start by reviewing the wave equation that guides the propagation of perturbations of generic spin around this kind of BH. In the second section, we digress about physical properties of waves around a BH.

3.1 Teukolsky Equation

3.1.1 Sub-extremal Case: $a < M$

In 1973, Saul A. Teukolsky [27] derived a linear master equation that drives a massless master field Ψ of helicity s (and spin $|s|$) propagating around a Kerr BH ($s = 0$ for scalar, $s = \pm 1/2$ for neutrino, $s = \pm 1$ for electromagnetic and $s = \pm 2$ for gravitational perturbations). This major achievement in linear perturbation theory of BH's was possible by means of the so-called Newman-Penrose formalism. In this formalism it is useful to work with the Kinnersley (null) tetrad basis

$$l^{\mu} = \left(\frac{r^2 + a^2}{\Delta}, 1, 0, \frac{a}{\Delta} \right), \tag{3.1}$$

$$n^{\mu} = \frac{1}{2\Sigma} \left(r^2 + a^2, -\Delta, 0, a \right), \tag{3.2}$$

$$m^{\mu} = \frac{1}{2^{1/2}(r + ia\cos(\theta))} \left(ia\sin(\theta), 0, 1, \frac{i}{\sin(\theta)} \right), \tag{3.3}$$

$$\text{and} \quad m^{\mu *}, \tag{3.4}$$

to construct the so-called Newman-Penrose scalars. For instance, in the electromagnetic case, the radiative components of the field are described by

$$\phi_0 \equiv F_{\mu\nu} l^\mu m^\nu, \quad \phi_2 \equiv F_{\mu\nu} m^{\mu *} n^\nu, \tag{3.5}$$

where $F_{\mu\nu}$ is the Maxwell tensor. Here, ϕ_0 represents the $s = 1$ field and ϕ_2 the $s = -1$ field.

In the gravitational case, the radiative components of the field are described by

$$\psi_0 \equiv -C_{\alpha\beta\gamma\delta} l^\alpha m^\beta l^\gamma m^\delta, \quad \psi_4 \equiv -C_{\alpha\beta\gamma\delta} n^\alpha m^{\beta *} n^\gamma m^{\delta *}, \tag{3.6}$$

where $C_{\alpha\beta\gamma\delta}$ is the Weyl tensor. In this case, ψ_0 represents the $s = 2$ field and ψ_4 the $s = -2$ field.

Via independent derivations for each spin, Teukolsky could prove in his groundbreaking work that field perturbations of generic spin around a rotating BH obey the following linear partial differential equation (PDE)

$$\begin{aligned}
&\left[\frac{(r^2+a^2)^2}{\Delta} - a^2\sin^2(\theta)\right]\frac{\partial^2\Psi}{\partial t^2} + \frac{4Mar}{\Delta}\frac{\partial^2\Psi}{\partial t\partial\varphi} + \left[\frac{a^2}{\Delta} - \frac{1}{\sin^2(\theta)}\right]\frac{\partial^2\Psi}{\partial\varphi^2} \\
&- \Delta^{-s}\frac{\partial}{\partial r}\left(\Delta^{s+1}\frac{\partial\Psi}{\partial r}\right) - \frac{1}{\sin(\theta)}\frac{\partial}{\partial\theta}\left(\sin(\theta)\frac{\partial\Psi}{\partial\theta}\right) - 2s\left[\frac{a(r-M)}{\Delta} + \frac{i\cos(\theta)}{\sin^2(\theta)}\right]\frac{\partial\Psi}{\partial\varphi} \\
&- 2s\left[\frac{M(r^2-a^2)}{\Delta} - r - ia\cos(\theta)\right]\frac{\partial\Psi}{\partial t} + (s^2\cot^2(\theta) - s)\Psi = 4\pi\Sigma T,
\end{aligned} \tag{3.7}$$

where T is a source term. We shall set T to be equal to zero throughout this work, corresponding to the vacuum case. This set-up is justified since QNM frequencies are source-independent quantities, as it will become clear later on. In this last equation, the master field Ψ is understood as

$$\Psi \rightarrow \begin{cases} & \Phi \quad \text{for} \quad s=0, \\ \phi_0 \quad \text{for} \quad s=1, & \rho^{-2}\phi_2 \quad \text{for} \quad s=-1, \\ \psi_0 \quad \text{for} \quad s=2, & \rho^{-4}\psi_2 \quad \text{for} \quad s=-2, \end{cases} \tag{3.8}$$

where $\rho \equiv -(r - ia\cos(\theta))^{-1}$.

If we decompose Ψ into Fourier-harmonic components and angular multipoles as

$$\Psi = \frac{1}{2\pi}\int_{-\infty}^{\infty} e^{-i\omega t}\sum_{l=|s|}^{\infty}\sum_{m=-l}^{l} e^{im\varphi}{}_sS_{lmc}(\theta){}_sR_{lm\omega}(r)d\omega, \tag{3.9}$$

it can be shown that the equations for $R_{lm\omega}(r)$ and $S_{lmc}(\theta)$ can be written as two linear ordinary differential equations (ODE's)

$$\begin{aligned} &\frac{1}{\sin(\theta)}\frac{d}{d\theta}\left(\sin(\theta)\frac{d_sS_{lmc}(\theta)}{d\theta}\right) \\ &+\left(c^2\cos^2(\theta) - \frac{m^2}{\sin^2(\theta)} - 2cs\cos(\theta) - \frac{2ms\cos(\theta)}{\sin^2(\theta)} - s^2\cot^2(\theta) + s + {}_sA_{lmc}\right){}_sS_{lmc}(\theta) = 0, \end{aligned} \tag{3.10}$$

with $c \equiv a\omega$ and

$$\Delta^{-s}\frac{d}{dr}\left(\Delta^{s+1}\frac{d_sR_{lm\omega}(r)}{dr}\right) + \left(\frac{K^2 - 2is(r-M)K}{\Delta} + 4is\omega r - {}_s\lambda_{lmc}\right){}_sR_{lm\omega}(r) = 0, \tag{3.11}$$

where $K \equiv (r^2+a^2)\omega - am$ and ${}_s\lambda_{lmc} \equiv {}_sA_{lmc} + c^2 - 2mc$, which is a separation constant. This pair of equations are the angular and the radial Teukolsky equations, respectively.

The angular equation has as solutions the spin-weighted spheroidal harmonics, which have ${}_sA_{lmc}$ (or, equivalently, ${}_s\lambda_{lmc}$) as its eigenvalue. It is important to notice that equation (3.10) has regular singular points at $\cos(\theta) = \pm 1$ and a irregular singular point at $\cos(\theta) = \infty$, and that its solutions satisfy:

$$\int_0^{2\pi} d\varphi e^{i(m-m')\varphi} \int_0^{\pi} d\theta {}_sS_{lmc}(\theta) {}_sS^*_{l'm'c}(\theta) \sin(\theta) = 2\pi \delta^{l'}_{l} \delta^{m'}_{m}. \tag{3.12}$$

The spin-weighted spheroidal harmonics are standard functions in BH perturbation theory [28] and can be computed numerically using the toolkit available at [29]. This toolkit also allows us to calculate ${}_s\lambda_{lmc}$. In the static limit where $a \to 0$, they reduce to the spin-weighted spherical harmonics, which have ${}_s\lambda_{lmc} = l(l+1)$. For the scalar case ($s = 0$) they are the spheroidal wave functions.

It is important to notice some symmetries of the eigenvalues ${}_sA_{lmc}$. These symmetries can be shown to be

$${}_sA_{lmc} = {}_sA_{l,-m,-c} = {}_sA^*_{lmc^*} = {}_{-s}A_{lmc} - 2s. \tag{3.13}$$

For the radial Teukolsky equation (3.11) we can identify two regular singular points at $r = r_\pm$ and an irregular singular point at $r = \infty$. This structure classifies this equation as a confluent Heun's equation [30]. It is possible to find two linearly independent solutions to (3.11) with different asymptotic behaviors, which we denote by ${}_sR^{in}_{lm\omega}$ and ${}_sR^{up}_{lm\omega}$. Their behavior near the horizon ($r \to r_+$) and at radial infinity is

$${}_sR^{in}_{lm\omega} \sim \begin{cases} {}_sB^{trans}_{lm\omega} \Delta^{-s} e^{-ikr_*}, & \text{for} \quad r \to r_+, \\ {}_sB^{ref}_{lm\omega} \dfrac{e^{i\omega r_*}}{r^{2s+1}} + {}_sB^{inc}_{lm\omega} \dfrac{e^{-i\omega r_*}}{r}, & \text{for} \quad r \to \infty, \end{cases} \tag{3.14}$$

$${}_sR^{up}_{lm\omega} \sim \begin{cases} {}_sC^{ref}_{lm\omega} \Delta^{-s} e^{-ikr_*} + {}_sC^{up}_{lm\omega} e^{ikr_*}, & \text{for} \quad r \to r_+, \\ {}_sC^{trans}_{lm\omega} \dfrac{e^{i\omega r_*}}{r^{2s+1}}, & \text{for} \quad r \to \infty. \end{cases} \tag{3.15}$$

Here, we defined $k \equiv \omega - m\Omega_H$, ${}_sB^{inc/ref/trans}_{lm\omega}$ and ${}_sC^{inc/ref/trans}_{lm\omega}$ as the incidence/ reflection/ transmission coefficients of the ingoing and upgoing modes, respectively. The radial coordinate used was the usual tortoise coordinate, which is related to r as

$$r_* \equiv \int \frac{dr_*}{dr} dr = \int \frac{r^2 + a^2}{\Delta} dr = r + \frac{2Mr_+}{r_+ - r_-} \ln\left(\frac{r - r_+}{2M}\right) - \frac{2Mr_-}{r_+ - r_-} \ln\left(\frac{r - r_-}{2M}\right). \tag{3.16}$$

These two solutions have different physical meanings. A wave that behaves like $e^{-i\omega t}R^{in}_{lm\omega}$ can be seen as a wave that propagates initially from infinity towards the black hole, being partially reflected back to infinity by the potential barrier and partially transmitted into the black hole. On the other hand, a wave that behaves like $e^{-i\omega t}{}_sR^{up}_{lm\omega}$ can be understood as a wave that is initially outgoing near the horizon and is partially reflected back to the black hole and partially transmitted to radial infinity. This interpretation is depicted in figure 3.1.

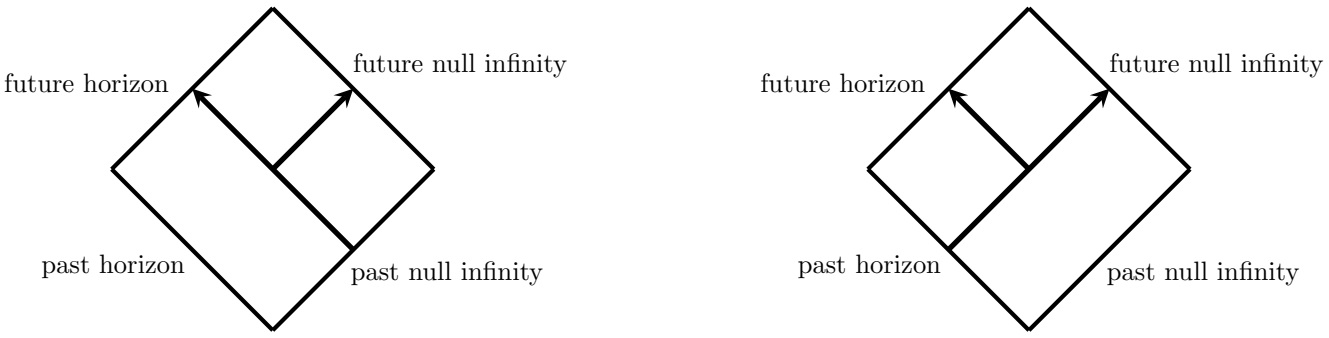

Figure 3.1: This figure shows Penrose diagrams with a schematic representation of the in- and up-modes of the solutions to the radial Teukolsky equation.

Defining ${}_s\bar{R}^{in}_{lm\omega}$ and ${}_s\bar{R}^{up}_{lm\omega}$ as

$$ {}_s\bar{R}^{in}_{lm\omega} = \frac{{}_sR^{in}_{lm\omega}}{{}_sB^{trans}_{lm\omega}} \quad , \quad {}_s\bar{R}^{up}_{lm\omega} = \frac{{}_sR^{up}_{lm\omega}}{{}_sC^{trans}_{lm\omega}}, \tag{3.17} $$

and performing a change of coordinate defined by

$$ \frac{dr}{d\bar{r}} = \Delta^{s+1}, \tag{3.18} $$

it can be seen that the resulting ODE will be of second order with no term of first order derivative. This means that the Wronskian with respect to $\bar{r}$ will be constant [31]. This Wronskian can be calculated as

$$ {}_sW_{lm\omega} \equiv \left({}_s\bar{R}^{in}_{lm\omega}\frac{d_s\bar{R}^{up}_{lm\omega}}{d\bar{r}} - {}_s\bar{R}^{up}_{lm\omega}\frac{d_s\bar{R}^{in}_{lm\omega}}{d\bar{r}} \right) = \Delta^{s+1}\left({}_s\bar{R}^{in}_{lm\omega}\frac{{}_sd\bar{R}^{up}_{lm\omega}}{dr} - {}_s\bar{R}^{up}_{lm\omega}\frac{d_s\bar{R}^{in}_{lm\omega}}{dr} \right) = 2i\omega\frac{{}_sB^{inc}_{lm\omega}}{{}_sB^{trans}_{lm\omega}}. \tag{3.19} $$

It is easy to check that ${}_sW_{lm\omega}$ also displays an interesting symmetry with respect to m and ω, similar to ${}_s\lambda_{lmc}$. The radial equation is complex conjugated if one performs the change $(m,\omega)\to(-m,-\omega^*)$. This means that ${}_sW_{lm\omega}={}_sW^*_{l,-m,-\omega^*}$.

3.1.2 Extremal case: $a=M$

The derivation of the Teukolsky equations is valid for arbitrary values of the spin parameter a. However, at extremality an important difference appears: although the angular equation does not show any special feature in this limit, the structure of the radial equation changes. In the extremal case the ODE has two irregular singular points: one at the horizon ($r=r_H=r_+=r_-$) and another one at infinity ($r=\infty$). This implies that the radial Teukolsky equation is now a doubly-confluent Heun equation [30] in contrast with the sub-extremal case. With this change, one might wonder if the transition from $a<M$ to $a=M$ in physical quantities of the BH, such as its QNM's, is smooth.

In order to address the above question properly, an analysis of the radial Teukolsky equation in the extremal case was performed in [32]. In this limit, it is possible to cast equations (3.14) and (3.15) in a more suitable form

$$ {}^x_sR^{in}_{lm\omega}\sim\begin{cases} {}^x_sB^{trans}_{lm\omega}e^{2M^2ik/x}x^{-2s}e^{-2Mi\omega\ln(x/(2M))}, & \text{for}\quad x\to 0^+,\\ {}^x_sB^{ref}_{lm\omega}\dfrac{e^{i\omega(x+2M\ln(x/(2M)))}}{x^{2s+1}}+{}^x_sB^{inc}_{lm\omega}\dfrac{e^{-i\omega(x+2M\ln(x/(2M)))}}{x}, & \text{for}\quad x\to\infty,\end{cases} \tag{3.20}$$

$$ {}^x_sR^{up}_{lm\omega}\sim\begin{cases} {}^x_sC^{ref}_{lm\omega}e^{2M^2ik/x}x^{-2s}e^{-2Mi\omega\ln(x/(2M))}+{}^x_sC^{up}_{lm\omega}e^{-2M^2ik/x}e^{2Mi\omega\ln(x/(2M))}, & \text{for}\quad x\to 0^+,\\ {}^x_sC^{trans}_{lm\omega}\dfrac{e^{i\omega(x+2M\ln(x/(2M)))}}{x^{1+2s}}, & \text{for}\quad x\to\infty,\end{cases} \tag{3.21}$$

where $x\equiv r-r_H=r-M$ and k is defined in the usual way. Equations (3.20) and (3.21) are simple limits of (3.14) and (3.15) respectively, but it is worth noticing that the coefficients will differ from the sub-extremal ones by a phase shift. However, it is easy to

check that the Wronskian will have a similar expression

$$ {}^{x}_{s}W_{lm\omega} \equiv \Delta^{s+1}\left({}^{x}_{s}\hat{R}^{in}_{lm\omega}\frac{d^{x}_{s}\hat{R}^{up}_{lm\omega}}{dx} - {}^{x}_{s}\hat{R}^{up}_{lm\omega}\frac{d^{x}_{s}\hat{R}^{in}_{lm\omega}}{dx}\right) = 2i\omega\frac{{}^{x}_{s}B^{inc}_{lm\omega}}{{}^{x}_{s}B^{trans}_{lm\omega}}, \tag{3.22} $$

which is also constant with respect to r and obeys the same symmetry under $(m,\omega)\rightarrow(-m,-\omega^{*})$. In equation (3.22) ${}^{x}_{s}\hat{R}^{in}_{lm\omega}$ and ${}^{x}_{s}\hat{R}^{up}_{lm\omega}$ are the same as in (3.21) but normalized by ${}^{x}_{s}B^{trans}_{lm\omega}$ and ${}^{x}_{s}C^{trans}_{lm\omega}$ respectively.

3.2 Physical Properties of Waves Around Black Holes

3.2.1 Quasi-Normal Modes

As an analogy to QNM's, we can start by looking at the case of a vibrating bell. When someone hits a bell, one can see that it will vibrate emitting a sound that will fade away with time and it will return to its initial shape. It is an experimental fact that different bells have different sounds even if they are hit in the same way. The different sound is a consequence of having a different set of characteristic frequencies. So one can expect that the sound emitted by the perturbed bell can tell us something about the bell, such as its shape or material. This idea is largely explained in [33] for the undamped case.

Similarly, we can introduce the concept of QNM's in the context of BH perturbation theory. As in the case of the bell, if we perturb a BH by an external field, we can expect the "sounds" emitted by the black hole to present characteristic frequencies. In this new context, the perturbations can be, for example, caused by a particle falling into the BH (gravitational case) or a gamma-ray burst nearby (electromagnetic case), and now the sound in the bell analogy can be compared with electromagnetic and gravitational waves respectively.

Since we expect these frequencies of the modes of vibration to be intrinsic, it is natural that they are determined by the source-free differential equation, justifying the

analysis of the vacuum case in (3.7). In order to search for the QNM's we have to introduce appropriate boundary conditions. On causal grounds, we impose that no waves are coming out from the BH and that no waves are coming in from radial infinity. In this picture we should expect that the physical field modes behave as

$$\Psi \propto \begin{cases} \Delta^{-s} e^{-i\omega t} e^{-ikr_*} & \text{as} \quad r \to r_+, \\ \dfrac{e^{-i\omega(t-r_*)}}{r^{2s+1}} & \text{as} \quad r \to \infty, \end{cases} \tag{3.23}$$

where the proportionality factors are r- and t-independent.

Because of the dissipative nature of the problem, we expect the frequencies that satisfy both boundary conditions in (3.23) to be complex-valued, where the imaginary part of these frequencies will give the decay rate of the field. Given a spin-field s, there are an infinite (but countable) number of QNM's for each set of multipole numbers (l, m), and they are enumerated by the so-called overtone number $n = 0, 1, 2, ...$ Accordingly, we shall denote the QNM frequencies by ω_{lmn}. Typically, the value of n increases with decreasing imaginary part of ω_{lmn}. The imaginary part of ω_{lmn} is related to the damping time of the mode; the $n = 0$ QNM being by definition the longest-lived mode. Both the real and imaginary parts of ω_{lmn} are determined by the BH's initial configuration (mass, spin and charge) and the spin of the perturbation. The imaginary part the QNM frequencies can tell us about an important property of the BH space-time. If $\Im(\omega_{lmn}) > 0$ for a particular mode, this mode will grow exponentially in time and this will indicate that this space-time is linearly (mode-) unstable [10, 21].

Even if ω_{lmn} has a negative imaginary part, one might be concerned about the fact that if we trace the mode perturbation back in time, it will grow, corresponding to initial data with infinite amplitude. This is due to the fact that QNM's do not form a complete set of eigenfunctions, meaning that an expansion in terms of QNM's is not always possible [34–37]. Astrophysically, this means that QNM's are excited only during a certain period

of time [38]. This period where the QNM's are excited corresponds to the ringdown phase in the waveform, as we can see in numerical waveform calculations [40–42] and as seen recently in LIGO's observations [3–8].

Another way of understanding QNM's, and the one that will be largely used in this work, is via the retarded Green function (GF) [37]. The retarded GF is a solution to the wave equation with $4\pi\Sigma\delta_4(x,x')$ source, and which satisfies boundary conditions in order to respect the causality principle. In the section about the Teukolsky equation (3.1), we used as starting point a mode decomposition as in (3.9). Having constructed the solutions (3.14) and (3.15) (or (3.20) and (3.21) for the extremal case) we can write the GF of (3.11) as

$$ {}_sG_{lm\omega}(r|r') = -\frac{{}_s\bar{R}^{up}_{lm\omega}(r)\,{}_s\bar{R}^{in}_{lm\omega}(r')}{{}_sW_{lm\omega}}\Theta(r-r') - \frac{{}_s\bar{R}^{up}_{lm\omega}(r')\,{}_s\bar{R}^{in}_{lm\omega}(r)}{{}_sW_{lm\omega}}\Theta(r'-r), \tag{3.24}$$

then the full retarded GF, in the time-domain, will be

$$ {}_sG(x^\mu|x^{\mu\prime}) = -2\Delta^s(r')\sum_{l=|s|}^{\infty}\sum_{m=-l}^{l}\int_{-\infty+i\mathscr{C}}^{+\infty+i\mathscr{C}} d\omega e^{-i(\omega t-m\varphi)}\,{}_sS_{lmc}(\theta)\,{}_sS^*_{lmc}(\theta')\,{}_sG_{lm\omega}(r|r'), \tag{3.25}$$

for $\mathscr{C} > 0$ and $x^\mu = (t, r, \theta, \varphi)$. Because of the time invariance and axisymmetry of this space-time, we have set $t' = \varphi' = 0$ in (3.25) without loss of generality.

In order to obtain the solution of the wave equation for an arbitrary source term, one needs to integrate the retarded GF against the source term. When performing the Laplace transform as in (3.25), one notices that there are different possible contributions to this integral: from simple poles, branch cuts (see section 3.2.2) and from other irrelevant (at least after a certain time) contributions [37, 39] (see figure 3.2). The first contribution to the master field can be written as a sum of terms behaving in time like $e^{-i\omega_p t}$, where ω_p's are simple poles of ${}_sG_{lm\omega}(r|r')$ in the frequency-domain. By the same reasoning applied

in the bell case, these frequencies are the QNM's. By construction, the simple poles of ${}_sG_{lm\omega}(r|r')$ correspond to the zeros of ${}_sW_{lm\omega}$. Because of the equivalence between ω_{lmn} and zeros of ${}_sW_{lm\omega}$ we will be looking for the zeros of equations (3.19) and (3.22) in order to find ω_{lmn}.

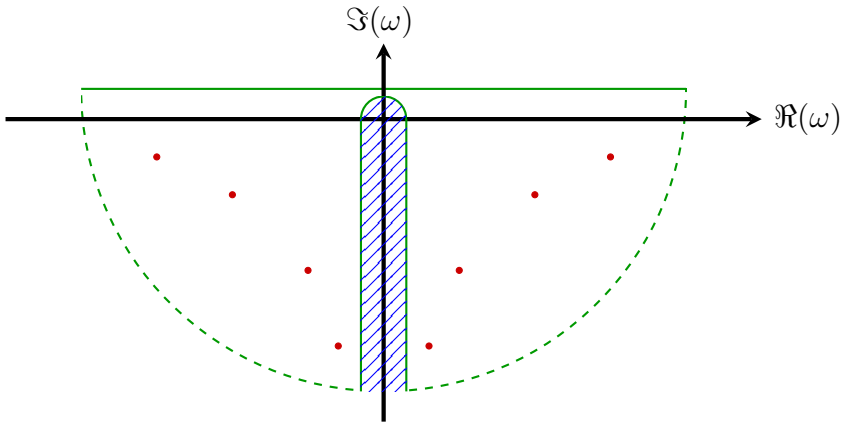

Figure 3.2: This figure is an illustrative representation of the contour deformation on the complex-frequency plane for the modes of the GF of the radial Teukolsky equation, for the static case ($a = 0$). The red dots represent simple poles of the GF and are the QNM frequencies. The dashed green line is the high-frequency arc of integration. The solid green line is the original integration for the Laplace transform. The blue hatched region represents the BC that stems from the origin ($\omega = 0$) that appear in the radial functions. In the case where $a > 0$, more BC's will appear in the complex-frequency plane, and they come from spin-weighted spheroidal harmonics. It is worth noticing that there might exist other types of BC's that we are not aware of. The contour of integration here should be taken in a clockwise sense.

3.2.2 Branch Cuts and Tails

Earlier in this chapter we said that the Green Function has three major contributions due to the different parts of the integration contour chosen when performing integral (3.25). Mathematically, this means that we can decompose the full GF (3.25) like

$$ {}_sG(x^\mu|x^{\mu\prime}) = {}_sG_{QNM}(x^\mu|x^{\mu\prime}) + {}_sG_{BC}(x^\mu|x^{\mu\prime}) + {}_sG_F(x^\mu|x^{\mu\prime}), \tag{3.26} $$

where ${}_sG_{QNM}(x^\mu|x^\mu)$ is the QNM contribution explained in the previous section, ${}_sG_F(x^\mu|x^{\mu\prime})$ is the contribution of the high frequency arc (which reduces to the flat-space GF in the

limit where $M, a \to 0$) and ${}_sG_{BC}(x^\mu|x^{\mu\prime})$ is the BC contribution (see figure 3.2). This section will be dedicated to the BC contribution to the GF (3.25).

It was in 1986 that this idea was explored for the first time in a work by Leaver [37]. Leaver worked on the Schwarzschild geometry (setting $a = 0$ in (2.1)). It was in his original work that Leaver proved that in this geometry the contribution coming from the BC in the contour of integration contributes to the late-time decay tails of the (Schwarzschild) GF.

Since Leaver found that for the Schwarzschild case the ${}_sG_{BC}$ contribution was the leading term in (3.26) at the late-time regime [37], it would be expected that the same is true in the Kerr metric. Following this train of though the authors of [39] computed (3.28) via the MST expressions for ${}_sR^{up}_{lm\omega}$. The starting point of the paper was the realization that the BC in the GF comes from a discontinuity in the Wronskian, inherited from ${}_sR^{up}_{lm\omega}$[1]. Because of the discontinuity in ${}_sR^{up}_{lm\omega}$, it was proved that there is a discontinuity in (3.25), that stems from the origin and goes down the imaginary axis of the complex-ω plane.

Formally, the BC contribution to (3.25) can be expressed as

$$ {}_sG_{BC}(x^\mu|x^{\mu\prime}) = -2\Delta^s(r')\sum_{l=|s|}^{\infty}\sum_{m=-l}^{l} e^{im\varphi}\int_0^\infty d\omega e^{-i\omega t}\,{}_sS_{lmc}(\theta)\,{}_sS^*_{lmc}(\theta')\delta_s G_{lm\omega}(r|r'), \quad (3.27) $$

where

$$ \delta_s G_{lm\omega}(r|r') = lim_{\bar\rho\to 0^+}\left({}_sG_{l,m,\omega+\bar\rho}(r|r') - {}_sG_{l,m,\omega-\bar\rho}(r|r')\right) \neq 0 \quad \text{for} \quad i\omega > 0. \quad (3.28) $$

Doing so, they reproduced the leading order behavior at timelike infinity as t^{-2l-3} and computed a third order correction behaving as $t^{-2l-5}\ln(t)$ in the scalar case. This

[1]It was argued that ${}_sR^{in}_{lm\omega}$ can not have BC's. The main argument was that this solution has a Jaffé series representation that is absolutely convergent $\forall\ \omega \in \mathbb{C}$ and $r_+ \leq r < \infty$.

leading order behavior is also correct for electromagnetic and gravitational fields and it was first found in [43,44]. This result together with the mode stability (proved in [46]) can be understood as an indication for the linear stability of the Kerr BH. If it was found that the GF has a **growth** due to this BC, it would be seen as an instability of this space-time. An instability due to the BC can occur if the branch point from which the BC stems from happens to be in the upper part of the complex-frequency plane, i.e. $\Im(\omega) > 0$. This motivates us to search for possible new BC's in the Wronskian (3.19), see our results in sections 5.2.2 and 5.3.3.

In 1974, Hartle and Wilkins performed an investigation of the analytic properties of the solutions to the Teukolsky equation in the complex-frequency plane [47]. The MST method was not used, since it was only developed 22 year later. They were able to perform such a study by means of a perturbative technique. It was defined

$$\begin{aligned} \frac{d\hat{r}_*}{dr} &= \frac{r^2}{\Delta}, \\ \Upsilon(\hat{r}_*) &= \Delta^{s/2} r_s R_{lm\omega}(r), \end{aligned} \tag{3.29}$$

for which the radial Teukolsky equation takes the general form

$$\frac{d^2\Upsilon(\hat{r}_*)}{d\hat{r}_*^2} + V(\hat{r}_*)\Upsilon(\hat{r}_*) = 0, \tag{3.30}$$

where $V(\hat{r}_*)$ is the potential obtained after performing transformation (3.29) on the radial Teukolsky equation (3.11).

By working in two different asymptotic regimes ($\hat{r}_* \to \infty$) of (3.30) they were able to construct two linearly independent solutions in each regime. These solutions are $A_{\pm}^{\infty}$ for $\hat{r}_* \to \infty$ and $A_{\pm}^{-\infty}$ for $\hat{r}_* \to -\infty$[2]. By separating the potential $V(\hat{r}_*)$ at $\hat{r}_* \to \pm\infty$ in

[2]The $\pm$ sub-index refer to the mode of the wave. The minus sign (plus) stands for ingoing (outgoing) wave. The super-index refer to which region the asymptotic behavior is valid. The minus (plus) sign refer to the $\hat{r}_* \to -\infty(+\infty)$. The same is valid for other quantities.

two terms ($V_0^{\pm\infty}(\hat{r}_*)$ and $V_1^{\pm\infty}(\hat{r}_*)$) and treating $V_1^{\pm\infty}(\hat{r}_*)$ as a perturbation, they wrote these solutions in the following manner

$$A_{\pm}^{\pm\infty} = A_{\pm}^{\pm\infty(0)} + \sum_{n=1}^{\infty} A_{\pm}^{\pm\infty(n)}, \tag{3.31}$$

where $A_{\pm}^{\pm\infty(0)}$ is a solution to a ODE of the form

$$\frac{d^2\Upsilon(\hat{r}_*)}{d\hat{r}_*^2} + V_0^{\pm\infty}(\hat{r}_*)\Upsilon(\hat{r}_*) = 0, \tag{3.32}$$

and

$$A_{\pm}^{\infty(n)} = \int_{\hat{r}_*}^{\infty} d\hat{r}_*^{(1)} \int_{\hat{r}_*^1}^{\infty} d\hat{r}_*^{(2)} ... \int_{\hat{r}_*^{(n-1)}}^{\infty} d\hat{r}_*^{(n)} G_0^{\infty}(\hat{r}_*|\hat{r}_*^{(1)}) G_0^{\infty}(\hat{r}_*^{(1)}|\hat{r}_*^{(2)}) ... \\ ... \times G_0^{\infty}(\hat{r}_*^{(n-1)}|\hat{r}_*^{(n)}) V_1^{\infty}(\hat{r}_*^{(1)}) ... V_1^{\pm\infty}(\hat{r}_*^{(n)}) A_{\pm}^{\infty(0)}, \tag{3.33}$$

and

$$A_{\pm}^{-\infty(n)} = \int_{-\infty}^{\hat{r}_*} d\hat{r}_*^{(1)} \int_{-\infty}^{\hat{r}_*^1} d\hat{r}_*^{(2)} ... \int_{-\infty}^{\hat{r}_*^{(n-1)}} d\hat{r}_*^{(n)} G_0^{-\infty}(\hat{r}_*|\hat{r}_*^{(1)}) G_0^{-\infty}(\hat{r}_*^{(1)}|\hat{r}_*^{(2)}) ... \\ ... \times G_0^{-\infty}(\hat{r}_*^{(n-1)}|\hat{r}_*^{(n)}) V_1^{-\infty}(\hat{r}_*^{(1)}) ... V_1^{-\infty}(\hat{r}_*^{(n)}) A_{\pm}^{-\infty(0)}, \tag{3.34}$$

where $G_0^{\pm\infty}(r_*|r_*^{(1)})$ is the GF to (3.32). With this technique, they thought there might be a branch point at

$$\omega_{HW} = m\Omega_H + i(s-1)\frac{r_+ - M}{2Mr_+}, \tag{3.35}$$

in the solution $A_-^{-\infty}$.

This frequency is now known as the Hartle-Wilkins frequency. Notice that if $s = 2$, this frequency is in the upper-half complex-ω plane, and if this BC exists and contributes to the GF (3.25), we might expect an instability of the space-time.

Although Hartle and Wilkins were inclined to believe in the existence of a branch point at $\omega = \omega_{HW}$, it was discussed by Glampedakis and Andersson that this indication is misleading (see [45]). Since the MST method was not used on [45] we decided to investigate whether we can find this BC or not by using the MST method.

There is also in [45] a discussion about extremal Kerr black holes. They wrote the radial Teukolsky equation in a similar form to (3.30) and studied its behavior as $r \to r_+$ for $a = M$. In this regime the Teukolsky equation can be approximated to

$$\begin{aligned} \frac{d^2 {}_sR_{lm\omega}(r_*)}{dr_*^2} + \left(\hat{\Omega}^2 + \frac{\mu}{r_*}\right) {}_sR_{lm\omega}(r_*) = 0, \\ \hat{\Omega} = \omega - m\Omega_H, \\ \mu = -2(m - is)\hat{\Omega}. \end{aligned} \tag{3.36}$$

The ODE (3.36) can be transformed to a Whittaker equation with two independent solutions:

$$W_{\pm \mathrm{j},\mathrm{i}}(\pm 2i\hat{\Omega} r_*) = (\pm 2i\hat{\Omega} r_*)^{1/2+\mathrm{i}} e^{\mp i\hat{\Omega} r_*} U(1/2 + \mathrm{i} \mp \mathrm{j}, 1 + 2\mathrm{i}, \pm 2i\hat{\Omega} r_*)^3 \tag{3.37}$$

for

$$\mathrm{j} = im + s \quad \text{and} \quad \mathrm{i} = \pm 1/2. \tag{3.38}$$

The Whittaker function is multi-valued when its argument is zero, i.e. $2i\hat{\Omega} r_* = 0$. This condition is equivalent to $\omega = m\Omega_H$[4]. This leads to the conclusion that there is a BC in the extremal Kerr BH that is absent for the sub-extremal Kerr BH. The BC in the superradiance bound frequency will be referred to as "superradiant" BC.

This BC was found to be related with a blow up of the Weyl scalar ψ_4 (see [50]). However in [48, 51] it was shown that this does not constitute an instability and that the blow up in ψ_4 is due to the choice of the tetrad basis.

[3]Notice that there is a degeneracy when using the name W both for the Wronskian and for the Whittaker function. This is the only time the we are referring to the Whittaker function, so no confusion should be expected.

[4]The condition is also met when $r_* = 0$, but equation (3.37) is only valid for $r_* \to -\infty$. For this reason one can not conclude about a branch point at $r_* = 0$.

3.2.3 Superradiance

In 1969, R. Penrose discovered a process that enables the extraction of energy from a rotating black hole [49], this process is now widely known as the "Penrose process". In this thought experiment, Penrose made use of a small massive object that, passing by the vicinity of a BH, breaks into two fragments, one falling into the BH, and the second one escaping to infinity. Penrose showed that if the breaking-up of the original object happens inside the ergoregion, the fragment that crosses the horizon may have negative energy with respect to a distant observer and the escaping particle has energy larger than the original one. Thus, an extraction of rotational energy and a decrease in the BH's spin takes place.

The so-called superradiance phenomenon is the wave analogue to the Penrose process. In this phenomenon, it is useful to use the fractional variation of energy

$$Z_{slm\omega} \equiv \frac{dE_{out}}{dt}\left(\frac{dE_{in}}{dt}\right)^{-1} - 1, \tag{3.39}$$

where E_{in} and E_{out} are the energy of the incident and the reflected part of an initially ingoing scattered wave at infinity. The quantity $Z_{slm\omega}$ is known in the literature as the amplification factor and it is possible to show that it satisfies $Z_{slm\omega} = Z_{s,l,-m,-\omega}$. For this reason, in this sub-section, we will be assuming $\omega > 0$.

The physical meaning of $Z_{slm\omega}$ is that, when it is larger than 0 the wave is carrying away energy from the BH because $dE_{out}/dt > dE_{in}/dt$. This is the superradiance phenomenon. This condition is met when $k < 0$, in other words, when $\omega < m\Omega_H$ [5]. For that reason $\omega_{SR} \equiv m\Omega_H$ is called the superradiant bound frequency.

[5]The most general condition is $k\omega < 0$, which can also be met for $k > 0$ if $\omega < 0$. Since in this section we assumed $\omega > 0$, we found the superrandiance condition to be $k < 0$.

By means of the stress-energy tensor in the scalar and electromagnetic cases, and of the area theorem in the gravitational case, one can relate the energy fluxes in (3.39) with the asymptotic amplitudes in (3.19) and find the amplification factors in terms of them as [53, 54]

$$Z_{slm\omega} \equiv \begin{cases} \left|\dfrac{{}_sB^{ref}_{lm\omega}}{{}_sB^{inc}_{lm\omega}}\right|^2 - 1 & \text{for} \quad s = 0, \\ \left|\dfrac{{}_sB^{ref}_{lm\omega}}{{}_sB^{inc}_{lm\omega}}\right|^2 \left(\dfrac{16\omega^4}{B^2}\right)^{s/|s|} - 1 & \text{for} \quad |s| = 1, \\ \left|\dfrac{{}_sB^{ref}_{lm\omega}}{{}_sB^{inc}_{lm\omega}}\right|^2 \left(\dfrac{256\omega^8}{|C|^2}\right)^{s/|s|} - 1 & \text{for} \quad |s| = 2, \end{cases} \tag{3.40}$$

where we define B and C via

$$\begin{aligned} B^2 &\equiv Q^2 + 4(mc - c^2), \\ |C|^2 &\equiv B^2\left((Q-2)^2 + 36(mc-c^2)\right) + 48(2Q-1)(2c^2 - mc) + 144\omega^2(M^2 - a^2), \\ Q &\equiv {}_s\lambda_{lmc} + s(s+1). \end{aligned} \tag{3.41}$$

If we keep $Z_{slm\omega}$ as in equation (3.40) it will not be useful for the purposes of this work. As already stated in the previous section, our main goal is to compute the QNM's by means of the Wronskian as defined in (3.19) and (3.22), which we wrote as a function of the incidence and transmission coefficients, but not of the reflection one. The idea is to use this $Z_{slm\omega}$ in order to perform a consistency check of our numerical calculations. So it would be useful to write the amplification factor as a function of the previously defined Wronskian ${}_sW_{lm\omega}$. In order to do so, we can use a (different) Wronskian between the solutions ${}_sY^{in}_{lm\omega}$ and ${}_{-s}Y^{in*}_{lm\omega}$ with respect to r_*, which is also r-independent. Then, we can write the following identity using this second Wronskian :

$$\left[{}_{-s}Y^{in*}_{lm\omega}\frac{d_sY^{in}_{lm\omega}}{dr_*} - {}_sY^{in}_{lm\omega}\frac{d_{-s}Y^{in*}_{lm\omega}}{dr_*}\right]_{r=r_+} = \left[{}_{-s}Y^{in*}_{lm\omega}\frac{d_sY^{in}_{lm\omega}}{dr_*} - {}_sY^{in}_{lm\omega}\frac{d_{-s}Y^{in*}_{lm\omega}}{dr_*}\right]_{r=\infty}, \tag{3.42}$$

where

$$ {}_sY^{in}_{lm\omega} \equiv \Delta^{s/2}(r^2+a^2)^{1/2}\, {}_sR^{in}_{lm\omega} \tag{3.43} $$

which reflects conservation of energy [53,55]. The Teukolsky-Starobinsky identities [2,53] allow us to correlate the asymptotic coefficients in (3.14) for fields of spins s and $-s$ in the following manner

$$ \begin{aligned} {}_sB^{inc}_{lm\omega}\big|_{s=1} &= -\frac{8\omega^2}{B}\, {}_sB^{inc}_{lm\omega}\big|_{s=-1}, \quad {}_sB^{ref}_{lm\omega}\Big|_{s=1} = -\frac{B}{2\omega^2}\, {}_sB^{ref}_{lm\omega}\Big|_{s=-1}, \\ {}_sB^{inc}_{lm\omega}\big|_{s=2} &= \frac{64\omega^4}{C}\, {}_sB^{inc}_{lm\omega}\big|_{s=-2}, \quad {}_sB^{ref}_{lm\omega}\Big|_{s=2} = \frac{C^*}{4\omega^4}\, {}_sB^{ref}_{lm\omega}\Big|_{s=-2}. \end{aligned} \tag{3.44} $$

Using the set of relations (3.42) and (3.44), it is possible to rewrite $Z_{slm\omega}$ as

$$ Z_{slm\omega} = \begin{cases} -\dfrac{8\omega M k r_+}{|{}_sW_{lm\omega}|^2} & \text{for} \quad s=0, \\ -\dfrac{2\omega^3}{Mkr_+|{}_sW_{lm\omega}|^2} & \text{for} \quad s=1, \\ -\dfrac{4\omega^5}{k(2Mr_+)^3(k^2+4\bar{\epsilon}^2)}\dfrac{1}{|{}_sW_{lm\omega}|^2} & \text{for} \quad s=2, \end{cases} \tag{3.45} $$

with

$$ \bar{\epsilon} \equiv \frac{(M^2-a^2)^{1/2}}{4Mr_+} \tag{3.46} $$

and ${}_sW_{lm\omega}$ appearing in (3.45) is defined via (3.19) and/or (3.22) . Here we have given an expression for the amplification factor for positive helicity. The expressions for negative helicity can be obtained in a similar way.

We developed a code in Mathematica [58] that will allow us to calculate the amplification factor as defined by (3.45), but in order to test our results it will be useful to have an analytical small-ω asymptotic behavior in order to verify the validity of our results. Such expression was obtained in [56, 57], where it was used the assumption $\omega \ll m\Omega_H$, and it reads

$$ \begin{aligned} Z_{slm\omega} \sim & 8r_+^2\omega^{2l+1}(r_+-r_-)^{2l}\hat{T}\left[\frac{\Gamma(1+l-s)\Gamma(1+l+s)}{(2l+1)!!\Gamma(l+1)\Gamma(2l+1)}\right]^2 \times \\ & \sinh\left(\frac{m\Omega_H}{\hat{T}r_+}\right)\Gamma\left(1+l-\frac{im\Omega_H}{\pi r_+\hat{T}}\right)\Gamma\left(1+l+\frac{im\Omega_H}{\pi r_+\hat{T}}\right), \end{aligned} \tag{3.47} $$

where we have included the definition $\hat{T} \equiv (r_+ - r_-)/(4\pi r_+^2)$.

In the extremal Kerr case, $\hat{T}$ is equal to zero, and one can easily check that equation (3.47) for the small-frequency regime is no longer valid. However, in [57], Starobinsky performed an approximation for our case of interest. This approximation is now valid for $\omega \to \omega_{SR}$. Using the definition of $\hat{\delta}^2 \equiv 2m^2 - {}_sA_{lmc} - (a\omega)^2 - (s+1/2)^2$, $\alpha \equiv (1 - \omega/\omega_{SR})$ and $S_\alpha \equiv \alpha/|\alpha|$, Starobinsky found

$$Z_{slm\omega} \sim \frac{\sinh^2(2\pi\hat{\delta})}{S_\alpha e^{\pi m(S_\alpha - 1)}} \Big(\cosh^2\Big(\pi(m-\hat{\delta})\Big) e^{\pi\hat{\delta}(S_\alpha - 1)} + \cosh^2\Big(\pi(m+\hat{\delta})\Big) e^{-\pi\hat{\delta}(S_\alpha-1)} \\ -2\cosh\Big(\pi(m-\hat{\delta})\Big)\cosh\Big(\pi(m+\hat{\delta})\Big)\cos\Big(\gamma_0 - 2\hat{\delta}\log(2m^2|\alpha|)\Big)\Big)^{-1}, \quad (3.48)$$

for $\hat{\delta}^2 > 0$ and $|\alpha| \ll m^{-4}\max(1, |\alpha|^2)$, where the definition

$$\gamma_0 = 4\arg\Big(\Gamma(1+2\mathrm{i}\hat{\delta})\Big) + 2\arg\Big(\Gamma\Big(1/2 + s + i(m-\hat{\delta})\Big)\Big) + 2\arg\Big(\Gamma\Big(1/2 + s - i(m+\hat{\delta})\Big)\Big), \quad (3.49)$$

was used. In the regime $\alpha \approx 0$, modes that have $\hat{\delta}^2 < 0$ will have its amplification factor expressed as

$$Z_{slm\omega} \sim 4S_\alpha |\delta|^2 (2m^2|\alpha|)^{2|\hat{\delta}|} e^{\pi m(1-S_\alpha)} \frac{|\Gamma(1/2 + s + |\hat{\delta}| + im)|^2 |\Gamma(1/2 - s + |\hat{\delta}| + im)|^2}{\Gamma(1 + 2|\hat{\delta}|)^4}. \quad (3.50)$$

At this stage the reader may be wondering about the absence of the amplification factors for the $s = 1/2$ field. The reason why these equations are not shown here is because *in the neutrino case superradiance simply does not happen* [2, 55].

Chapter 4

Linear Perturbation Methods

Now we are equipped with the most relevant equations of linear perturbation theory in BH, the Teukolsky equations. The next most natural step is to investigate methods that allow us to extract physical information from them, as well as the wave solution itself. This chapter is devoted to a review of methods that allow us to perform such analysis.

4.1 Three-term Recurrence Relations and Continued Fractions

In this chapter we will be using a result that is extremely useful when trying to find solutions to ODE's as series expansions. When dealing with series, one may encounter a recurrence relation that connects the series coefficients (f_n's). If such relation is homogeneous and have three terms it can be written like:

$$\alpha_n f_{n+1} + \beta_n f_n + \gamma_n f_{n-1} = 0, \tag{4.1}$$

where α_n, β_n and γ_n are the recurrence relation coefficients. We shall denote recurrence relations like (4.1) as single-ended if $n \in \mathbb{N}$ and as double-ended if $n \in \mathbb{Z}$.

It is known in the literature that the theory of three-term recurrence relations is linked to the theory of continued fractions. For instance, with the recurrence coefficients of (4.1) it is possible to contruct the a CF such as:

$$\frac{-\gamma_0}{\beta_0-}\frac{\alpha_0\gamma_1}{\beta_1-}\frac{\alpha_1\gamma_2}{\beta_2-}... \tag{4.2}$$

In his work [59], Gautschi made use of the concept of *minimal* and *dominant* solutions of (4.1). It can be seen that a three-term recurrence relation, such as (4.1), possesses two linearly independent solutions, say, $\hat{f}_n^{(1)}$ and $\hat{f}_n^{(2)}$. Gautschi studied the special case where these two solutions satisfy:

$$\lim_{n\to\infty}\frac{\hat{f}_n^{(1)}}{\hat{f}_n^{(2)}}=0. \tag{4.3}$$

Because of this behavior, $\hat{f}_n^{(1)}$ ($\hat{f}_n^{(2)}$) is called the *minimal* (*dominant*) solution of (4.1) as $n\to\infty$. The minimal solution is unique up to an overall factor.

Studying the behavior of minimal and dominant solutions, Gautschi provided the proof that the CF (4.2) is convergent if and only if the recurrence relation satisfied by f_n's possesses a minimal solution, with $f_0\neq 0$. In this case it is possible to prove that

$$\frac{f_n}{f_{n-1}}=\frac{-\gamma_n}{\beta_n-}\frac{\alpha_n\gamma_{n+1}}{\beta_{n+1}-}\frac{\alpha_{n+1}\gamma_{n+2}}{\beta_{n+2}-}... \tag{4.4}$$

When dealing with double-ended three-term recurrence relation, there will be two infinite continued fractions analogous to (4.2). The first one with the index embracing all positive integers, and the second with the index running over all negative integers. The main difference is that now we might also have a solution which is minimal as $n\to-\infty$. The convergence result is applicable in both limits. If there exist a minimal solution as $n\to\infty$ ($n\to-\infty$), the infinite CF, analogous to (4.2), holding positive (negative) index will be convergent. It is important to notice that the minimal solution as $n\to\infty$ and the minimal solution as $n\to-\infty$ will not necessarily be the same. Such imposition can be made at some stage, but it is important to keep in mind that this is not a general rule.

With this result in mind, when dealing with recurrence relations in the next sections, we will always require the solutions to be minimal, for $n \to \infty$ and (in double-ended cases) for $n \to -\infty$.

4.2 Leaver's Method

4.2.1 Continued Fractions for Eigenvalues and QNM's

Eigenvalue

An important method in BH perturbation theory relies on solving homogeneous three-term recurrence relations by means of continued fraction (CF) techniques. As far as we know, the first time this method was used in the context of black hole physics was in [60], where it was used to calculate the angular eigenvalues. It was only in 1985 that Leaver [61] showed that this method could also be applied to the QNM problem. Here we give a brief review of this method.

The first step to calculate the angular eigenvalues consists in writing the solutions to equation (3.10) as a power series. In order to construct a solution which is regular at $u = \cos(\theta) = \pm 1$, one needs to notice that its behaviors at these points are

$$ {}_sS_{lmc}(u) \sim \begin{cases} (1+u)^{|m-s|/2}, & \text{for} \quad u \to -1, \\ (1-u)^{|m+s|/2}, & \text{for} \quad u \to +1. \end{cases} \tag{4.5} $$

Because of (4.5) we can write an appropriate ansatz to the solutions of (3.10) as

$$ {}_sS_{lmc}(u) = e^{cu}(1+u)^{|m-s|/2}(1-u)^{|m+s|/2} \sum_{n=0}^{\infty} a_n^{\theta}(1+u)^n, \tag{4.6} $$

where a_n^{θ} are the series coefficients for the solution of the angular Teukolsky equation.

Inserting (4.6) in (3.10) one can find a recurrence relation that connects a_n^{θ} for different n's. Defining the recurrence coefficients

$$
\begin{aligned}
\alpha_n^\theta \equiv & -2(n+1)(n+|m-s|+1), \\
\beta_n^\theta \equiv & n(n-1)+2n(|m-s|/2+|m+s|/2+1-2c)-2c(|m-s|+s+1) \\
& +(|m-s|/2+|m+s|/2)(|m-s|/2+|m+s|/2+1) \\
& -c^2-s(s+1)-{}_sA_{lm}, \\
\gamma_n^\theta \equiv & 2c(n+|m-s|/2+|m+s|/2+s),
\end{aligned} \tag{4.7}
$$

the relation is single-ended and reads

$$
\begin{cases}
\alpha_0^\theta a_1^\theta + \beta_0^\theta a_0^\theta = 0, \\
\alpha_n^\theta a_{n+1}^\theta + \beta_n^\theta a_n^\theta + \gamma_n^\theta a_{n-1}^\theta = 0, \quad \text{for} \quad n \in \mathbb{N}.
\end{cases} \tag{4.8}
$$

If there exists a minimal solution to (4.8) it is possible to invert this relation and find that

$$
\beta_0^\theta - \frac{\alpha_0^\theta\gamma_1^\theta}{\beta_1^\theta -}\frac{\alpha_1^\theta\gamma_2^\theta}{\beta_2^\theta -}\frac{\alpha_2^\theta\gamma_3^\theta}{\beta_3^\theta -}\ldots = 0, \tag{4.9}
$$

which is an infinite CF. The correct eigenvalue will be given by the root of equation (4.9). This choice of ${}_sA_{lmc}$ ensures that the coefficients of (4.6) correspond to the minimal solution of (4.8) [59, 61]. In [60] it is found an equivalent equation to (4.8), but with different coefficients α_n^θ, β_n^θ and γ_n^θ. This is due to the fact that the expansion was not written as in (4.6) but as an expansion in terms of Jacobi polynomials.

QNM's

When looking for QNM's one might check that the correct asymptotic behavior of the solutions of (3.11) that satisfy the QNM's boundary conditions are:

$$
{}_sR_{lm\omega}(r) \sim \begin{cases} \left(\dfrac{r-r_+}{2M}\right)^{-s-i\sigma_+}, & \text{for} \quad r \to r_+, \quad \text{purely ingoing,} \\ \left(\dfrac{r}{2M}\right)^{-1-2s+i2M\omega} e^{i\omega r}, & \text{for} \quad r \to \infty, \quad \text{purely outgoing.} \end{cases} \tag{4.10}
$$

This justifies the use of

$$
{}_sR_{lm\omega}(r) = e^{i\omega r}\left(\frac{r-r_-}{2M}\right)^{-1-s+i(2M\omega+\sigma_+)}\left(\frac{r-r_+}{2M}\right)^{-s-i\sigma_+}\sum_{n=0}^{\infty} a_n^r \left(\frac{r-r_+}{r-r_-}\right)^n, \tag{4.11}
$$

as an ansatz for the solution of (3.11) that satisfies the QNM boundary conditions. It was defined $\sigma_+ \equiv (\omega r_+ - am/(2M))\,/\sqrt{1-a^2/M^2}$.

When substituting (4.11) into (3.11) it is straightfoward to prove that a single-ended relation similar to (4.8) holds for the radial coefficients, provided the change of index $(\theta \to r)$ and

$$
\begin{aligned}
\alpha_n^r =& (n+1)\,(n+b_0)\,, \\
\beta_n^r =& 2n(1-n) + nb_1 + b_2, \\
\gamma_n^r =& n(n-3) + 2 + b_3(n-1) + b_4,
\end{aligned} \tag{4.12}
$$

where we have defined

$$
\begin{aligned}
b_0 \equiv & +1-s-2M\omega i-2ib, \\
b_1 \equiv & -4+4M\omega i\left(2+\sqrt{1-a^2/M^2}\right)+4ib, \\
b_2 \equiv & (2M\omega)^2\left(4+2\ \sqrt{1-a^2/M^2}-\frac{a^2}{4M^2}\right)-2am\omega \\
& -s-1+(2+\sqrt{1-a^2/M^2})i(2M\omega)-{}_sA_{lm}+(8M\omega+2i)b, \\
b_3 \equiv & s+3-6Mi\omega-2ib, \\
b_4 \equiv & s+1-8(M\omega)^2-(2s+3)i(2M\omega)-(8M\omega+2i)b, \\
b \equiv & \frac{1}{\sqrt{1-a^2/M^2}}\left(M\omega-\frac{am}{2M}\right).
\end{aligned}
\tag{4.13}
$$

Similarly to the case of the angular eigenvalue, the problem of finding QNM frequencies is now a matter of finding the roots of the CF analogous to (4.9), but with the radial recurrence coefficients. This is also a sufficient condition to ensure the solution of the radial recurrence relation (analogous to (4.8)) to be minimal.

As already mentioned, the structure of the radial Teukolsky equation changes from $a < M$ to $a = M$. For this reason the previous equation to find QNM's are valid only for $a < M$. Motivated by a search of QNM's in extremely rotating and extremely charged BH, Richartz adapted this method in [11]. By using an expansion around $r = 2M$ as an ansatz for a solution of (3.11), Richartz found that the extremal a_n^r's satisfy a recurrence relation similar to the one presented above. His recurrence coefficients are related to the sub-extremal ones as given by equations (A23) and (A25) in [11].

Although this seems to address the problem of the extremal Kerr QNM's, Richartz's method might not be well-suited for all regions of the complex-ω plane, such as near the point $\omega = \omega_{SR}$. The region near this point of the complex-frequency plane is of high importance in the extreme Kerr case. The reason is that it has been shown that when $a \to M$, an infinite set of QNM's "pile up" near this point [17]. In [18, 19] it was shown

that for $m > 0$ modes, all QNM's seem to accumulate to that point if $m/(l+1/2) \gtrsim 0.74$, while for modes with $m/(l+1/2) \lesssim 0.74$ there seems to be a few modes that do not follow this pattern. The point $\omega = \omega_{SR}$ is also a branch point in the extremal case [45], hence the question of what happens to the modes that accumulate at ω_{SR} in the exact extreme case is still an open and interesting issue. This seems to be an indication that QNM's get arbitrarily close and form a BC as extremality is approached.

4.2.2 Derivative of the Eigenvalue

The eigenvalue of equation (3.10) can be calculated as discussed in the previous section, but one might ask if it is possible to find an analytical expression for its derivative throughout the complex-c plane. At a first glance, this might be a purely technical question, but there is some value to it.

A quantity of great interest in BH perturbation theory is the excitation factor of each mode [37, 62, 63]. These factors are source-independent quantities that are needed when one wishes to compute the excitation amplitudes of a given QNM.

By definition, the excitation factors are given by

$$ {}_sB^T_{lmn} \equiv \frac{1}{2\omega} \frac{{}_sB^{ref}_{lm\omega}}{{}_sB^{trans}_{lm\omega}} \left(\frac{d}{d\omega} \left(\frac{{}_sB^{inc}_{lm\omega}}{{}_sB^{trans}_{lm\omega}} \right) \right)^{-1} \Bigg|_{\omega=\omega_{lmn}} . \tag{4.14} $$

As one might suspect, the amplitudes ${}_sB^{inc/trans/ref}_{lm\omega}$ depend on ${}_sA_{lmc}$. Therefore, from the chain rule, an analytical expression for the derivative of this eigenvalue might be useful, not only for investigating analytical properties of ${}_sB^T_{lmn}$, but also as a practical way of calculating this quantity. This is only one of the possible applications of the eigenvalue derivative, and it was stated for illustrative reasons. As a matter of fact, the eigenvalue derivative deserves attention on its own right, independently from the excitation factors. One can use this result to study the analytical properties of ${}_sA_{lmc}$ itself.

To obtain the derivative of ${}_sA_{lmc}$ one might start by assuming that the CF (4.9) can be truncated at some finite order N in order to use as a "good enough" numerical approximation to the eigenvalue. As commonly done in numerical recipes, one only needs to demand N to be large enough in order for the CF to converge to some required precision. This may seem like a crude approximation, but we have numerically shown that this is not the case, as one can see in the results section.

In [64] it is given an analytical expression to the derivative of a finite CF (see its equation (6)). Assuming that our approximation to the infinite CF is good enough and making use of [64] we can take its derivative with respect to c $(= a\omega)$. Following the notation in [64], we can see that for the eigenvalue case this will yield a linear equation for its derivative. This linear equation can be inverted to find

$$\frac{d_s A_{lmc}}{dc} \approx \frac{-\frac{d\zeta_0^\theta}{dc} + \sum_{j=0}^{N}\left(\prod_{k=0}^{j}\frac{1}{\alpha_k^\theta\gamma_{k+1}^\theta}\right)\left(\frac{1}{t_j}\frac{d(\alpha_j^\theta\gamma_j^\theta)}{dc} + \frac{d\zeta_j^\theta}{dc}\right)}{1+\sum_{j=0}^{N}\prod_{k=0}^{j}\left(\frac{t_k^2}{\alpha_k^\theta\gamma_{k+1}^\theta}\right)},^{1} \tag{4.15}$$

where t_{N-k} is the k-th tail of the truncated finite CF (4.9) for the eigenvalue and $\zeta_n^\theta \equiv \beta_n^\theta + {}_sA_{lmc}$ [2]. The definition of the k-th tail of the finite CF is

$$t_{N-k} = \frac{\alpha_{N-k}^\theta\gamma_{N-k-1}^\theta}{\beta_{N-k-1}^\theta -}\frac{\alpha_{N-k-1}^\theta\gamma_{N-k-2}^\theta}{\beta_{N-k-2}^\theta -}\ldots\frac{\alpha_{N-2}^\theta\gamma_{N-1}^\theta}{\beta_{N-1}^\theta -}\frac{\alpha_{N-1}^\theta\gamma_N^\theta}{\beta_N^\theta}.$$

To the best of our knowledge this is the first time that an analytical method was developed to compute the eigenvalue derivative directly. We have numerical evidence that supports the validity of this method, see section 5.1.

[1] This expressions is said to be an approximation in the sense that we achieved the derivative of the finite CF, which was used as an approximation of the actual CF that defines the angular eigenvalue. Thus that is what we mean when talking about an approximation for the derivative.

[2] Inspecting the expression for β_n^θ (4.7) it can be seen that ζ_n^θ has no term that depends on ${}_sA_{lmc}$. Then the derivative of ζ_n^θ will not contain the eigenvalue.

4.3 The MST method

4.3.1 Sub-extremal Case

In 1996, Mano, Suzuki and Takasugi [65] developed an analytic method in BH perturbation theory, which is now widely known as the MST method. When developing this method, they assumed $\Re(\omega) > 0$. Because of the the complex conjugation of (3.11) under the transformation $(m, \omega) \to (-m, -\omega^*)$ [39] one can use the following equation to obtain results for $\Re(\omega) < 0$. This method is based on a series expansion of the solutions to (3.11) in terms of hypergeometric functions (4.16) and confluent hypergeometric functions (4.17). These expansions are

$$
\begin{aligned}
{}_sR^{in}_{lm\omega} &= e^{i\epsilon\kappa y}(-y)^{-s-i(\epsilon+\tau)/2}(1-y)^{i(\epsilon-\tau)/2}\sum_{n=-\infty}^{\infty} a_n p_{n+\nu}(y), \qquad (4.16)\\
p_{n+\nu}(y) &= {}_2F_1(n+\nu+1-i\tau, -n-\nu-i\tau; 1-s-i\epsilon-i\tau; y),
\end{aligned}
$$

and

$$
\begin{aligned}
{}_sR^{up}_{lm\omega} &= 2^\nu e^{-\pi\epsilon} e^{-i\pi(\nu+1+s)} e^{i\hat{z}}\hat{z}^{\nu+i\epsilon_+}(\hat{z}-\epsilon\kappa)^{-s-i\epsilon_+}\\
&\times \sum_{n=-\infty}^{\infty} i^n \frac{(\nu+1+s-i\epsilon)_n}{(\nu+1-s+i\epsilon)_n} a_n (2\hat{z})^n U(n+\nu+1+s-i\epsilon, 2n+2\nu+2; -2i\hat{z}). \qquad (4.17)
\end{aligned}
$$

In these last expressions we have defined $\epsilon \equiv 2M\omega$, $q \equiv a/M$, $\kappa \equiv \sqrt{1-q^2}$, $\tau \equiv (\epsilon - mq)/\kappa$, $y \equiv \omega(r_+ - r)/(\epsilon\kappa)$, $\hat{z} \equiv \epsilon\kappa(1-y)$ and $\epsilon_+ \equiv (\epsilon+\tau)/2$. The notation $(y)_n = \Gamma(y+n)/\Gamma(y)$ stands for the Pochhammer symbol. Here, ν appears as a generalization of l. This new parameter will be crucial for imposing the convergence of (4.16) and (4.17), as will be clearer later on. To ν is given the name of renormalized angular momentum. This parameter is a function of (l, m, ω).

Inserting equation (4.16) into (3.11) it is possible to find another double-ended three-term recurrence relation. This time for a_n, that holds as

$$
\alpha_n^\nu a_{n+1} + \beta_n^\nu a_n + \gamma_n^\nu a_{n-1} = 0, \quad \text{for} \quad n \in \mathbb{Z} \qquad (4.18)
$$

with the following recurrence coefficients

$$\alpha_n^\nu = \frac{i\epsilon\kappa(n+\nu+1+s+i\epsilon)(n+\nu+1+s-i\epsilon)(n+\nu+1+i\tau)}{(n+\nu+1)(2n+2\nu+3)},$$
$$\beta_n^\nu = -{}_s\lambda_{lmc} - s(s+1) + (n+\nu)(n+\nu+1) + \epsilon^2 + \epsilon(\epsilon - mq) + \frac{\epsilon(\epsilon-mq)(s^2+\epsilon^2)}{(n+\nu)(n+\nu+1)},$$
$$\gamma_n^\nu = -\frac{i\epsilon\kappa(n+\nu-s+i\epsilon)(n+\nu-s-i\epsilon)(n+\nu-i\tau)}{(n+\nu)(2n+2\nu-1)}. \tag{4.19}$$

Notice that, by doing the same procedure with equation (4.17) one can check that its series coefficients a_n satisfy the same relation. This justify the use of the same notation for the expansion coefficients of the two different solutions.

This time we are dealing with double-ended three-term recurrence relation. In this case, we have already explained that now we may have two minimal solutions, one for $n \to -\infty$ (a_n^-), and a second one for $n \to \infty$ (a_n^+). As stated previously in this chapter, three-term recurrence relations are connected with CF. This time we encounter two infinite continued fractions, one for positive n, and another one for negative n. According to the theory of CF's we have seen that it is possible to write

$$R_n^\nu = \frac{a_n}{a_{n-1}} = \frac{-\gamma_n^\nu}{\beta_n^\nu + \alpha_n^\nu R_{n+1}^\nu}, \tag{4.20}$$
$$L_n^\nu = \frac{a_n}{a_{n+1}} = \frac{-\alpha_n^\nu}{\beta_n^\nu + \gamma_n^\nu L_{n-1}^\nu}, \tag{4.21}$$

where the CF representation of R_n (L_n) is only valid if it is convergent for $n \to \infty$ ($n \to -\infty$),i.e. if the solutions for (4.18) are minimal for $n \to \infty$ ($n \to -\infty$). This means that we need to search for a solution that is minimal in both cases.

In theorem 2.3 of [59], it is given a way to analyze the asymptotic behavior of the two solutions of three-term recurrence relations. In our study case, this theorem was used to show that [66]

$$\begin{cases} \left|\dfrac{a_n^+}{a_{n-1}^+}\right| \sim \left|\dfrac{i\epsilon\kappa}{2n}\right| & \text{as} \quad n \to \infty, \\ \left|\dfrac{a_n^-}{a_{n+1}^-}\right| \sim \left|\dfrac{i\epsilon\kappa}{2n}\right| & \text{as} \quad n \to -\infty. \end{cases} \tag{4.22}$$

Here the importance of ν is made clear. The renormalized angular momentum was introduced in order to impose the convergence of the CF representation for both R_n (for $n \to \infty$) and L_n (for $n \to -\infty$). To do so, ν has to be calculated in such a way that guarantees that the relation

$$R_n^\nu L_{n-1}^\nu = 1, \tag{4.23}$$

is valid for an arbitrary integer n. Equation (4.23) is equivalent to

$$g_n(\nu) = \beta_n^\nu + \alpha_n^\nu R_{n+1}^\nu + \gamma_n^\nu L_{n-1}^\nu = 0. \tag{4.24}$$

If conditions (4.23) and (4.24) are met for a single value of $n \in \mathbb{Z}$, it is automatically satisfied $\forall\, n \in \mathbb{Z}$.

Having convergent expressions for R_n and L_n and choosing a particular normalization where $a_0 = 1$, we can compute $a_n\ \forall\ n \in \mathbb{Z}$. To many purposes, it is useful to provide a small ϵ-expansion for ν, this expansion reads

$$\nu = l + \nu_2\epsilon^2 + O(\epsilon^3), \tag{4.25}$$

where

$$\nu_2 \equiv \frac{1}{2l+1}\left(-2 - \frac{s^2}{l(l+1)} + \frac{\left((l+1)^2 - s^2\right)^2}{(2l+1)(2l+2)(2l+3)} - \frac{\left(l^2 - s^2\right)^2}{(2l-1)2l(2l+1)}\right). \tag{4.26}$$

A higher order expansion for ν can be found in [39].

The imposition that makes a_n to be minimal both to $n \to -\infty$ and $n \to \infty$ at the same time, together with the asymptotic (as $|n| \to \infty$) properties of the (confluent) hypergeometric functions guarantees the convergence of (4.16) for $|y| < \infty$ ($r < \infty$) and (4.17) for $r > r_+$ [65, 66].

As explained before, the radial Teukolsky equation is complex-conjugated under $(m,\omega) \to (-m,-\omega^*)$. Because of this property we henceforth assume $\Re(\omega) > 0$, if one wishes to compute MST quantities for $\Re(\omega) < 0$ one can obtain them by using this symmetry.

Noticing that solution (4.16) converges for $r_+ \leq r < \infty$ and (4.17) converges for $r_+ < r \leq \infty$, one can construct a solution that is convergent everywhere. In order to do so, a matching procedure is performed. During this matching procedure the following useful quantities arise :

$$A^{\nu}_{+} \equiv e^{-\frac{\pi}{2}\epsilon} e^{\frac{\pi}{2} i(\nu+1-s)} 2^{-1+s-i\epsilon} \frac{\Gamma(\nu+1-s+i\epsilon)}{\Gamma(\nu+1+s-i\epsilon)} \sum_{n=-\infty}^{+\infty} a_n, \tag{4.27}$$

$$A^{\nu}_{-} \equiv 2^{-1-s+i\epsilon} e^{-\frac{\pi}{2} i(\nu+1+s)} e^{-\frac{\pi}{2}\epsilon} \sum_{n=-\infty}^{+\infty} (-1)^n \frac{(\nu+1+s-i\epsilon)_n}{(\nu+1-s+i\epsilon)_n} a_n,$$

and

$$\begin{aligned} K_\nu \equiv & \frac{e^{i\epsilon\kappa}(2\epsilon\kappa)^{s-\nu-\eta} 2^{-s} i^{\eta} \Gamma(1-s-2i\epsilon_+)\Gamma(\eta+2\nu+2)}{\Gamma(\eta+\nu+1-s+i\epsilon)\Gamma(\eta+\nu+1+i\tau)\Gamma(\eta+\nu+1+s+i\epsilon)} \\ & \times \left(\sum_{n=\eta}^{\infty} (-1)^n \frac{\Gamma(n+\eta+2\nu+1)}{(n-\eta)!} \frac{\Gamma(n+\nu+1+s+i\epsilon)}{\Gamma(n+\nu+1-s-i\epsilon)} \frac{\Gamma(n+\nu+1+i\tau)}{\Gamma(n+\nu+1-i\tau)} a_n \right) \\ & \times \left(\sum_{n=-\infty}^{\eta} \frac{(-1)^n}{(\eta-n)!(\eta+2\nu+2)_n} \frac{(\nu+1+s-i\epsilon)_n}{(\nu+1-s+i\epsilon)_n} a_n \right)^{-1}, \end{aligned} \tag{4.28}$$

where η is an arbitrary integer. Here, K_ν is independent of the value of η.

Via this matching procedure, it is now possible to calculate the asymptotic amplitudes defined in (3.14). Obtaining:

$$B^{trans}_{lm\omega} = \left(\frac{\epsilon\kappa}{\omega}\right)^{2s} e^{i\kappa\epsilon_+(1+2\log\kappa/(1+\kappa))} \sum_{n=-\infty}^{\infty} a_n, \tag{4.29}$$

$$B^{inc}_{lm\omega} = \omega^{-1} \left(K_\nu - ie^{-i\pi\nu} \frac{\sin(\pi(\nu-s+i\epsilon))}{(\sin\pi(\nu+s-i\epsilon))} K_{-\nu-1} \right) A^{\nu}_{+} e^{-i(\epsilon\ln\epsilon - \frac{1-\kappa}{2}\epsilon)}, \tag{4.30}$$

$$B^{ref}_{lm\omega} = \omega^{-1-2s} \left(K_\nu + ie^{i\pi\nu} K_{-\nu-1} \right) A^{\nu}_{-} e^{i(\epsilon\ln\epsilon - \frac{1-\kappa}{2}\epsilon)}. \tag{4.31}$$

Now we are able to calculate the Wronskians (3.19) and (3.22) and then calculate the QNM's by searching for its zeros.

4.3.2 Extremal Case

Based on the idea of Mano, Suzuki, and Takasugi, [32] has adapted the MST method to the extremal Kerr case. By noticing the different singularity structure of (3.11) for $a = M$, it was possible to find analogous expressions to the sub-extremal ones. All these extremal quantities will be referred to with similar notation but with an extra "x" super-index on them.

By using an expansion for ${}_sR^{in}_{lm\omega}$ and ${}_sR^{up}_{lm\omega}$ in terms of confluent hypergeometric functions, the series coefficients ${}^xa_n$ were defined. This leads to a modification in the recurrence relation coefficients (4.19). They were exchanged by

$$ {}^x\alpha_n^\nu = \frac{\epsilon_x(q_n^\nu + \chi_s)(q_n^\nu - \chi_{-s})}{q_n^\nu(2q_n^\nu + 1)}, \tag{4.32} $$

$$ {}^x\beta_n^\nu = (q_n^\nu - 1)q_n^\nu - {}_s\hat{A}_{lmc} - \epsilon_x\frac{\chi_{-s}\chi_s}{(q_n^\nu - 1)q_n^\nu}, \tag{4.33} $$

$$ {}^x\gamma_n^\nu = \frac{\epsilon_x(q_n^\nu - 1 - \chi_s)(q_n^\nu - 1 + \chi_{-s})}{(q_n^\nu - 1)(2q_n^\nu - 3)}, \tag{4.34} $$

with the definitions

$$ \begin{aligned} \epsilon_x &\equiv 4M^2\omega k = 4M^2\omega(\omega - m^x\Omega_H), \\ q_n^\nu &\equiv n + \nu + 1, \\ \chi_s &\equiv s - i2M\omega, \\ {}_s\hat{A}_{lmc} &\equiv -7(M\omega)^2 + s(s+1) + {}_sA_{lm\omega}. \end{aligned} \tag{4.35} $$

With these new recurrence relation coefficients, one can now calculate the CF's ${}^xR_n$ and ${}^xL_n$. These CF's play the same role as in the sub-extremal case. They are also used in order to write analogous conditions to calculate ν for the convergence of the

CF, see equations (4.23) and (4.24). It is worth mentioning that the extreme recurrence relations are the $a \to M$ limit of the sub-extreme ones with a sign change in the ${}^{x}\alpha_n^{\nu}$ and ${}^{x}\gamma_n^{\nu}$ coefficients with respect to their sub-extreme equivalents. It is important to notice that the sign change in these coefficients cancel out when constructing R_n^{ν} and L_n^{ν}, this cancellation assures that the $a \to M$ limit of (4.23) and (4.24) are exactly the same as their extreme equivalent constructed with the coefficients (4.32).

Similar arguments to the ones employed in the sub-extremal case allowed the authors to calculate the asymptotic amplitudes that are needed to compute the extremal Wronskian (3.22). The two coefficients needed in this work are ${}^{x}B_{lm\omega}^{inc/trans}$.

$$ {}^{x}B_{lm\omega}^{trans} = (2M)^{2s}\varsigma_{+}^{(0)}(2Mk)^{\nu+1}(-i2Mk)^{-\nu-1+s+i2M\omega}e^{-i\pi\chi_{-s}/2}e^{-i\pi(\nu+1/2)}\sum_{n=-\infty}^{\infty}\frac{\Gamma(q_n^{\nu}+\chi_s)}{\Gamma(q_n^{\nu}-\chi_s)}{}^{x}a_n \tag{4.36} $$

and

$$ \begin{aligned} {}^{x}B_{lm\omega}^{inc} =& 2M\varsigma_{+}^{(\infty)}\left({}^{x}K_{\nu}-(-i2M\omega)^{-2\nu}(i2M\omega)^{2\nu}\,e^{-2\pi i\nu}\,{}^{x}K_{-\nu-1}\right)2^{s-i2M\omega}(2M\omega)^{\nu+s}(i2M\omega)^{-\nu-i2M\omega} \\ &\times e^{-3\pi M\omega}e^{-\pi i}\frac{\sin(\pi(\nu+i2M\omega))}{\sin(2\pi\nu)}\sum_{n=-\infty}^{\infty}(-1)^n\,{}^{x}a_n. \end{aligned} \tag{4.37} $$

In the last equation ${}^{x}K_{\nu}$ is by construction

$$ \begin{aligned} {}^{x}K_{\nu} \equiv& \frac{\varsigma_{+}^{(0)}}{\varsigma_{+}^{(\infty)}}(2Mk)^{\nu+1}(-i2Mk)^{-2\nu-1}(4M\omega)^{-\nu-1}e^{i\pi s} \\ &\times\left(\sum_{n=\eta}^{\infty}\frac{\Gamma(q_n^{\nu}+\chi_s)}{\Gamma(q_n^{\nu}-\chi_s)}\frac{\Gamma(2q_n^{\nu}-1)}{\Gamma(q_n^{\nu}+\chi_{-s})}\frac{(1-q_n^{\nu}+\chi_{-s})_{n-\eta}}{(2-2q_n^{\nu})_{n-\eta}(n-\eta)!}{}^{x}a_n(-i2Mk)^{-\eta}\right)\times \\ &\times\left(\sum_{n=-\infty}^{\eta}\frac{\Gamma(q_n^{\nu}+\chi_s)}{\Gamma(q_n^{\nu}-\chi_s)}\frac{\Gamma(1-2q_n^{\nu})}{\Gamma(1-q_n^{\nu}+\chi_s)}\frac{(q_n^{\nu}+\chi_s)_{\eta-n}}{(2q_n^{\nu})_{\eta-n}(\eta-n)!}{}^{x}a_n(-4iM\omega)^{\eta}\right)^{-1}, \end{aligned} \tag{4.38} $$

where η is again an arbitrary integer. The $\varsigma_{+}^{(0)}$ and $\varsigma_{+}^{(\infty)}$ are normalization factors chosen as

$$\varsigma_+^{(0)} \equiv (2Mk)^{-\nu}(-i2Mk)^{\nu}e^{i\pi\nu}\left(\frac{\sin\left(\pi(\nu-i2M\omega)\right)}{\sin\left(\pi(\nu+i2M\omega)\right)}\right)^{1/2},$$
$$\varsigma_+^{(\infty)} \equiv (2M\omega)^{-\nu}(-i2M\omega)^{\nu}e^{i\pi\nu}\left(\frac{\sin\left(\pi(\nu-i2M\omega)\right)}{\sin\left(\pi(\nu+i2M\omega)\right)}\right)^{1/2}.$$

These are the quantities needed to the construction of the extremal Wronskian. This will allow us to perform a search for BC's and QNM's in the exactly extremal Kerr BH like in the sub-extremal case.

4.4 Monodromy Method

Another powerful technique that can be used when dealing with BH linear perturbation theory is the monodromy method. This method starts by complexifying the radial coordinate of the radial Teukolsky equation. The failure of the field to be globally holomorphic in the complex-r plane is encoded in the so-called *monodromy matrices*. In this section we will give a small review about the monodromy method and state a couple of its applications in the context of BH linear perturbation theory. In this section we summarize the discussions in [67], where further details can be found.

4.4.1 Overview

Suppose that $\Lambda(z)$ is a function of a complex variable z that satisfies a ODE of the type:

$$\partial_z\left(P(z)\partial_z\Lambda(z)\right) - Q(z)\Lambda(z) = 0. \tag{4.39}$$

This equation is equivalent to a first order ODE for a two component vector Ξ that reads

$$\partial_z\begin{pmatrix}\Xi_1\\ \Xi_2\end{pmatrix} = \begin{pmatrix}0 & P(z)^{-1}\\ Q(z) & 0\end{pmatrix}\begin{pmatrix}\Xi_1\\ \Xi_2\end{pmatrix} \equiv A(z)\Xi, \tag{4.40}$$

where $\Xi_1 = \Lambda(z)$ and $\Xi_2 = P(z)\partial_z\Lambda(z)$ are the components of Ξ. The functions $P(z)$ and $Q(z)$ are such that $A(z)$ is meromorphic.

This ODE has two linearly independent solutions $\Xi^{(1)}$ and $\Xi^{(2)}$, which are two-dimensional vectors. With these solutions, we can construct the fundamental matrix $\vartheta(z)$ as

$$\vartheta(z) \equiv \left(\Xi^{(1)} \;\; \Xi^{(2)}\right). \tag{4.41}$$

Following a closed loop γ in the complex-z plane around an arbitrary point z the fundamental matrix is found to be equal to $\vartheta_\gamma(z)$. From this construction it is possible to define the *monodromy matrix* M_γ via

$$\vartheta_\gamma(z) \equiv \vartheta(z) M_\gamma. \tag{4.42}$$

In general we will have that the value of the function is not equal at the beginning and at the end of γ, i.e. $\vartheta_\gamma(z) \neq \vartheta(z)$. If the path γ does not enclose any branch point in $\vartheta(z)$ then $M_\gamma = \mathbb{1}$. When the path encloses a branch point M_γ is non trivial and a measure of the lack of meromorphicity of $\vartheta(z)$.

4.4.2 Calculating ν

In our study case, the Kerr metric, the relevant ODE that we are interested in studying is the radial Teukolsky equation (3.11). In the sub extremal case it has been argued that the monodromy matrix for $r = \infty$ is related to the renormalized angular momentum (ν) [67]. More precisely, the monodromy matrix around $r = \infty$ has $e^{2\pi i \alpha_{irr}}$ as its eigenvalues, and this eigenvalues relate with ν as:

$$\nu = l + i\alpha_{\text{irr}}, \tag{4.43}$$

where l is the angular momentum multipole index. This is the way that we chose to compute ν throughout this work, except when explicitly said otherwise. In order to compute α_{irr} we used the code developed in [67] and publicly available at [68].

The expression (4.43) is shown to be true in the sub-extremal Kerr case, but in this dissertation we worked under the assumption that it still holds for the extremal case as well. It is also important to notice that we have calculated ν both for $a = 0.999M$ and for $a = M$ and compared the two results. After this comparison we were convinced that ν (as calculated by the monodromy technique) is smooth in the transition from sub-extremal to extremal Kerr.

4.4.3 Calculating QNM's

Although we have used the monodromy technique only in order to perform a numerical calculation of ν, this technique has been adapted to the numerical calculation of the QNM frequencies as well. To those whom may be interested in this method to calculate QNM frequencies in the Kerr space-time we direct to the papers [67, 69, 70].

Chapter 5

Results

In the previous chapter, we studied relevant methods for obtaining physical information about waves around a BH. With such methods, we were able to investigate several properties, such as the presence of possible new BC's, the amplification factor, and most importantly the QNM's. We analyzed these properties both in the sub-extremal and extremal Kerr cases. This chapter is dedicated to our findings.

5.1 Eigenvalue Derivative

When deriving equation (4.15) for the eigenvalue derivative, we assumed that truncating the infinite CF (4.9) at a high enough finite order N provided a good approximation to the original CF. In order to check this assumption, we wrote a code in Mathematica [58] and carried out numerical tests.

As it can easily be seen, equation (4.15) for the derivative of ${}_sA_{lmc}$ depends implicitly on the eigenvalue itself. Therefore, when writing the derivative code, one needs to calculate eigenvalues as well. We calculated the eigenvalues by means of the publicly available Mathematica package [29].

In order to implement an algorithm for the derivative code we included a loop that increases N by steps of 100. In each loop, equation (4.15) is computed and the result

is compared with the one obtained for the previous value of N. The loop stops at a given N, determined when the relative error, both in the imaginary and real parts of $d_s A_{lmc}/dc$, is smaller than a required precision. In this work we required an agreement of 16 digits when comparing the results from two consecutive iterations. However, all the quantities inside the code were always being calculated with 128 digits. We chose to keep the number of digits higher than the precision required in our derivative code because we did not know how fast the convergence of (4.15) would be. By taking steps in N of 100, we may be including more terms than the necessary to achieve 16 digits of precision, therefore achieving a higher precision, this will be shown to be true when computing relative differences.

In order to compare the efficiency and the applicability of this code we performed a couple of tests. As a first test, we compared an analytical fourth order small-c expansion for the eigenvalue [28] against our numerical results. The results for some modes are shown in figure 5.1.

As a second test, we compared the results obtained using the Mathematica derivative operator (Mdo) upon the eigenvalue function of the package [29] against the ones obtained by our new method. The comparison was accomplished via the computation of the relative difference between the two methods, which permitted us to test our code where the small-c expansion fails. For the modes where this test was applied we notice that our code works at least 5 times faster than by computing the derivative using the Mdo method. By the time we perform these tests, we notice that the Mdo direct application on the package eigenvalue function was not able to obtain a result for some complex frequencies. Although our CF derivative code could access these frequencies, we could not compare the results with an alternative method. That is why we show results only for real values of c.

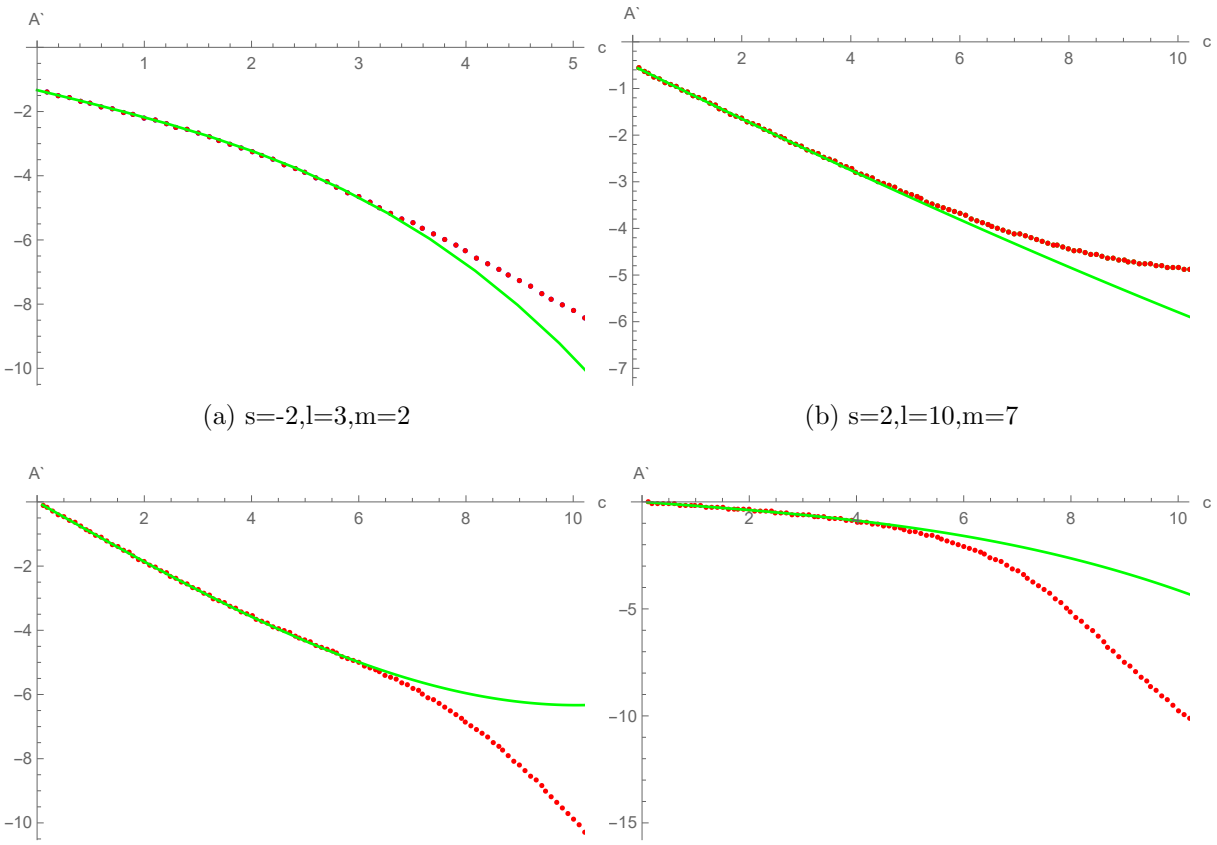

(a) s=-2,l=3,m=2

(b) s=2,l=10,m=7

(c) s=1,l=5,m=0

(d) s=0,l=4,m=-4

Figure 5.1: These plots show the comparison between the c-derivative of the angular eigenvalue obtained from two methods. Green solid curves represent the results obtained from the small-c expansion. Red dotted curves represent the results obtained from our CF derivative code. Their agreement is very good up to $c \sim 4$ for every mode tested. The results shown here are for several different modes and spins.

Figure 5.2 shows that our concern about the convergence of (4.15) with respect to a increase in N was in fact correct. It is worth noticing that even requiring a precision of 16 digits, our code obtained a much higher agreement when compared with the results obtained via the Mdo method, as can be seen in figures 5.2. This means that the series in (4.15) must converge faster than we originally expected and the code could in principle be made to be even faster. A possible way to speed up our code is by taking smaller steps in N.

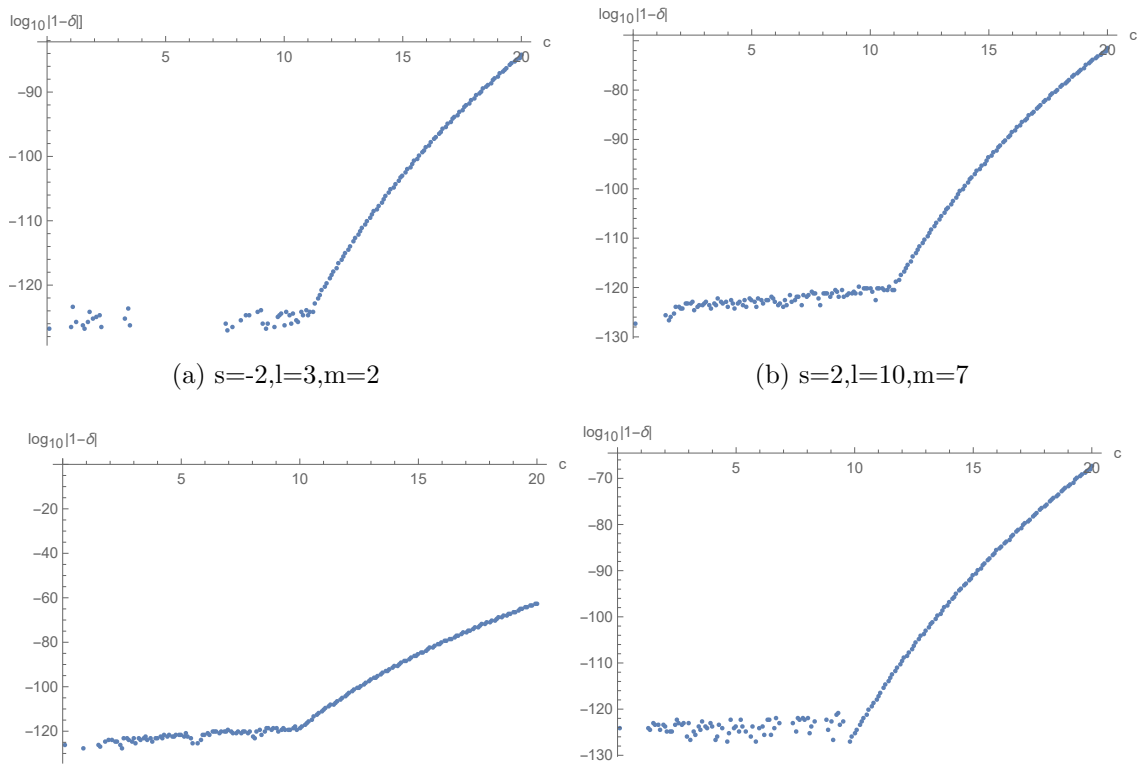

(a) s=-2,l=3,m=2 (b) s=2,l=10,m=7

(c) s=1,l=5,m=0 (d) s=0,l=4,m=-4

Figure 5.2: These plots show the results for the relative difference between the derivatives found by means of (4.15) and by the Mdo method. Here, δ is defined as the ratio between the values obtained in each method. Notice that the results show that the achieved precision is higher than the 16 digits that we required. For one of the modes some of the points seem to be missing. This is due to the fact that the agreement in those points was exact, leading to a zero relative difference, and the logarithm of this value is minus infinity, so the points are not in the range of the plot.

5.2 Sub-extremal Kerr

In this section we are going to present our results on sub-extremal Kerr case. This section is organized in two sub-sections. The first one is dedicated to tests that we performed in order to check for the convergence of our code and its ability to reproduce well-known results, such as the superradiance amplification factor. The second sub-section is dedicated to our results on the search for possible unknown BC's in the complex-ω plane and on the search for QNM frequencies. The code developed and used in this section uses expressions from the sub-extremal MST method available in section 4.3.1.

5.2.1 Tests

Convergence Tests

The first test that we performed was in order to check the convergence of our code. The MST expressions presented in section 4.3.1 depend on several different sums, such as the ones appearing in equations (4.27)-(4.29). The sums that we are concerned with here are the ones appearing in (4.28). The reason for ignoring the sums in (4.27) and (4.29) is that they cancel out when calculating the Wronskian via (3.19).

Because a_n is chosen to be a minimal solution of the MST recurrence relation, the solutions (4.16) and (4.17) of the radial Teukolsky equation are convergent. Since the asymptotic amplitudes of these solutions depend linearly on K_ν (see (4.30) and (4.31)), one may also expect K_ν to be convergent. The question that we address here is whether our code is implemented in such a way that convergence is achieved. Our code has an internal loop for calculating the sums in K_ν. This loop only stops when the relative error in imaginary and real part of K_ν for two consecutive steps of the loop is smaller than a certain required precision. We need to check that this condition is not met before convergence has taken place.

The answer to this question can be found by performing a calculation of K_ν, and saving the value of each partial sum ($K_\nu^{(n)}$) in a table. Then we plot the values of $K_\nu^{(n)}$ against n (the index of the sums in (4.28)) in figure 5.3. When analyzing these plots we can see whether convergence is numerically achieved or not by looking at the asymptotic behavior of $K_\nu^{(n)}$ for large n. We performed the designed test for the summation in the real and in the imaginary part of $K_\nu^{(n)}$ for several frequencies. Figure 5.3 corroborate the fact that our code is indeed reaching convergence when calculating K_ν. For these plots the required precision was of 20 digits. We chose these particular complex-values frequencies because they are the values of the QNM frequencies, which are already known

from previous works [61, 71]. The results shown in figures 5.3 are for only one mode ($s = 2, l = 2, a = 0$) but we executed the same test for different modes and different values of a and the results were conceptually the same. We choose to display here only the case for $a = 0$ for brevity.

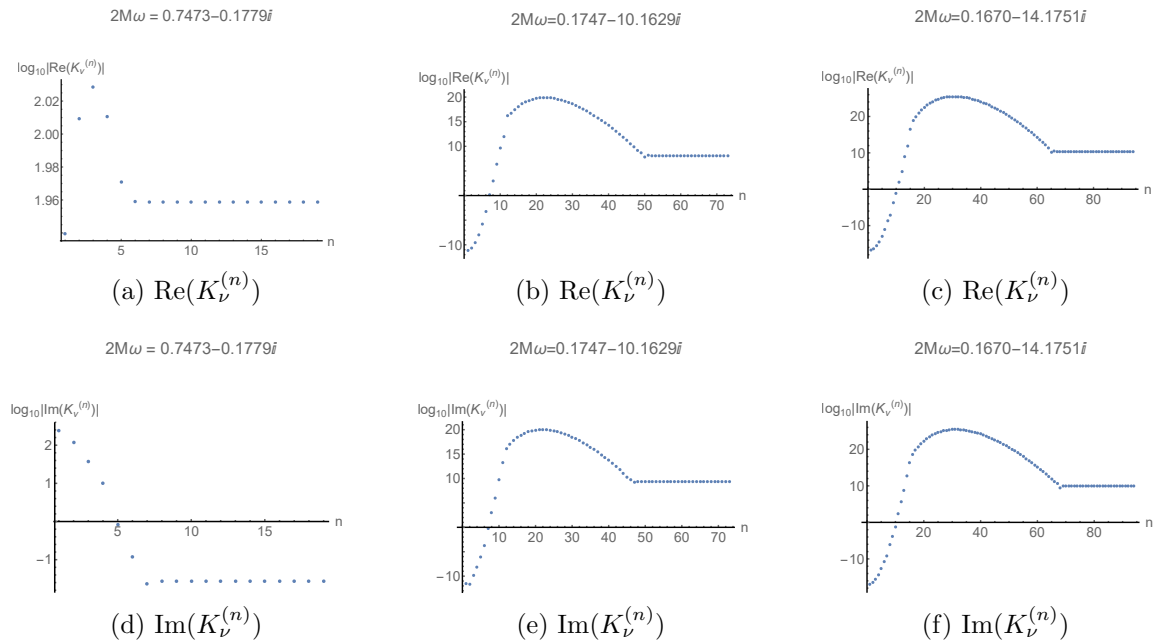

(a) $\mathrm{Re}(K_\nu^{(n)})$ (b) $\mathrm{Re}(K_\nu^{(n)})$ (c) $\mathrm{Re}(K_\nu^{(n)})$

(d) $\mathrm{Im}(K_\nu^{(n)})$ (e) $\mathrm{Im}(K_\nu^{(n)})$ (f) $\mathrm{Im}(K_\nu^{(n)})$

Figure 5.3: We show the results for the convergence test in the series in the definition of K_ν. Each plot shows the partial sum $K_\nu^{(n)}$ as functions of n for various frequencies. As one can see on the tables in Appendix B, these values of the frequencies are QNM frequencies. These plots indicate that we have achieved convergence correctly. The results shown here are for the mode $s = 2, l = 2, a = 0$.

When calculating K_ν, we were also saving the value of each summand in a table. Then we plot the values of this table against n in figure 5.4. As we can see in our results the values of the summands can start increasing in the first few steps. The results found in figures 5.4 were obtained by also requiring 20 digits of precision both in the imaginary and real parts of each sum.

As we can see from figure 5.4, we calculated the sums at least to the required precision. The same figure show that for the same frequency all sums have the same number of

terms, the final value of n. However, the sums in the denominator seem to achieve a larger precision than the required one. The reason for this is that in our code the final precision was required in the final fraction in (4.28), not in the denominator and numerator separately. As one can clearly see, the convergence of the denominator is reached faster and we can use this fact to speed up our code in future works.

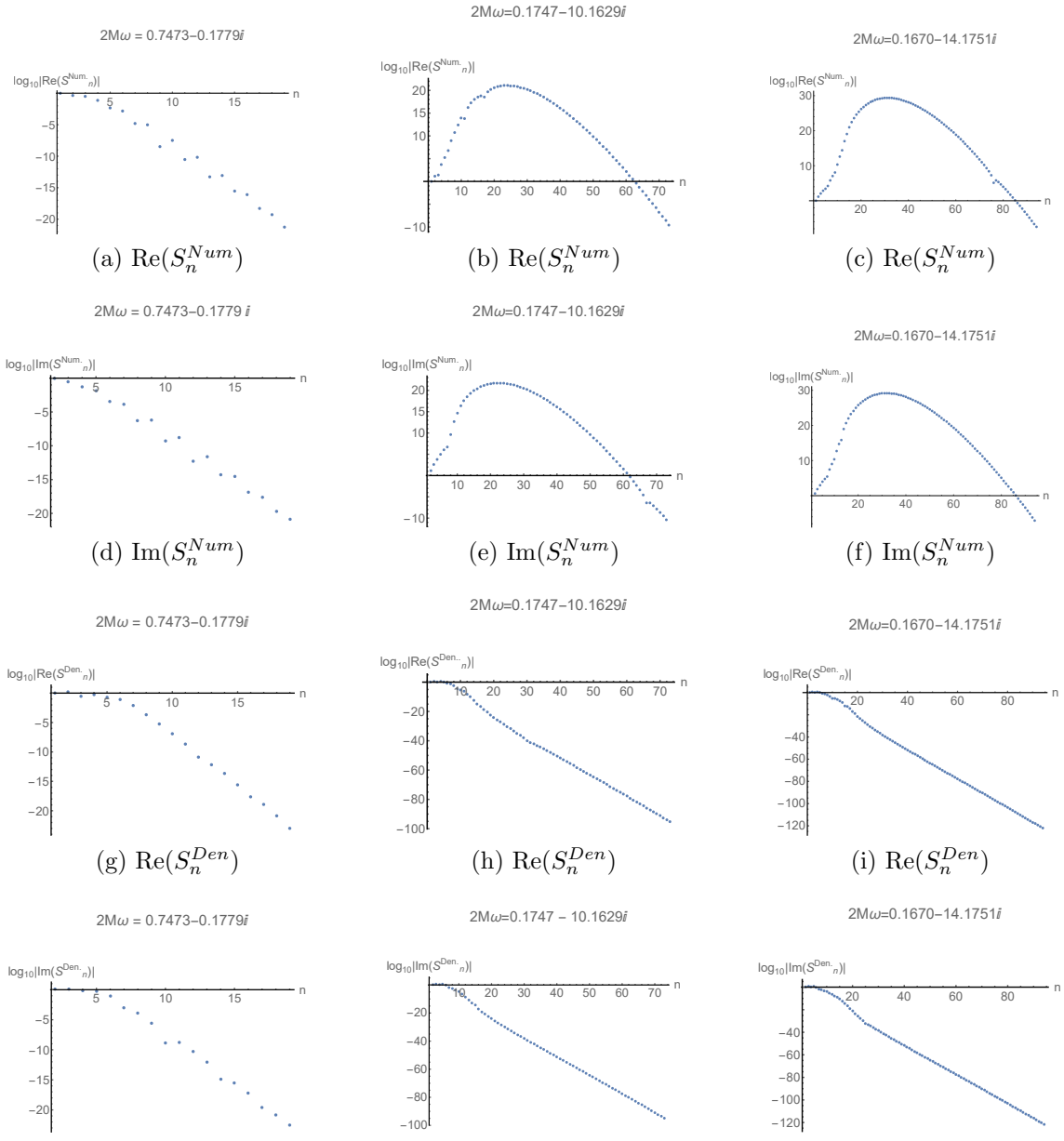

(a) $\mathrm{Re}(S_n^{Num})$ (b) $\mathrm{Re}(S_n^{Num})$ (c) $\mathrm{Re}(S_n^{Num})$

(d) $\mathrm{Im}(S_n^{Num})$ (e) $\mathrm{Im}(S_n^{Num})$ (f) $\mathrm{Im}(S_n^{Num})$

(g) $\mathrm{Re}(S_n^{Den})$ (h) $\mathrm{Re}(S_n^{Den})$ (i) $\mathrm{Re}(S_n^{Den})$

(j) $\mathrm{Im}(S_n^{Den})$ (k) $\mathrm{Im}(S_n^{Den})$ (l) $\mathrm{Im}(S_n^{Den})$

Figure 5.4: Each plot shows the summands in the sums in the denominator (S_n^{Den}) and in the numerator (S_n^{Num}) as functions of n. As one can see on the tables in Appendix B, these values of the frequencies are QNM frequencies. These plots indicate that we have achieved convergence correctly. The results shown here are for the mode $s = 2, l = 2, a = 0$.

Superradiance Test

In this section we will be showing the results found when calculating $Z_{slm\omega}$ via equations (3.19), (3.45), (4.29) and (4.30). Our results are displayed in figure 5.5 and they can

be compared with the ones shown in figure 12 in [54].

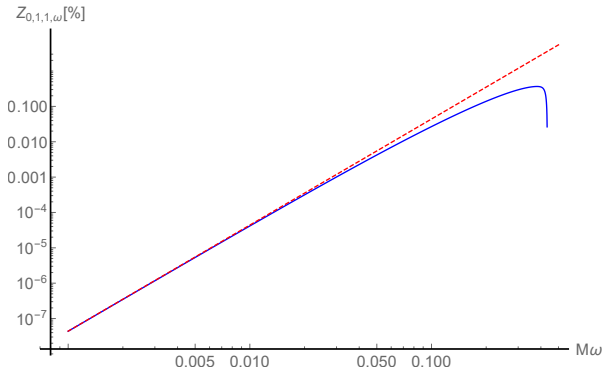

(a) s=0,l=1,m=1,a=0.99M

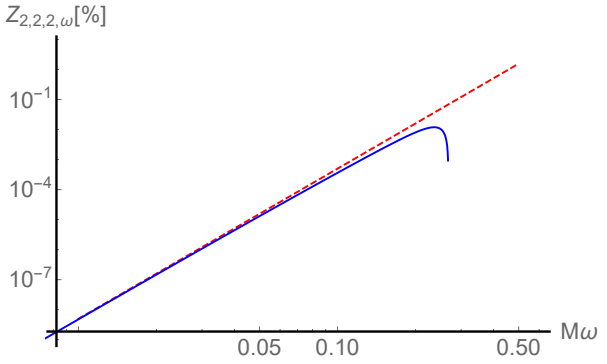

(b) s=2,l=2,m=2,a=0.5M

Figure 5.5: This figure shows our results of the calculation of $Z_{slm\omega}$ for two different modes. The blue solid lines are the results of our code for $Z_{slm\omega}$ as defined in (3.45). The red dashed lines were obtained via the small-ω approximation for $Z_{slm\omega}$, given in (3.47). These results are shown in a log-log scale, where the vertical axis is $Z_{slm\omega}$ in the percentage form and the horizontal axis is $M\omega$. The top panel is to be compared with figure 12 in [54] and the bottom panel is original from this work. Notice that for the mode displayed on the top panel $M\omega_{SR} \approx 0.4338$, while for the mode displayed on the bottom panel $M\omega_{SR} \approx 0.2679$.

As already explained in section 3.2.3, the amplification factor can only take positive values for $\omega \leq \omega_{SR}$. For $l = 1, m = 1$ and $a = 0.99M$ (top panel of figure 5.5) we have $M\omega_{SR} \approx 0.4338$, while for $l = 2, m = 2$ and $a = 0.5M$ (bottom panel of figure 5.5) $M\omega_{SR} \approx 0.2679$. The results from our code not only found the correct threshold for the superradiance phenomenon but also show the correct behavior for small frequencies.

The results of the convergence test show us that our code is reaching 20 digits of precision accurately and the results of the superradiance test is in agreement with the literature [54]. These facts give confidence on our code.

5.2.2 Results

Finding BC's

We have discussed in a previous section, 3.2.2, how BC's can be either unphysical (e.g., angular BC's, see appendix A of [39]) or, by contrast, can have physical consequences (e.g., instability). For this reason, BC's deserve some attention and this section is dedicated to looking for possible new BC's in the sub-extremal Kerr case. If they exist the following question is whether they have physical implications or if they are carried away in the sums performed in the full retarded GF.

In order to search for BC's we start by pointing out the possible sources of BC's in the complex-ω plane in (3.25). A discontinuity would manifest itself through the radial solution(s), meaning that they would reveal themselves in the Wronskian. We can point out that possible sources are ν, ${}_s\lambda_{lm\omega}$ and a_n. We designed a routine that allows us to numerically check for the presence of BC's inside a finite region of the complex-ω plane. This routine consists of few simple steps. We start by choosing a point that we suspect that might be a branch point or at least nearby a branch point. With this particular choice we calculate the particular quantity of interest (ν, ${}_s\lambda_{lm\omega}$, a_n or ${}_sW_{lm\omega}$) around this point. We performed this calculation and plotted these quantities as a function of ϕ on the circle $\omega = \omega_c + \varpi e^{i\phi}$, for $0 \leq \phi < 2\pi$, where ω_c is the point that we are investigating, and ϖ is the radius of this circle. A discontinuity in these plots would suggest the presence of a BC passing by that circle, but it does not necessarily indicate the presence of a branch point *inside* the particular region. However, at this stage, we are interested in the existence of the BC, so the test is still useful to us.

We applied this routine to each of the quantities cited above for some modes. At first we chose the central point to be the origin and the radius ϖ was set large enough to include the superradiance bound frequency (ω_{SR}) and the Hartle-Wilkins frequency (ω_{HW}). In this section we show the results of our search for BC's.

It is worth noticing that we did not plot ν directly. The reason for this is that ν is discontinuous, but these discontinuities are related to the symmetry properties of MST equations. The MST symmeries under the change $\nu \to -\nu - 1$ and the addition of an integer to ν imply that whenever we find a discontinuity on ν we would need to check if they can be carried away by using these symmetries. If ν can be made to be continuous using these symmetries, the BC's found are unphysical. A systematic way that we can take these symmetries in to account is to plot $|\sin(2\pi\Re(\nu))|$ and $|\Im(\nu)|$ due to the symmetric properties of these functions. In these ν plots the unphysical BC's due to these symmetries will not manifest themselves.

We can see that the plots for ν and ${}_s\lambda_{lm\omega}$ do not show any discontinuity in the region, so they can not contribute to the formation of a BC. The renormalized angular momentum ν and its properties were largely studied in [72, 73]. In these papers, it was reported that in the real frequency line ν is either an arbitrary real number or a complex number with a half integer real part. We have numerically checked this property to true in all our cases of interest. When performing the search for BC's on ν, we evaluate ν for complex-valued frequencies. It is clear from figure 5.7 that for frequencies away from the real axis ν is complex-valued with an arbitrary real part. However, if one looks carefully to the same figure at $\phi = 0, 2\pi$, the function $|\sin(2\pi\Re(\nu))|$ is zero, meaning that ν has a half-integer real part at this point.

Inspecting the plots of the coefficients a_n's (figure 5.8) around the origin, we can see several discontinuities. In these plots we display the coefficients a_n's for n running

from 1 to 4 [1], and all of them show discontinuities happening for the same values of ϕ. But looking at the plots of the Wronskian itself (figue 5.9), we only found a BC at $\phi = 3\pi/2$ which is an already known BC. This is the BC that stems from the origin and goes down the imaginary axis in the complex-ω plane [37, 39]. The fact that the several discontinuities in a_n's that happen for $\phi \neq 3\pi/2$ do not appear in the Wronskian implies that they are unphysical. These discontinuities in a_n's coefficients were found to be related to the discontinuities on ν that can be ruled out by the symmetries of the MST equations, reinforcing the idea that they are unphysical. Somewhere in the fourth quadrant, we can also see an indication that the "superradiant" BC is being formed. It may seem that there is a discontinuity in the fourth quadrant, but it is just a very steep structure in the Wronskian. If we had chosen a smaller value of a this structure would have been less steep (see figure 5.20). The formation of this BC will be seen in further details when we discuss the results on extremal Kerr, see section 5.3.3.

In figures 5.6-5.9 , we show the results of our analysis when encircling the origin. We chose to display the results of only one particular mode for brevity, but other modes were tested and all the results were conceptually the same, so all the information is contained in the images shown here. The mode that we chose to display here is $s = l = m = 2$, for which $M\omega_{SR} \approx 0.2679$ and $M\omega_{HW} \approx 0.2679 + 0.2320i$. We set $M\varpi = 1$ because it guarantees that both $M\omega_{SR}$ and $M\omega_{HW}$ are inside the circle. This investigation leads to the conclusion that no physical BC's were found in the Wronskian around $\omega = 0$, $\omega = \omega_{SR}$ and $\omega = \omega_{HW}$, other then the known one down the imaginary axis in the sub-extremal case and an indication that a second one going down from ω_{SR} is forming when a approaches M.

[1] Remember that we set $a_0 = 1$, so no discontinuity can come from this particular coefficient.

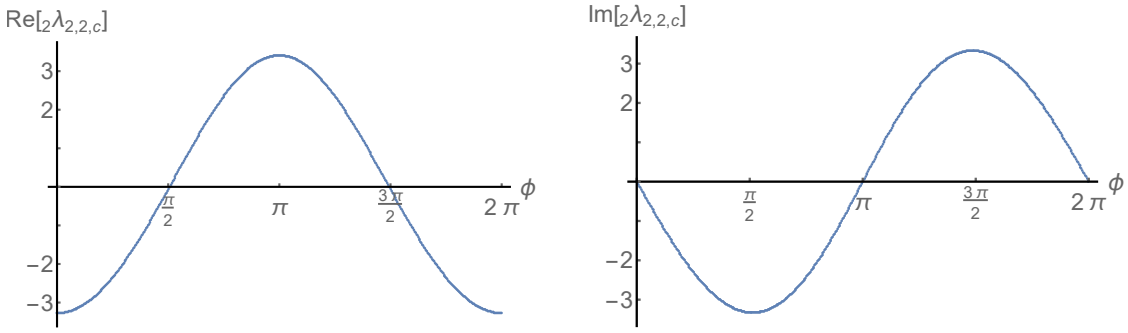

(a) Real part (b) Imaginary part

Figure 5.6: This figure shows ${}_2\lambda_{2,2,c}$, on the circle of $|c|$=0.5, for $\omega_c = 0$. We can not see any discontinuity here.

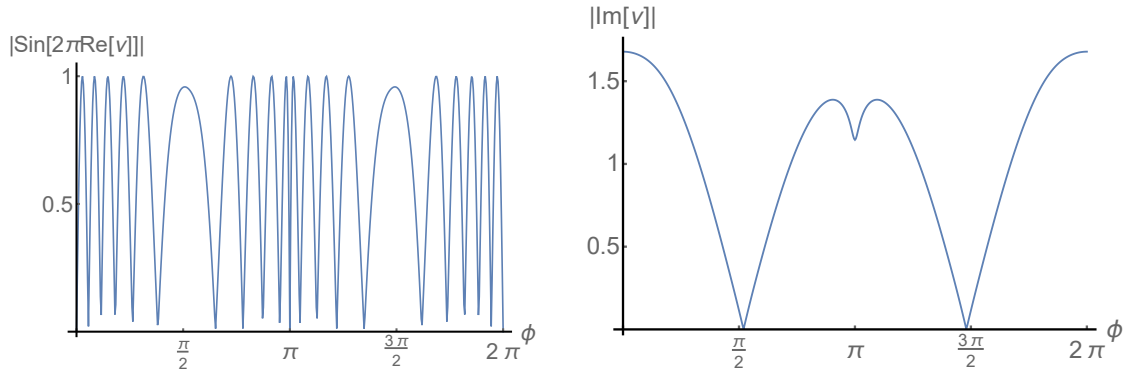

(a) Real part (b) Imaginary part

Figure 5.7: This figure shows ν, on the circle of $|M\omega| = 1$, for $\omega_c = 0$. We can not see any discontinuity here. The mode is $s = l = m = 2$, for $a = 0.5M$.

It was not by chance that we chose to display the results for the mode $s = l = m = 2$. As we explained in section 3.2.2, [47] suggested that if $s = 2$ there might be a BC in the upper-half complex-ω plane that stems from ω_{HW} (see equation (3.35)), which could lead to an instability. Although this frequency is inside the contour chosen to encircle the origin, one might be concerned that the BC could be of finite size. This happens, for example, in the function $f(z) = \sqrt{z^2 + 1}$ which has branch points in $z = \pm i$. If a particular choice of foliation is assumed, there will be only one BC connecting both of the branch points. Being concerned with the possibility that a similar structure could be taking place here, we performed the same search for BC's, but this time for $\omega_c = \omega_{HW}$

and $\varpi = |\omega_{HW}|/5$. Although the search for BC's around ω_{HW} in the quantities ν, ${}_s\lambda_{lmc}$, a_n's display the same qualitative results, we also chose to display our results for the search for BC's in the Wronskian as a stronger evidence that there is no BC in this point. This result can be seen in figure 5.10.

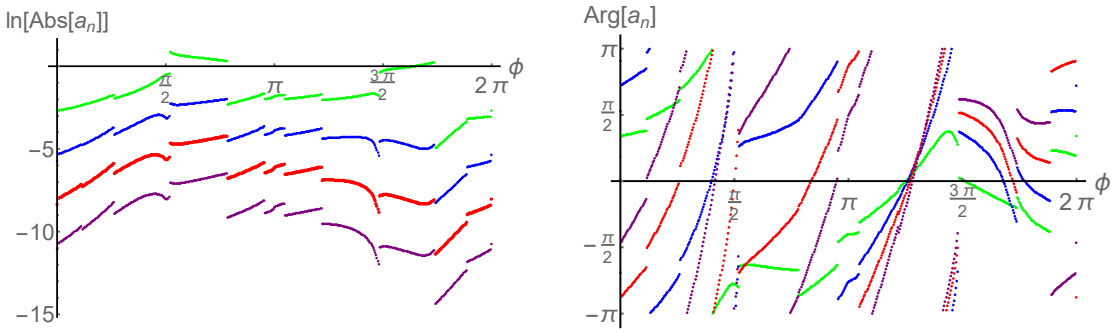

(a) Absolute value (b) Argument

Figure 5.8: This figure shows a_n coefficients for $n = 1$ (green lines), $n = 2$ (blue lines), $n = 3$ (red lines) and $n = 4$ (purple lines). We can see discontinuities that are related to the symmetries of the MST equations with respect to ν. For this reason they are unphysical and should not appear as BC's in the GF. The mode is $s = l = m = 2$, for $a = 0.5M$ for $\omega_c = 0$. Here it was used $M = 1$.

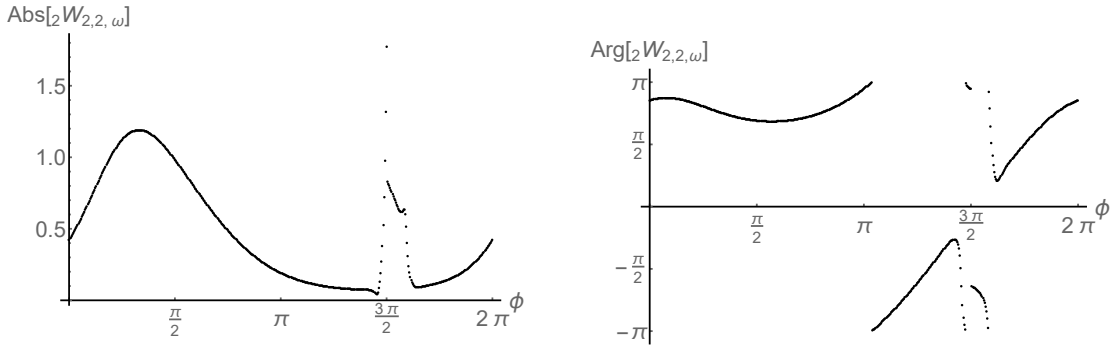

(a) Absolute value (b) Argument

Figure 5.9: This figure shows ${}_2W_{2,2,\omega}$, on the circle of $|M\omega| = 1$, for $\omega_c = 0$. We can see a discontinuity at $\phi = 3\pi/2$. This discontinuity is the manifestation of the already known BC that stems from the origin and goes down the imaginary axis [37,39]. A steep structure is seen in the fourth quadrant. This is related to the formation of the BC in the extremal case. The mode is $s = l = m = 2$, for $a = 0.5M$. Here it was used $M = 1$.

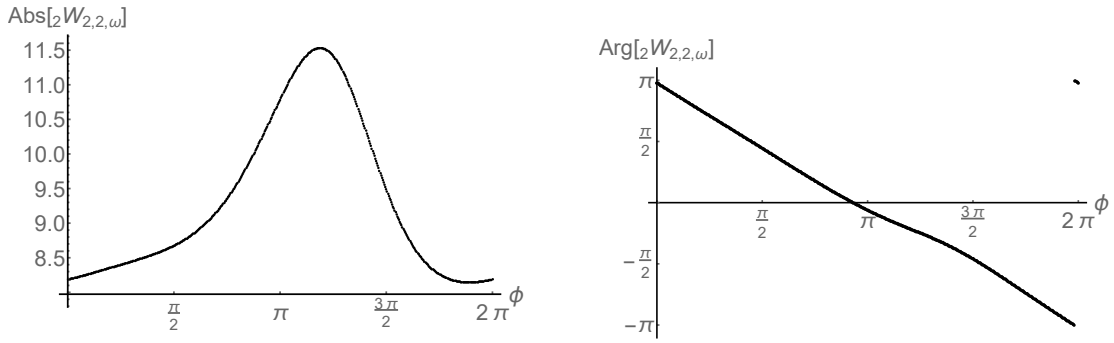

(a) Absolute value (b) Argument

Figure 5.10: This figure shows ${}_2W_{2,2,\omega}$, on the circle of radius $\varpi = \omega_{HW}$, for $\omega_c = \omega_{HW}$. No discontinuity can be seen at the entire range of ϕ apart from the one near $\phi = 2\pi$.This discontinuity is merely due to the choice of parametrization, i.e. a phase shift from π to $-\pi$ represent the same point. The mode is $s = l = m = 2$, for $a = 0.5M$. Here it was used $M = 1$.

Finding QNM's

When looking for QNM frequencies we did not use the Wronskian (3.19) directly. By noticing that ${}_sW_{lm\omega}$ has some overall factors that can not lead to a zero, meaning that they can not lead to a QNM, we defined what we call the (dimensionless) Wronskian factor:

$$
\begin{aligned}
{}_sW^f_{lm\omega} &\equiv (2i)^{-1}\left(\frac{\omega}{\epsilon\kappa}\right)^{-2s}\frac{e^{i\kappa\epsilon_+(1+2\log\kappa/(1+\kappa))}}{e^{-i(\epsilon\ln\epsilon-\frac{1-\kappa}{2}\epsilon)}e^{-\frac{\pi}{2}\epsilon}e^{\frac{\pi}{2}i(\nu+1-s)}2^{-1+s-i\epsilon}}\frac{e^{-i\epsilon\kappa}2^s i^{-\eta}}{\Gamma(1-s-2i\epsilon_+)}{}_sW_{lm\omega} \quad (5.1)\\
&= \left(\hat{K}_\nu - ie^{-i\pi\nu}\frac{\sin(\pi(\nu-s+i\epsilon))}{\sin(\pi(\nu+s-i\epsilon))}\hat{K}_{-\nu-1}\right)\frac{\Gamma(\nu+1-s+i\epsilon)}{\Gamma(\nu+1+s-i\epsilon)},
\end{aligned}
$$

where

$$
\hat{K}_\nu \equiv \frac{e^{-i\epsilon\kappa}2^s i^{-\eta}}{\Gamma(1-s-2i\epsilon_+)}K_\nu. \quad (5.2)
$$

We now have an expression that contains only the factors that can lead to zeros of the Wronskian. We can use ${}_sW^f_{lm\omega}$ to search for QNM's.

We calculated the Wronskian factor over a region by requiring 16 digits of precision and we performed contour plots to estimate the locations of the zeros of this function. By means of a minimization method routine, we used the estimated positions for the zeros

as initial guesses to find minima of $|{}_sW^f_{lm\omega}|$. These minima are zeros of the Wronskian, so they correspond to QNM frequencies. One might be concerned that it was argued before that ω_{lmn} are zeros of ${}_sW_{lm\omega}$ and now we are using a different condition. However, these two conditions are in fact equivalent. As claimed by minimum modulus principle in the theory of analytic functions, it is known that an analytic function can only have a local minimum within its region of analyticity if this point is a zero of the function [31, 74]. In fact the Wronskian has poles and BC's and it is not analytic everywhere. However, poles can clearly not correspond to minima in $|{}_sW_{lm\omega}|$. In their turn, branch points could correspond to local minima which are not zeros of ${}_sW_{lm\omega}$, but they can easily be eliminated by spotting the appearance of a discontinuity from such points.

The minimization routine chosen in this work is the Nelder-Mead method [75]. This method is applicable for minimizing a real n-dimensional function $f : \mathbb{R}^n \to \mathbb{R}$, for which the derivatives may not be known. It works by calculating and comparing the value of the function of interest at $n+1$ points $p^i = (x^i_1, x^i_2, ..., x^i_n)$ for $1 \leq i \leq n+1$. Among these $n+1$ points, the one that leads to the largest value of the function is excluded and a new point that is closer to the point with the lowest value of $f(x_1, x_2, ..., x_n)$ is chosen. Then a new comparison is made and this process is repeated until all the points are close enough to each other, i.e. they are separated by a distance smaller than a required precision. After this condition is met, the point that leads to the smallest value of $f(x_1, x_2, ..., x_n)$ is the one that we consider to be its numerical minimum. In appendix A this method is explained more carefully.

When using the Nelder-Mead routine with the initial guess obtained from the contour plots, we require at least 8 digits of precision in both imaginary and real parts of ω_{lmn}, in the Schwarzschild case it was required 16 digits of precision. We compared the results obtained from our method with QNM frequency data publicly available in [71]. We found

the agreement between them to be within their error bars.

Since all sub-extremal MST expressions are valid for $0 \leq a < M$, an obvious starting point to check our code for calculating the Wronskian factor (5.1) is the static case $a = 0$. The results for this case can be seen in figure 5.11.

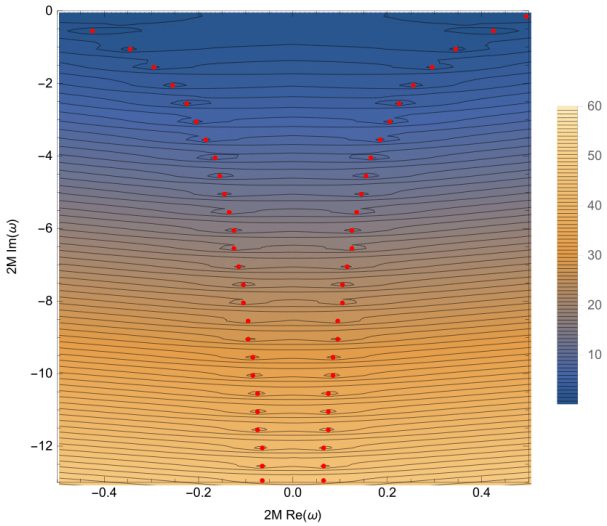

(a) s=1,l=1

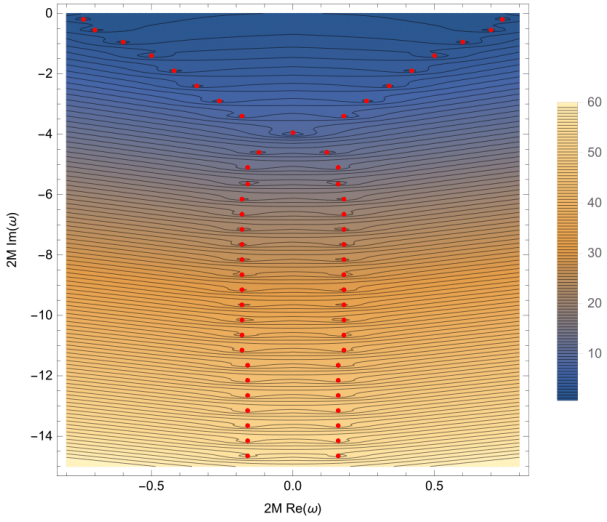

(b) s=2,l=2

Figure 5.11: This figure shows the contour plot of $\log_{10} |{}_sW^f_{lm\omega}|$ for the electromagnetic ($s = 1$) and gravitational cases ($s = 2$) in the complex-ω plane. The red dots are ω_{lmn} for these two particular modes, as obtained from our method. Note that m is not specified here because it is of no relevance for $a = 0$.

As stated before, all Schwarzschild QNM frequencies found in this work reproduce previous data [71] within their error bars and can be found in appendix B. For $s = 2$, there is one frequency that we found to be on the imaginary axis, within the 16 digits of precision that we used. This point correspond to the $n = 8$ overtone. Leaver [61] calculated this QNM frequency as being very close to but not exactly at $2M\omega = -4i$. This frequency ($2M\omega = -4i$) has drawn much interest in the literature [76–78], and it is called the algebraically special frequency (AS). The interest is based in some peculiar behaviors. In the static limit ($a = 0$) metric perturbations around this BH can be described by two different equations: Regge-Wheeler equation (axial perturbations) and Zerilli equation (polar perturbations). Although these two equations are in general isospectral [79], i.e. have the same set of QNM frequencies, this particular point seems to be a QNM for the Zerilli equation but not for the Regge-Wheeler equation [76]. When dealing with the Teukolsky equation for a small, van den Brink [76] showed that there is a branch of QNM which, in the Schwarzschild limit, stems from $2M\omega = -4i$ for $s = l = 2$ (see equation (7.30) of [76]). A careful reader may have noticed that at this point, there is a pole of $\Gamma(1 - s - 2i\epsilon_+)$ for $a = 0, s = 2$, a factor that was present in ${}_sW_{lm\omega}$ but was excluded in our definition of $W^f_{lm\omega}$, see equation (5.1). This factor could in principle cancel out the contribution that leads to a zero in $W^f_{lm\omega}$. In order to check whether the use of the Wronskian factor leads to misleading results about this frequency, we performed a plot with the full Wronskian around this frequency. The result of this approach is shown in figure 5.12.

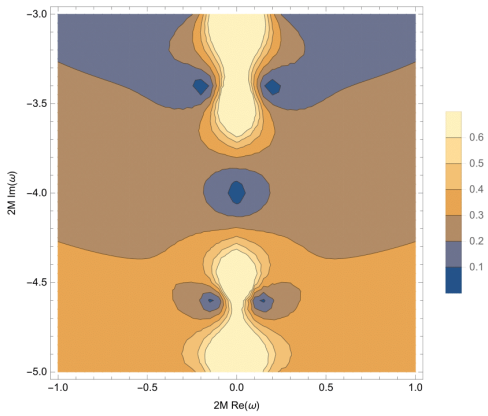

Figure 5.12: Contour plot of $|{}_sW_{lm\omega}|$, as defined by (3.19), which includes the term $\Gamma(1-s-2i\epsilon_+)$. Here we can see that the point $2M\omega=-4i$ is numerically found to be a zero of the Wronskian. This plot refers to the mode $s=2, l=2, a=0$, and should be compared with the central region of figure 5.11b.Here it was used $M=1$.

It is clearly seen from figure 5.12 that the concern about the cancellation of the QNM, although justifiable, is not correct and $2M\omega=-4i$ is numerically found to be a QNM of the Teukolsky equation for the mode $s=l=2$ with $a=0$.

After the successful calculation of ω_{lmn} via the MST method in the static case, we moved on to the near extreme Kerr (NEK), $a\approx M$. This regime was studied largely in [18, 20], but in these previous works the method applied was the CF method explained in section 4.2.1. We note a known particular behavior for modes with $m>0$. In the NEK case all these modes present overtones that tend to accumulate near the point $\omega=\omega_{SR}$, which is real-valued. These modes are called zero-damped modes (ZDM) due to the lack of imaginary part in the asymptotic limit $a\to M$. If a mode also satisfies $m/(l+1/2)\lesssim 0.74$, we found that some overtones that maintain a finite imaginary part do exist. To these overtones it is given the name of damped modes (DM). These results are consistent with the ones found in [18, 20], where this terminology of ZDM and DM was first proposed.

In the NEK case, we choose modes in order to compare our results with the ones found on figure 7 on [18]. The only studied mode with $s=-2$ that has $m/(l+1/2)\gtrsim 0.74$ is the one shown in panel 5.13d. For this mode we did not found any DM, in agreement with

findings in [18, 20]. All the ZDM's for the various modes on figure 5.13 are accumulated near $\omega = \omega_{SR}$, as expected. Panel 5.13b is a zoom of a specific region of panel 5.13a. In figure 7 of [18], it was performed a plot of the CF in Leaver's method to compute QNM frequencies with the recurrence coefficients (4.12). This plot shows poles that can be "very close" to the QNM frequencies. Our method of plotting the Wronskian factor did not display poles around the QNM frequencies. This is again a reflection of the terms that were ruled out from ${}_sW_{lm\omega}$ when defining $W^f_{lm\omega}$. This can be seen as an advantage of our approach to QNM, once these poles become arbitrarily close to $\omega_{lm\omega}$, as seen on the bottom left panel of figure 7 on [18], the presence of these poles can lead to numerical issues when going to the NEK case. The values for the QNM's frequencies found for the modes shown in figure 5.13 can be seen on the tables of appendix C, QNM frequencies in the NEK case were calculated with 8 digits of precision and agree with data from [18,20,71]

.

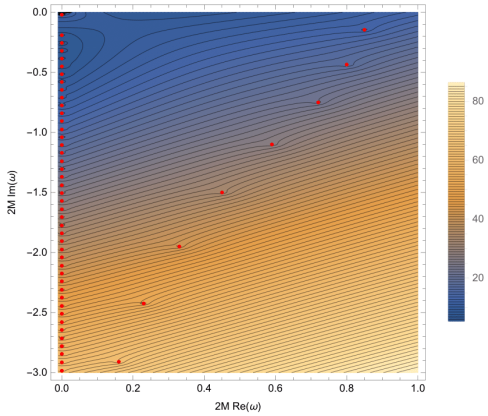

(a) s=-2,l=2,m=0,a=0.998M

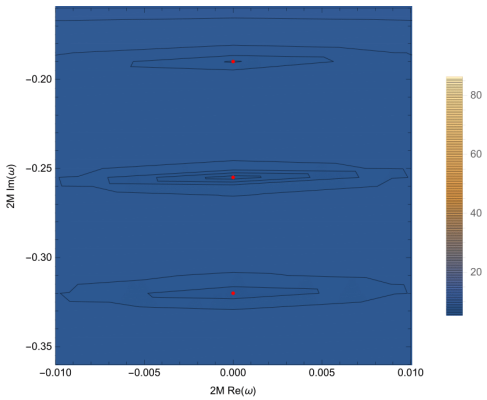

(b) s=-2,l=2,m=0,a=0.998M, zoom in

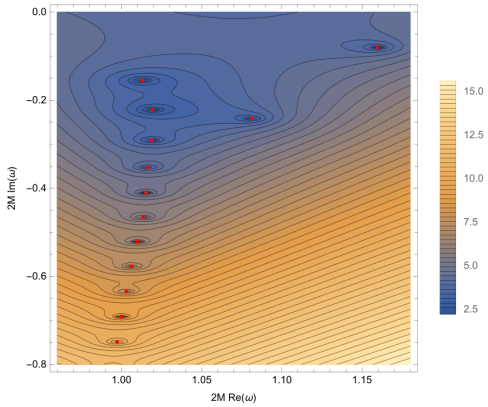

(c) s=-2,l=2,m=1,a=0.998M

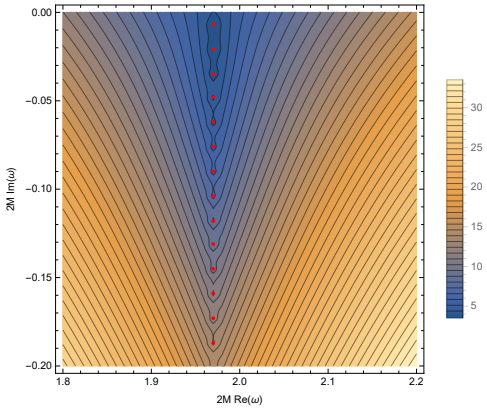

(d) s=-2,l=2,m=2,a=0.9999M

Figure 5.13: In these figures we show some of the modes investigated in the NEK case. These are contour plots of $\log_{10}|{}_sW^f_{lm\omega}|$. Here, we show the results for $|s| = 2$ and $l = 2$ for values of $0 \leq m \leq 2$. Panel 5.13b exhibits the same mode as panel 5.13a, but it displays a zoom over a smaller region.The superradiance bound frequencies for these modes are $2M\omega_{SR} = 0$ (for $m = 0$), ≈ 0.938 (for $m = 1$) and ≈ 1.972 (for $m = 2$).

At this stage a valid question can be made: what happens with QNM's under the reflection $s \to -s$? This question is easily answered by means of the Teukolsky-Starobinsky relations. Because of these relations, the solution with s can be written in terms of the solution with $-s$, due to these relations we are inclined to believe that these two solutions are isospectral. We have numerically checked that our code obtained the same set of QNM's for two modes differing only by the sign of its helicity. Those modes were $s = \pm 2$, $l = m = 2$. However, this is not sufficient to assert that there is not an exception to the isospectrality.

In this section we have seen that our method of searching for QNM can provide correct results. Bearing this in mind, we are now going to use an analogue expression for the extreme Kerr case and investigate the same properties as in the sub-extremal case.

5.3 Extremal Kerr

In the previous section we applied the MST method to the sub-extremal case and we could correctly calculate quantities such as the amplification factors and QNM frequencies for several different modes. In this section we show our findings after we performed a similar analysis in the extremal case.

5.3.1 Large ν Expansion

As stated earlier in this work, the physically meaningful MST equations satisfy some symmetries with respect to ν. These symmetries are under the change $\nu \to -\nu - 1$ and an addition of an arbitrary integer [66]. By making use of these last properties of the MST equations, Throwe was able to find an analytical approximation for large ν [80] in the sub-extreme case. Following his idea, we found a large ν expansion for the continued fraction equation that defines ν in the extremal case. This expansion reads as follows:

$$\begin{aligned} {}^{x}g_0(\nu_*) \approx & (\nu_* + 1/2)^2 - 1/4 - {}_s\lambda_{lmc} - s(s+1) - 2Mm\omega + 8(M\omega)^2 + \\ & 2M\omega(-ms^2 - m^2M\omega + 2s^2M\omega + 4M^3\omega^3)(\nu_* + 1/2)^{-2}, \end{aligned} \tag{5.3}$$

where ${}^{x}g_0(\nu_*)$ is the three-term recurrence relation for the extreme Kerr case, analogous to equation (4.24), with $n = 0$ for simplicity [2]. It is worth mentioning that equation (5.3) is not reproduced by taking the $a \to M$ limit of Throwe's large ν expansion. This has to do with the fact that Throwe used different recurrence coefficients in the sub-extremal equations than the ones defined in (4.19). His choice of sub-extremal recurrence coefficients are a multiple of (4.19) by the factor $F \equiv (n+\nu)(1+n+\nu)(-1+2n+2\nu)(3+$

[2]Remember that ν should not change for different choices of n in the equivalent equations to (4.23) and (4.24) in the extremal case. See [32].

$2n + 2\nu$), which is of fourth order in ν. This justifies the fact that Throwe's polynomial expression and (5.3) have different orders, while Throwe found a sixth order polynomial for the sub-extremal case we found a "second" order one. Both choices of recurrence coefficients are valid since equation (4.18) can be re-scaled by an overall factor and still lead to the same value of ν via (4.24). The polynomial that we achieved for the extremal case can be also found by taking the $a \to M$ limit of Throwe's expansion and dividing it by F.

The values of ν_* that are the roots of ${}^{x}g_0(\nu_*)$ are the ones to be used in the MST expressions as ν. The exact three-term recurrence relation satisfied by ν in the extreme Kerr case is available in [32]. Although this approximation was not implemented in our code, future works might find it quite useful to use this expression in order to speed up numerical calculation like the ones presented in the next few sections.

Having this approximation, we can now try to find its roots for a given frequency. We have numerically checked that in the extremal case ν has similar properties in the real line as in the sub-extremal case reported in [72, 73]. Specifically, in the real line, it is either an arbitrary real number or a complex number with half integer real part. By noticing this property of ν, one can search for roots of ${}^{x}g_0(\nu_*)$ on the real ν_* line, or in the line $\nu_* = 1/2 + i\hat{\nu}$ for $-\infty < \hat{\nu} < \infty$, if $\omega \in \mathbb{R}$. We performed a test in order to verify equation (5.3). We plotted ${}^{x}g_0(\nu_*)$ as a function of (real-valued) ν_* for a value of ω that leads to a real-valued ν for the mode $s = 2, l = 3, m = 2$. The result is shown in figure 5.14.

In figure 5.14 we can find a blue line representing the results from our numerical exact calculation of ν by plotting the extremal case analogous to (4.24), as a function of ν_*, a red line representing our large ν expansion (5.3) and a green line for Throwe's large ν expansion for $a = 0.9999M$, see equation (3.15) in [80]. They respectively give

the values for ν as being equal to 1.835, 1.851 and 1.866. We understood these results as a confirmation that the analytical expression we found performs better than Throwe's expansion for $a = M$. However, we checked that the value of ν at the extremal case and to the sub-extremal case for $a \to M$ are the same.

Due to the degeneracy in ν ($\nu \to -\nu - 1$ and/or $\nu \to \nu + n$ for $n \in \mathbb{Z}$) there will be an infinite amount of possible values of ν. In our plot the value $\nu \approx 2.165$ is correlated with the value $\nu \approx 1.835$ by the relation $\nu \to -\nu + 4$, so it would still be a valid choice for ν. Similarly to Throwe, we found that most of these valid roots of ${}^{x}g_0(\nu_*)$ are close to its poles (for example the zero at $\nu \approx 2.165$), which can lead to numerical issues when using most of the root finding algorithms. He argued that these poles also indicate that the series for R_n and L_n are poorly behaved in the region, so if these roots are used to evaluate the coefficients a_n they will often lead to additional numerical errors. This may also be the case for the extremal MST expressions. One might also notice that there are actual spurious zeros appearing in the exact ${}^{x}g_0(\nu_*)$, i.e. they can not be correlated through these relations. They seem to be half integers, just like in the sub-extremal case in Throwe's work. These spurious zeros should be disregarded.

A careful reading of this section might lead to two subsequent questions. We stated that ν has two different behaviors in the real ω line. The first question that appears here is where does this behavior changes. The second question is, what is the behavior of ν away from the real ω line. The answer to the first of these questions was unclear to us and remains an open issue to the best of our knowledge. The answer to the second question is that ν seems to be an arbitrary complex number in the complex ω plane, like in the sub-extremal case. For this reason the search for a root of ${}^{x}g_0(\nu_*)$ is not limited to a particular line of the complex ν plane, as in the previous cases. Although the expression (5.3) should still be valid in the whole complex-ω plane, it is unclear to us how to distinguish possible

spurious zeros of ${}^{x}g_0(\nu_*)$ for $\Im(\omega) \neq 0$. These were the reasons why we chose not to use equation (5.3) in our current code, but this should not be seen as an impediment for future works.

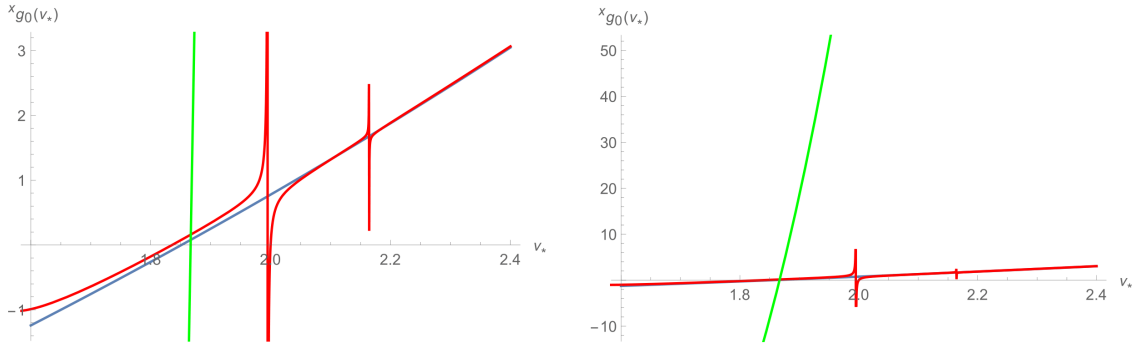

(a) zoom in (b) zoom out

Figure 5.14: Plot of the CF ${}^{x}g_0(\nu_*)$ as a function of ν_*. The roots of ${}^{x}g_0(\nu_*)$ define the value of ν that leads to a minimal solution. The mode presented here is $s = 2, l = 3, m = 2$ for the extremal case, for a given frequency of $M\omega = 0.9$. Here the red, blue and green lines represent, respectively, the numerical CF function, our large ν expansion (5.3) and Throwe's large ν expansion for $a = 0.999999M$, see equation (3.15) in [80]. Notice that because the two expansions are polynomials of different order the growth rate is different, but both still have similar zeros, i.e. they hold approximately the same value of ν.

5.3.2 Tests

As in the sub-extremal case, we also need to check for the convergence of our extremal MST code. Although the expressions are not the same, the tests that we designed in the sub-extremal case are still well suited for checking if our code for the extremal MST expression is correct. Thus, the tests performed here are similar to the ones performed in section 5.2.1. We organized this subsection in two parts: convergence tests and the superradiance test.

Convergence Tests

Just as in the sub-extremal case, we need to be careful about the convergence when computing the sums appearing in the extremal MST expressions. In the extreme case, we chose to apply the convergence test to the coefficients ${}^{x}B^{inc}_{lm\omega}$ (4.37) and ${}^{x}B^{trans}_{lm\omega}$ (4.36),

since they are needed to compute the Wronskian via equation (3.22). The test that we performed for this new code is similar to the one designed for K_ν in section 5.2.1. This means that we plotted the partial sums ${}^{x}B_n^{inc}$ and ${}^{x}B_n^{trans}$ as functions of n. Notice that the partial sum here, means that the sums in (4.37) and (4.36) were performed from $-n$ to n. The results for these convergence tests are shown in figures 5.15 and 5.16. While performing this test, we were requiring 20 digits of precision as the threshold for our internal loop used to perform the sums in both coefficients. The results found are displayed in figures 5.15 and 5.16.

Just as in the sub-extremal case for the summands in K_ν, we also plot the summands in ${}^{x}B_n^{inc}$ and ${}^{x}B_n^{trans}$. These plots range from negative to positive values of n. This is because the range of the index in these sums is now from $-\infty < n < \infty$, and the dominant terms are the ones near $n = 0$ as we can see in the plots shown in 5.18 and 5.17. Using this routine we plotted the summands and notice that our code is including summands for $n > 0$ that do not alter the value of the sum within our required precision. This happens because in order to perform the sums in ${}^{x}B_{lm\omega}^{trans}$ (4.36) and ${}^{x}B_{lm\omega}^{inc}$ (4.37), we wrote routines containing loops that add summands of both n and $-n$ index in each iteration. In other words, the sum will always have the same number of summands for negative and positive values of n. These loops stop when the relative difference between the values of the sum for $|n|$ and $|n-1|$ is smaller than the required precision. Our code can be made faster if we change the loops where the sum is performed, in a way not to include the negligible terms that are still appearing in our sum.

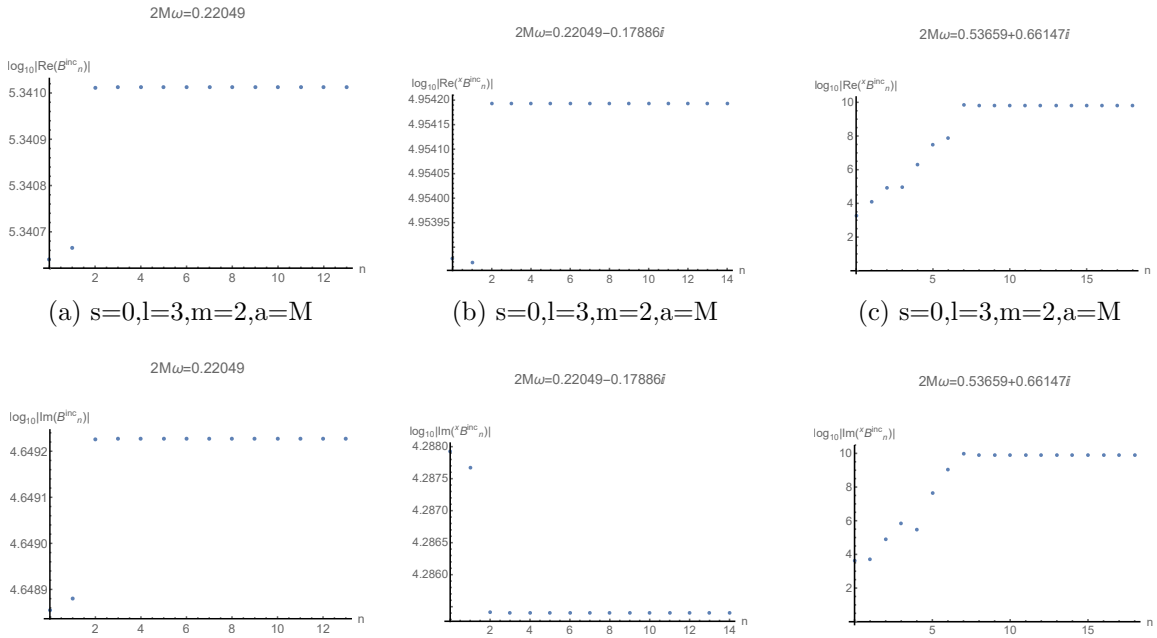

(a) s=0,l=3,m=2,a=M (b) s=0,l=3,m=2,a=M (c) s=0,l=3,m=2,a=M

(d) s=0,l=3,m=2,a=M (e) s=0,l=3,m=2,a=M (f) s=0,l=3,m=2,a=M

Figure 5.15: Here it is shown plots for the partial sum ${}^{x}B_n^{inc}$. The required precision in our code when generating these plots was of 20 digits. Here it was used $2M = 1$.

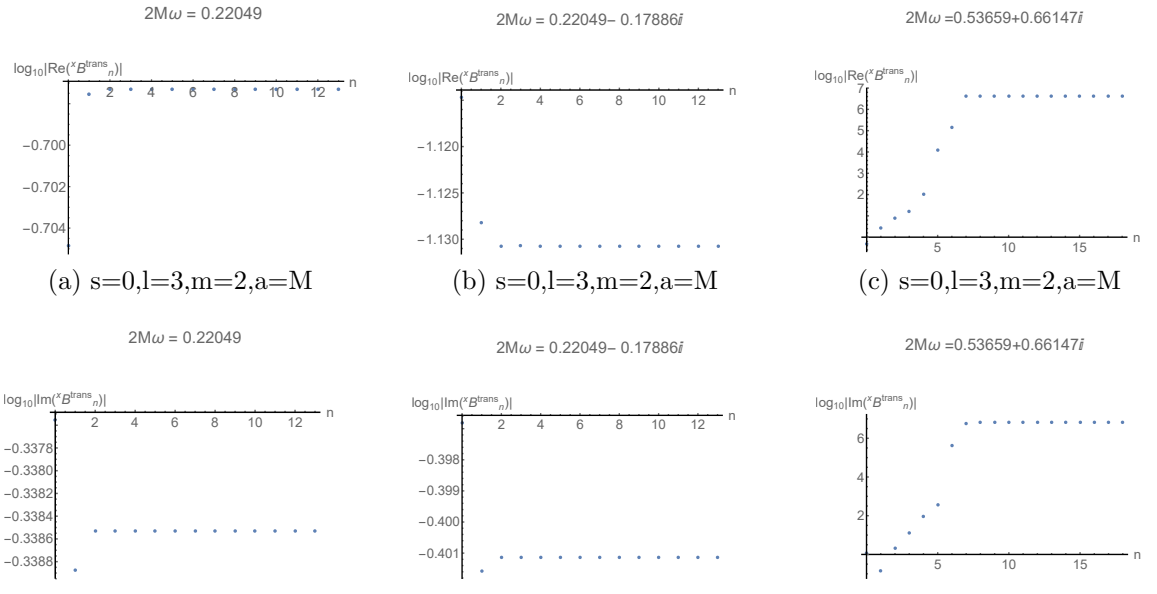

(a) s=0,l=3,m=2,a=M (b) s=0,l=3,m=2,a=M (c) s=0,l=3,m=2,a=M

(d) s=0,l=3,m=2,a=M (e) s=0,l=3,m=2,a=M (f) s=0,l=3,m=2,a=M

Figure 5.16: Here it is shown plots for the partial sum ${}^{x}B_n^{trans}$. The required precision in our code when generating these plots was of 20 digits. Here it was used $2M = 1$.

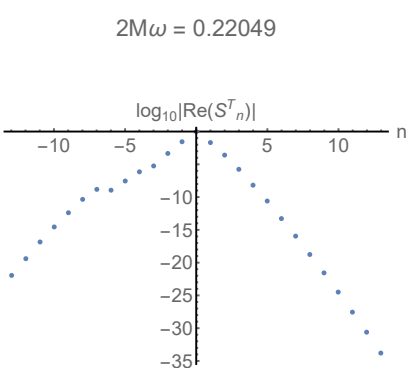

(a) s=0,l=3,m=2,a=M

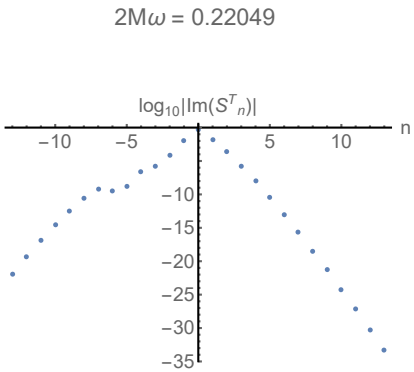

(b) s=0,l=3,m=2,a=M

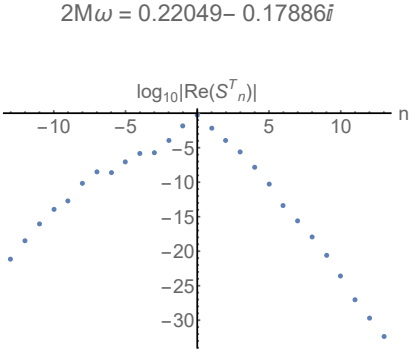

(c) s=0,l=3,m=2,a=M

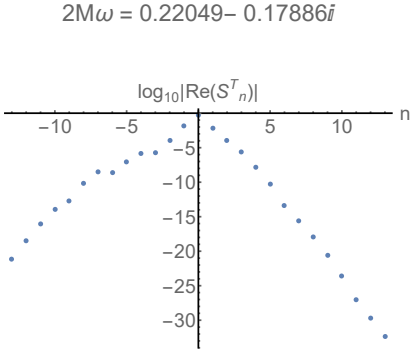

(d) s=0,l=3,m=2,a=M

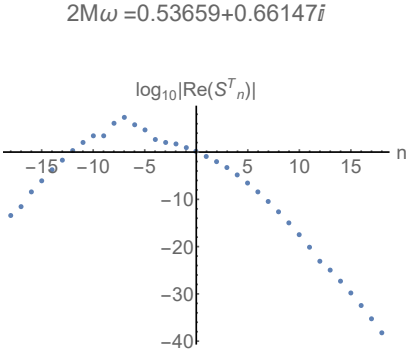

(e) s=0,l=3,m=2,a=M

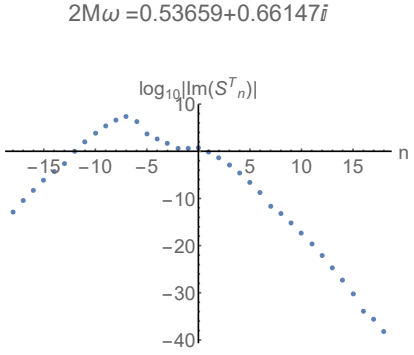

(f) s=0,l=3,m=2,a=M

Figure 5.17: Here it is shown plots for the summands (S_n^T) of the series for ${}^{x}B_{lm\omega}^{trans}$. The required precision in our code when generating these plots was of 20 digits. Here it was used $2M = 1$.

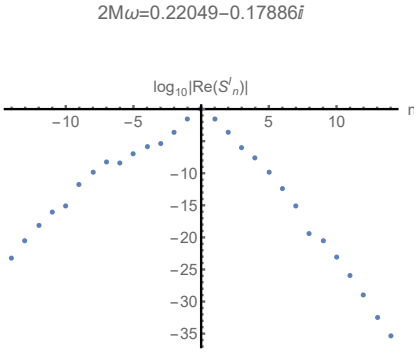

(a) s=0,l=3,m=2,a=M

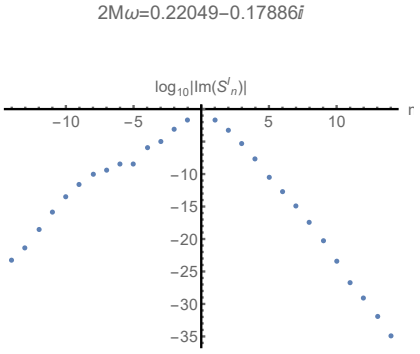

(b) s=0,l=3,m=2,a=M

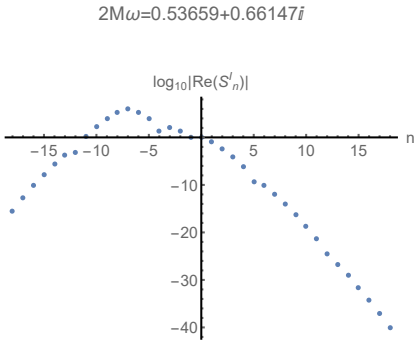

(c) s=0,l=3,m=2,a=M

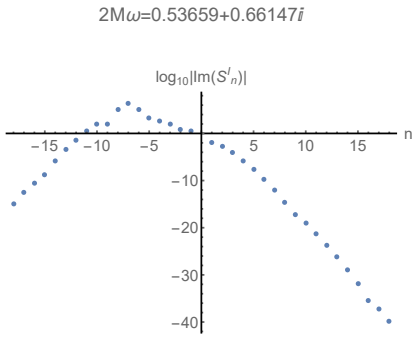

(d) s=0,l=3,m=2,a=M

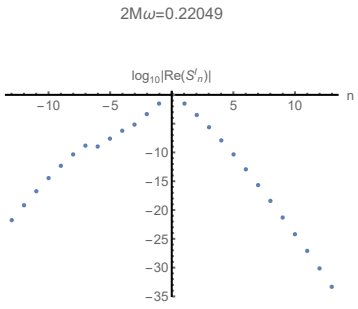

(e) s=0,l=3,m=2,a=M

Figure 5.18: Here it is shown plots for the summands (S_n^I) of the series for ${}^{x}B^{inc}_{lm\omega}$. The required precision in our code when generating these plots was of 20 digits. The plot for the imaginary part of S_n^I for $2M\omega = 0.22049$ is not shown here because for this frequency the summands were found to be real. Here it was used $2M = 1$.

Although, we only show here results for one mode for brevity, other modes were tested and the results were conceptually the same. Here, in contrast with the sub-extremal case, we choose not to use QNM frequencies when performing the tests. We made this choice because we performed all our numerical calculations in the extremal case oblivious to

Richartz findings [11], only comparing the final results. When analyzing the results in figures 5.15-5.18, we concluded that our code is reaching convergence up to a desired precision, and that our code is ready to be used for obtaining physical information.

Superradiance Test

Equation (3.45) is still valid for the extremal Kerr case. However, ${}_sW_{lm\omega}$ now has to be calculated via (3.22), i.e. using the extremal asymptotic amplitudes. The results shown in this section have the same motivation as in the sub-extremal case, but some differences do exist. The main difference is that there is no guarantee that (3.47) also holds in the extremal case, but it should be valid arbitrarily close to the extremal case. This difference will be useful as a test of how smooth $Z_{slm\omega}$ is in the transition from $a < M$ to $a = M$. We plotted (3.45) in the extremal case and (3.47) with a very close to M against each other. This plot (figure 5.19) allowed us to check if the value of the amplification factor in the extremal case is similar to sub-extreme one. We can also check our extremal $Z_{slm\omega}$ result against its behavior near ω_{SR} given by (3.48) and (3.50).

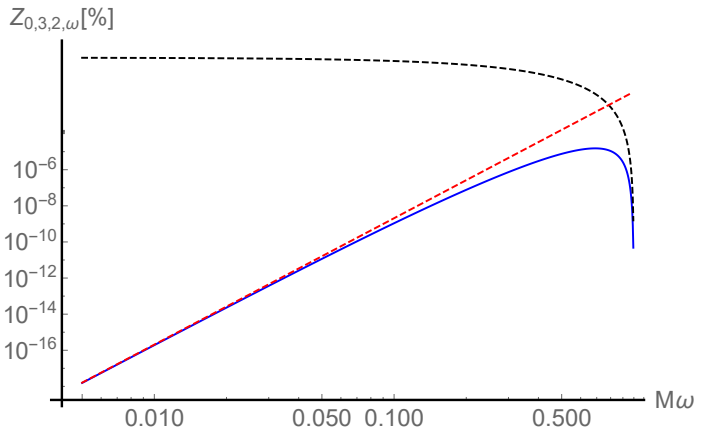

Figure 5.19: Log-log plot of our numerical result for the amplification factor (in percentage) for the extremal Kerr case as a function of the frequency, for the mode $s = 0, l = 3, m = 2, a = M$. The solid blue line is the result that we obtained using our own code via (3.45). The dashed red line is a plot of (3.47) with $a = 0.9999M$. The dashed black line is a plot of (3.48), where it was assumed $a = M$. For this mode in the extremal case we have $M\omega_{SR} = ma/2r_+ = 1$, in agreement with the plot.

Figure 5.19 shows that our numerical code agrees with the predicted analytical behavior near the threshold ($\omega \approx \omega_{SR}$). Furthermore, it shows that the behavior for small frequencies is very similar, if not the same, to that in the sub-extremal case with a arbitrarily close to M. We conclude that our code for the extreme case is correct, and so our code is ready to be used to search for QNM's.

5.3.3 Results

Formation of the Superradiant BC

A search for BC's in the extremal case was performed similarly to the one in section 5.2.2 and no BC's were found other then the expected ones at $\omega = 0$ and $\omega = \omega_{SR}$. This section is dedicated to show our results on the formation of the BC that happens to stem from the point $\omega = \omega_{SR}$, where the ZDM's accumulate in the NEK scenario as seen in figure 5.13, as predicted ins [45]. We used the full sub-extremal Wronskian for increasing value of a until the extremal Wronskian in needed in order to study the formation process of this BC through the accumulation of the ZDM's.

When looking at figure 5.20, it is clear to us that the formation process of the BC is more complicated then it might have been anticipated. Previous works have noticed the accumulation of QNM frequencies, but they are not the only modes that do so. As we can see, the poles in ${}_sW_{lm\omega}$ are also "piling up" at the same point. These poles represent the totally reflected modes (TRM). This can be seen on equation (3.19): when the mode is totally reflected we have $B^{trans}_{lm\omega} = 0$, leading to poles in ${}_sW_{lm\omega}$ unless $B^{inc}_{lm\omega} = 0$. Another fact that supports our interpretation of these poles as TRM's is that these are coming from the $\Gamma(1 - s - 2i\epsilon_+)$ factor which appears in the construction of the Wronskian. Such poles happen at $1 - s - 2i\epsilon_+ = -n$ for $n = 0, 1, 2, 3...$, which is a condition equivalent to

$$\omega = m\Omega_H - 2\pi i T_H(n - s + 1).^3 \tag{5.4}$$

[3]The equation shown here display the factor $(n-s+1)$ and in the original paper this factor is $(n-s)$.

Equation (5.4) was first found in [69] and it was derived as the sufficient condition for defining a TRM.

Figure 5.20 shows that the TRM's and QNM's are coming closer together as we increase the value of a. When $a = M$ an infinite amount of both mode classes accumulate and mix in a way that a BC finite discontinuity is formed. To the best of our knowledge, this is the first time that this accumulation of TRM's is reported in the literature.

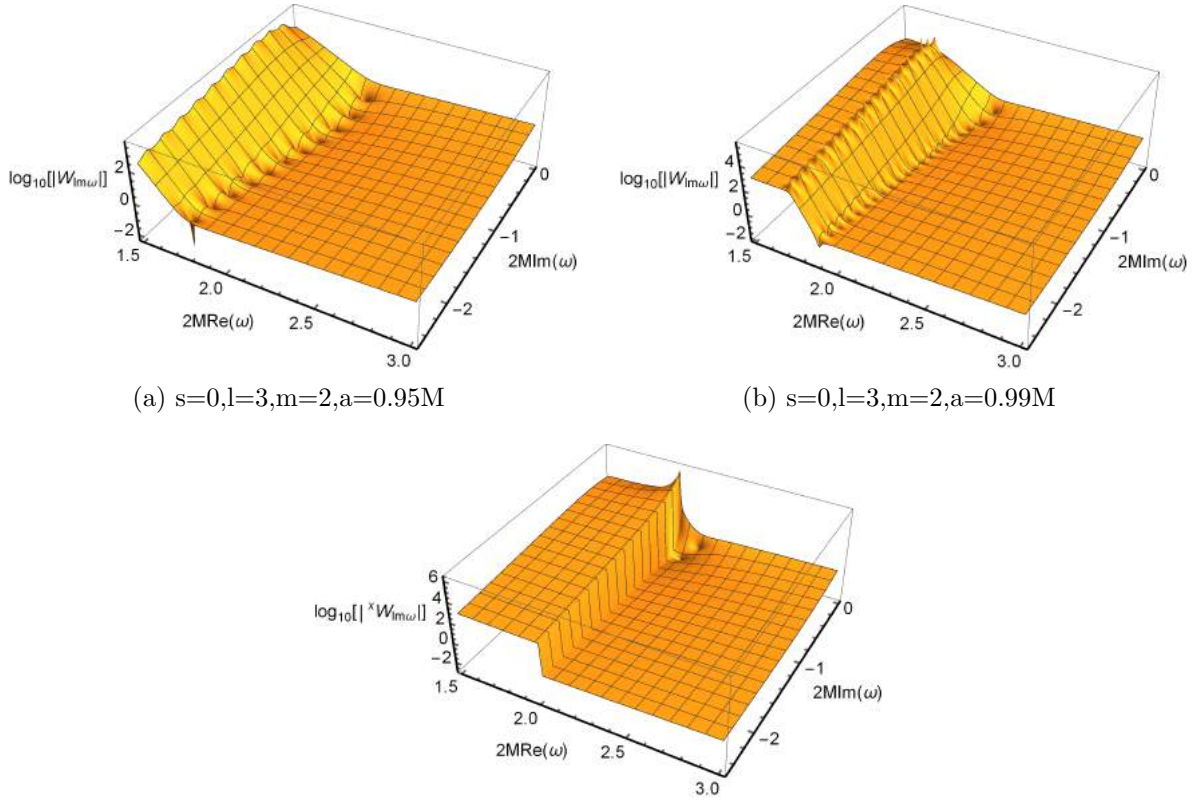

(a) s=0,l=3,m=2,a=0.95M

(b) s=0,l=3,m=2,a=0.99M

(c) s=0,l=3,m=2,a=M

Figure 5.20: Here it is shown the 3D plots for the absolute value of the Wronskian for different values of a. The images are ordered by increasing a. Notice that for this particular mode $s = 0, l = 3, m = 2$, $2M\omega_{SR} \approx 1.447$ (for $a = 0.95M$), $\approx$1.735 (for $a = 0.99M$), =2 (for $a = M$). For $s = 0$ the Wronskian defined via (3.19) is dimensionless.

This can be understood as a relabeling of the index n.

Finding QNM's

In this subsection we are going to summarize the results found when performing a search for QNM frequencies for extreme Kerr BH's. For the extreme case, we used the full Wronskian (3.22), with analogue expressions to (4.27)-(4.30) that can be found in [32].

In figure 5.20 we showed how ${}_sW_{lm\omega}$ transitions from sub-extremal to extremal Kerr. In panel 5.20c we can see two isolated QNM's frequencies appearing to the right of the BC, which correspond to the DM's found in the NEK case. We display in figure 5.21 the same data as in panel 5.20c, but in the form of a contour plot for clarity. We also applied the method to the mode $s = -2$ and $l = 2$ for $0 \leq m \leq 2$. Our results for this search for QNM frequencies are displayed in panel 5.22c.

In figure 5.22 we can see two different regimes: $0 < m \lesssim 0.74(l + 1/2)$ and $m \gtrsim 0.74(l + 1/2)$. For $l = 2$ and $m = 0$ there is an accumulation of QNM's at $\omega = \omega_{SR} = 0$ (see figure 5.13a) and we found several QNM frequencies in the analyzed region of the complex -ω plane. For $l = 2$ and $m = 1$ we have $m/(l+1/2) = 0.4 < 0.74$ and we can also see a BC that is formed from the accumulation of QNM's and TRM's - see previous section. Although this accumulation takes place, some QNM's (the DM's in [18, 20] notation) are still away from the accumulation point. These DM's seem to be always to the right of the BC. For $s = 2$, $l = 2$ and $m = 2$ we notice the absence of QNM's in this particular region of the complex-ω plane.

All QNM frequencies discussed in this section were calculated with 8 digits of precision and are displayed in appendix D. Only the first excited QNM's for each mode was computed in the exact extremal case in [11], some of the highly excited QNM's for this case were first calculated in this thesis.

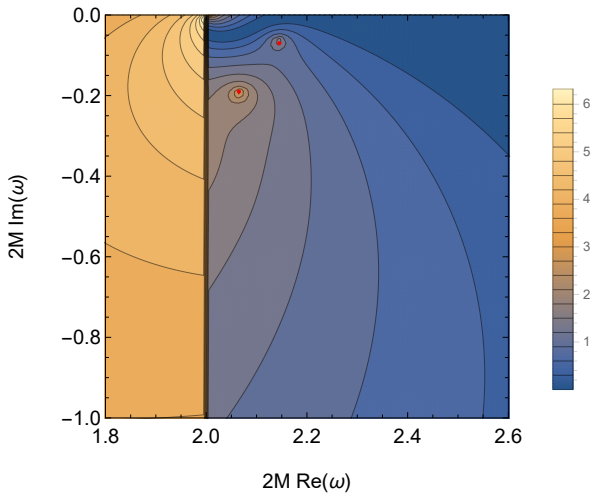

Figure 5.21: Contour plots of $\log_{10}|{}^{x}_{s}W_{lm\omega}|$ in the complex-frequency plane. The presence of two minima to the right of the BC is clearly seen. The mode analyzed here is $s = 0, l = 3, m = 2, a = M$. The superradiance bound frequency for this mode is $2M\omega_{SR} = 2$. Here it was used $2M = 1$.

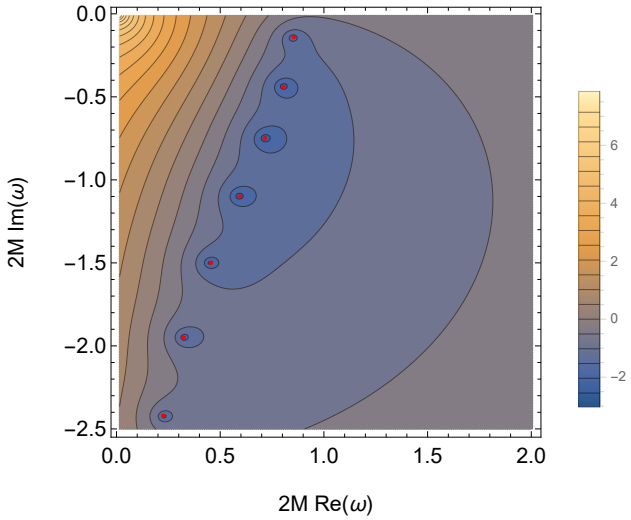

(a) s=-2,l=2,m=0,a=M

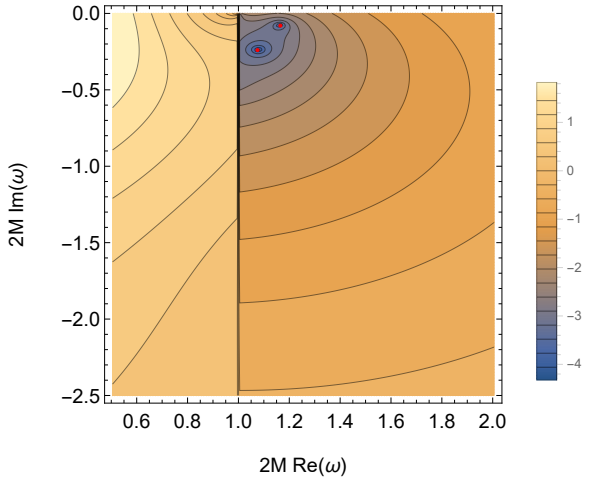

(b) s=-2,l=2,m=1,a=M

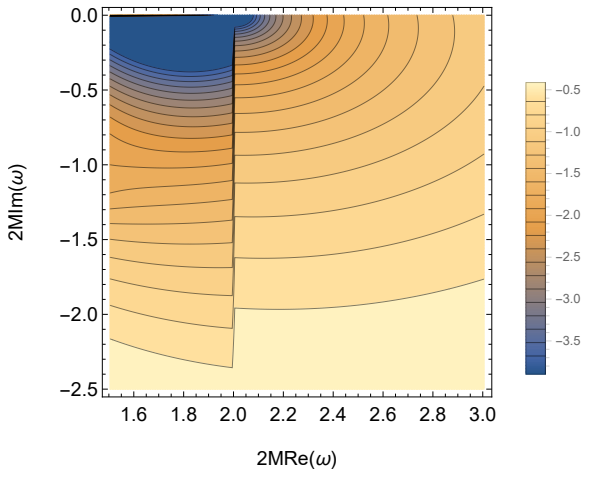

(c) s=-2,l=2,m=2,a=M

Figure 5.22: Contour plots of $\log_{10}|{}^{x}sW_{lm\omega}|$ in the complex-frequency plane. For the $m = 0$ mode we have $m/(l + 1/2) = 0 < 0.74$ and DM's do appear. For the $m = 1$ mode we have $m/(l + 1/2) = 0.4 < 0.74$, and for this reason DM's appear. For the $m = 2$ mode we have $m/(l + 1/2) = 0.8 > 0.74$, and for this reason DM's do not appear. The superradiance bound frequencies for these modes are $2M\omega_{SR} = 0$ (for $m = 0$), 1 (for $m = 1$) and 2 (for $m = 2$). Here it was used $2M = 1$.

Chapter 6

Conclusions

In this thesis we have reproduced literature results and obtained new results about wave propagation around a rotating black hole. We started by reviewing the Kerr metric and its properties. This was followed by a review on linear perturbation theory of rotating black holes. The main methods developed in the last few decades in the context of this theory are explained on first few chapters. Our first contribution to the theory, i.e the first (approximative) analytical method to calculate the angular eigenvalue derivative directly, can be found in those first capters.

The last chapter was dedicated to our numerical results. There we numerically demonstrated the validity of our angular eigenvalue derivative method. This result may be useful in the future for the study of the analytical properties of spin-weighted spheroidal harmonics. It is worth mentioning, that this result was sent to the authors of Black Hole Perturbation Toolkit [29] before the conclusion of this thesis, where we expect the method to be implemented. We have also applied the MST method to investigate the sub-extremal and extremal Kerr BH.

The main goal of this work was to obtain the QNM frequencies of the extremal Kerr BH. In order to obtain this result we chose to use the MST method. It seems to us that this was the first time that the MST method was used to perform a search

for QNM frequencies. For this reason we started by investigating whether our approach can reproduce results found in previous works for sub-extremal Kerr. By checking the convergence of our numerical methods and investigating the behavior of the amplification factor we convinced ourselves that our MST code was correct. The following step was to use our code to find QNM frequencies. We were able to calculate them with 16 digits of precision, and all the values found are in agreement with the ones available in the literature within their error bars. We also discussed the QNM problem in the algebraically special point in the static case. A search for possible new BC's in the complex-frequency plane for several quantities in the sub-extremal Kerr case was also performed. Although we have found BC's in the MST coefficients a_n's, we provide reasons to believe that they are unphysical due to the symmetries of the MST equations with respect to ν. Although we did not find any new physical BC's, we could see indications of the formation of the BC that is known to appear in the Wronskian for extremal Kerr case.

We also made use of the adaptation of the MST method to the extremal Kerr case provided in [32]. By making use of this adaptation, we performed similar analysis to the ones executed in the sub-extremal case, but this time in the exact extremal Kerr case. The BC analysis performed there provided an enlightenment about the formation process of the BC that appears in the extremal case at $\omega = \omega_{SR}$. We found that this BC is formed due to the accumulation not only of QNM frequencies, but also of totally reflected modes. To the best of our knowledge, this is the first time this TRM frequencies accumulation is reported. We concluded this section performing a QNM frequency search. Our results were consistent with the ones found in the first work -and, as far as we know, only work until now- on the QNM frequency problem in extreme Kerr [11], and we were also able to provide new modes.

We believe that our findings presented here constitute a contribution in the understanding of the rotating black hole spectroscopy and to the extremal Kerr perturbation theory.

Bibliography

[1] H. M. Nussenzveig, *Curso de Física Básica*, Vol.2, Editora Edgard Blucher LTDA. (1983), Brazil 1

[2] S. Chandrasekhar, *The Mathematical Theory of Black Holes*, Oxford University Press (1983), New York 1, 3, 4, 24, 25

[3] B.P. Abbott et al. (LIGO Scientific Collaboration and Virgo Collaboration), *Observation of Gravitational Waves from a Binary Black Hole Merger*, Phys. Rev. Lett. 116, 061102 (2016) 2, 16

[4] B.P. Abbott et al. (LIGO Scientific Collaboration and Virgo Collaboration), *GW151226: Observation of Gravitational Waves from a 22-Solar-Mass Binary Black Hole Coalescence*, Phys. Rev. Lett. 116, 241103 (2016) 2, 16

[5] B.P. Abbott et al. (LIGO Scientific and Virgo Collaboration), *GW170104: Observation of a 50-Solar-Mass Binary Black Hole Coalescence at Redshift 0.2*, Phys. Rev. Lett. 118, 221101 (2017) 2, 16

[6] B.P. Abbott et al. (LIGO Scientific and Virgo Collaboration), *GW170608: Observation of a 19 Solar-mass Binary Black Hole Coalescence*, Astrophys. J. L., Vol 851, No. 2 2, 16

[7] B.P. Abbott et al. (LIGO Scientific and Virgo Collaboration), *GW170814: A Three-Detector Observation of Gravitational Waves from a Binary Black Hole Coalescence*, Phys. Rev. Lett. 119, 141101 (2017) 2, 16

[8] B.P. Abbott et al. (LIGO Scientific and Virgo Collaboration), *GW170817: Observation of Gravitational Waves from a Binary Neutron Star Inspiral*, Phys. Rev. Lett. 119, 161101 (2017) 2, 16

[9] B.P. Abbott et al. (LIGO Scientific and Virgo Collaborations), *Tests of General Relativity with GW150914*, Phys. Rev. Lett. 116, 221101(2016) 2

[10] E. Berti, V. Cardoso and A. O. Starinets, *Quasinormal modes of black holes and black branes*, Class. Quant. Grav., 26, 16, 163001(2009) 2, 15

[11] M. Richartz, *Quasinormal modes of extremal black holes*, Phys. Rev. D **93**, no. 6, 064062 (2016) doi:10.1103/PhysRevD.93.064062, arXiv:1509.04260 [gr-qc] 2, 31, 72, 75, 79, 99

[12] K. S. Thorne, *Disk-Accretion onto a Black Hole. II. Evolution of the Hole*, Astrophys. J., 191, pp. 507-520 (1974) doi:10.1086/152991 2

[13] C. S. Reynolds, *The spin of supermassive black holes*,Class. Quant. Grav. 30, 244004 (2013), arXiv:1307.3246 2

[14] L. Brenneman, *Measuring the Angular Momentum of Supermassive Black Holes*, SpringerBriefs in Astronomy. ISBN 978-1-4614-7770-9. Laura Brenneman, 2013 (2013) 2

[15] M. C. Miller and J. M. Miller, *The masses and spins of neutron stars and stellar-mass black holes*, Phys. Rept. 548, 1 (2014), arXiv:1408.4145 2

[16] M. van de Meent, *Self-force corrections to the periapsis advance around a spinning black hole*, Phys. Rev. Lett. **118**, no. 1, 011101 (2017), doi:10.1103/PhysRevLett.118.011101, arXiv:1610.03497 [gr-qc] 2

[17] S. Detweiler, *Black holes and gravitational waves. III - The resonant frequencies of rotating holes*, Astrophys. J., Part 1, vol. 239, July 1, 1980, p. 292-295 2, 31

[18] H. Yang, A. Zimmerman, A. Zenginoğlu, F. Zhang, E. Berti and Y. Chen, *Quasinormal modes of nearly extremal Kerr spacetimes: spectrum bifurcation and power-law ringdown*, Phys. Rev. D **88**, no. 4, 044047 (2013), doi:10.1103/PhysRevD.88.044047, arXiv:1307.8086 [gr-qc] 2, 31, 61, 62, 75, 95

[19] A. Zimmerman, H. Yang, F. Zhang, D. A. Nichols, E. Berti and Y. Chen, *Reply to "On the branching of quasinormal resonances of near-extremal Kerr black holes" by Shahar Hod*, arXiv:1510.08159 [gr-qc] 2, 31

[20] H. Yang, F. Zhang, A. Zimmerman, D. A. Nichols, E. Berti and Y. Chen, *Branching of quasinormal modes for nearly extremal Kerr black holes*, Phys. Rev. D **87**, no. 4, 041502 (2013), arXiv:1212.3271 [gr-qc] 2, 61, 62, 75, 95

[21] T. Padmanabhan, *Gravitation, Foundations and Frontiers*, Cambridge University Press (2010), New York 3, 5, 15

[22] R. M. Wald, *General Relativity*, The University of Chicago Press (1984), Chicago and London 3, 7

[23] R. C. Henry, *Kretschmann scalar for a Kerr-Newman black hole*, Astrophys. J. 535, 350 (2000), arXiv: astro-ph/9912320 3

[24] C. W. Misner, K. S. Thorne and J. A. Wheeler, *Gravitation*, W.H. Freeman and Company (1973), San Francisco 4, 5

[25] R. M. Wald, *Gravitational collapse and cosmic censorship*,Fundam. Theor. Phys. **100**, 69 (1999), arXiv:gr-qc/9710068 [gr-qc] 4

[26] D. Raine and E. Thomas, *Black Holes, An Introduction*, Imperial College Press (2010) 6

[27] S. A. Teukolsky, *Perturbations of a rotating black hole. I. Fundamental equations for gravitational, electromagnetical and neutrino-field perturbations.*, Astrophys. J., 185, pp. 635-643 (1973) 8

[28] E. Berti, V. Cardoso and M. Casals, *Eigenvalues and eigenfunctions of spin-weighted spheroidal harmonics in four and higher dimensions*, Phys. Rev. D **73**, 024013 (2006), Erratum: Phys. Rev. D **73**, 109902 (2006), arXiv: [gr-qc/0511111] 11, 44

[29] BHPToolkit, *Black Hole Perturbation Toolkit* , `bhptoolkit.org` 11, 43, 44, 78

[30] A. Ronveaux, *Heun's Differential Equations*, Oxford University Press (1995) 11, 13

[31] E. Butkov, *Mathematical Physics*, Addison-Wesley Publishing Company (1973) 12, 58

[32] M. Casals and P. Zimmerman, *Perturbations of Extremal Kerr Spacetime: Analytic Framework and Late-time Tails*, arXiv:[gr-qc/1801.05830] 13, 38, 64, 65, 75, 79

[33] M. Kac, *Can One Hear the Shape of a Drum?*, Am. Math. Mon. 73, 1 (1966) 14

[34] K. D. Kokkotas and B. G. Schmidt, *Quasi-Normal Modes of Stars and Black Holes*, Living Rev. Rel. 2, 2 (1999), [gr-qc/9909058] 15

[35] H.-P. Nollert, *TOPICAL REVIEW: Quasinormal modes: the characteristic "sound" of black holes and neutron stars*, Class. Quant. Grav. 16, R159 (1999) 15

[36] H.-P. Nollert and B. G. Schmidt, *Quasinormal modes of Schwarzschild black holes: Defined and calculated via Laplace transformation*, Phys. Rev. D45, 2617 (1992) 15

[37] E. W. Leaver, *Spectral decomposition of the perturbation response of the Schwarzschild geometry*,Phys. Rev. D34, 384 (1986), Erratum Phys. Rev. D 38, 725 (1988) xii, 15, 16, 18, 32, 54, 56

[38] N. Andersson, *Evolving test-fields in a black-hole geometry*,Phys. Rev. D55, 468 (1997), [gr-qc/9607064] 16

[39] M. Casals, C. Kavanagh and A. C. Ottewill, *High-order late-time tail in a Kerr space-time*, Phys. Rev. D **94**, No. 12, 124053 (2016), doi:10.1103/PhysRevD.94.124053, arXiv:1608.05392 [gr-qc] xii, 16, 18, 34, 36, 52, 54, 56

[40] F. Pretorius, *Evolution of Binary Black Hole Spacetimes*, Phys. Rev. Lett. 95, 121101 (2005), [gr-qc/0507014] 16

[41] M. Campanelli, C. O. Lousto, P. Marronetti and Y. Zlochower, *Accurate Evolutions of Orbiting Black-Hole Binaries Without Excision*, Phys. Rev. Lett. 96, 111101 (2006), [gr-qc/0511048] 16

[42] J. G. Baker, J. Centrella, D.-I. Choi, M. Koppitz and J. van Meter, Gravitational wave extraction from an inspiraling configuration of merging black holes, Phys. Rev. Lett. 96, 111102 (2006), [gr-qc/0511103] 16

[43] S. Hod, *Radiative Tail of Realistic Rotating Gravitational Collapse*, Phys. Rev. Lett. 84, 10 (2000) 19

[44] S. Hod, *Mode coupling in rotating gravitational collapse: Gravitational and electromagnetic perturbations*, Physical Review D 61, 064018 19

[45] K. Glampedakis and N. Andersson, *Late-time dynamics of rapidly rotating black holes*, Phys. Rev. D 64, 104021(2001) 20, 21, 32, 73

[46] B. F. Whiting, *Mode stability of the Kerr black hole.*, J. Math. Phys., Vol. 30, No. 6, p. 1301 - 1305 (1989) 19

[47] J. B. Hartle and D. C. Wilkins, *Analytic Properties of the Teukolsky Equation*, Commun. math. Phys. 38, 47—63 (1974) 19, 55

[48] S. E. Gralla and P. Zimmerman, *Critical Exponents of Extremal Kerr Perturbations*, arXiv:1711.00855 [gr-qc] 21

[49] R. Penrose, *Nuovo Cimento*, J. Serie 1 (1969) 252 22

[50] M. Casals, S. E. Gralla and P. Zimmerman, *Horizon Instability of Extremal Kerr Black Holes: Nonaxisymmetric Modes and Enhanced Growth Rate*, Phys. Rev. D **94**, no. 6, 064003 (2016), doi:10.1103/PhysRevD.94.064003, arXiv:1606.08505 [gr-qc] 21

[51] L. M. Burko and G. Khanna, *Linearized Stability of Extreme Black Holes*, arXiv:1709.10155 [gr-qc] 21

[52] S. A. Teukolsky and W. H. Press, *Perturbations of a rotating black hole. II. Dynamical stability of the Kerr metric.* , Astrophys. J., 185:649-673 (1973)

[53] S. A. Teukolsky and W. H. Press, *Perturbations of a rotating black hole. III. Interaction of the hole with gravitational and electromagnetical radiation.* , Astrophys. J., 193:443-461 (1974) 23, 24

[54] R. Brito, V. Cardoso and P. Pani, *Superradiance*, Lecture Notes in Physics 906, Springer (2015) xii, 23, 51, 52

[55] J.A.H. Futterman, F.A. Handler and R.A. Matzsner, *Scattering from Black Holes*, Cambridge University Press (1988), New York 24, 25

[56] A. Starobinski, *Amplification of waves during reflection from a rotating black hole*, Zh. Eksp. Teor. Fiz. 64 (1973) 48. (Sov. Phys. - JETP, 37, 28, 1973) 24

[57] A. A. Starobinski and S. M. Churilov, *Amplification of electromagnetic and gravitational waves scattered by a rotating black hole*, Zh. Eksp. Teor. Fiz. 65 (1973) 3. (Sov. Phys. - JETP, 38, 1, 1973) 24, 25

[58] Mathematica, Wolfram Research, Inc., *Mathematica, Version 11.2*, Champaign, IL, 2017 24, 43

[59] W. Gautschi, *Computational Aspects of three-term recurrence relations*, SIAM Review, Vol.9, No. 1 (1967) 27, 29, 35

[60] E.D. Fackerell and G. Crossman, *Spin-weighted angular spheroidal functions*,J. Math. Phys. 18, 1849 (1977), https://doi.org/10.1063/1.523499 28, 29

[61] E.W. Leaver, *An Analytic Representation for the Quasi-Normal Modes of Kerr Black Holes*,Proc. Royal Soc. A, Vol. 402, No. 1823 pp. 285-298,(1985) 28, 29, 48, 60

[62] E. Berti and V. Cardoso, *Quasinormal ringing of Kerr black holes: The excitation factors*, Phys. Rev. D 74, 104020 (2006) 32

[63] Z. Zhang, E. Berti and V. Cardoso, *Quasinormal ringing of Kerr black holes. II. Excitation by particles falling radially with arbitrary energy*, Phys. Rev. D 88, 044018 (2013) 32

[64] J. Malila, *The Derivative Of A Finite Continued Fraction*, Applied Mathematics E-Notes, 14(2014), 13-19, available at `http://www.math.nthu.edu.tw/~amen/` 33

[65] Mano, S., Suzuki, H. and Takasugi, E., *Analytic solutions of the Teukolsky equation and their low frequency expansions*, Prog. Theor. Phys., 95, 1079–1096, (1996) 34, 36

[66] Sasaki, M. Tagoshi, *Analytic Black Hole Perturbation Approach to Gravitational Radiation*, H. Living Rev. Relativ. (2003) 6: `https://doi.org/10.12942/lrr-2003-6` 35, 36, 64

[67] A. Castro, J. M. Lapan, A. Maloney, and M. J. Rodriguez, *Black Hole Scattering from Monodromy*, Classical and Quantum Gravity 30, 165005 (2013) 40, 41, 42

[68] M. J. Rodriguez, `https://sites.google.com/site/justblackholes/techy-zone` 41

[69] U. Keshet and A. Neitzke, *Asymptotic Spectroscopy of Rotating Black Holes* ,Phys. Rev. D78, 044006 (2008), arXiv:0709.1532[hep-th] 42, 74

[70] H.-c. Kao and D. Tomino, *Quasinormal Modes of Kerr Black Holes in Four and Higher Dimensions* , Phys. Rev. D77, 127503 (2008), arXiv:[0801.4195] 42

[71] E. Berti, Ringdown webpage, `http://www.phy.olemiss.edu/~berti/ringdown/` 48, 58, 60, 62, 93, 94, 95

[72] Ryuichi Fujita and Hideyuki Tagoshi, *New numerical methods to evaluate homogeneous solutions of the Teukolsky equation*, Prog. Theor. Phys., 112(3):415–450, 2004 53, 65

[73] Ryuichi Fujita and Hideyuki Tagoshi, *New numerical methods to evaluate homogeneous solutions of the Teukolsky equation. II.*, Prog. Theor. Phys., 113(6):1165– 1182, 2005 53, 65

[74] P. Dennery and A. Krzywicki, *Mathematics for Physicists*, Dover Publications (1995), New York 58

[75] J. A. Nelder, R. Mead, *A Simplex Method for Function Minimization*, The Computer Journal, Volume 7, Issue 4,1965, Pages 308–313, https://doi.org/10.1093/comjnl/7.4.308 58, 92

[76] A. M. van den Brink, *Analytic treatment of black-hole gravitational waves at the special frequency*, Phys. Rev. D62, 064009 (2000), [gr-qc/0001032] 60

[77] H. Onozawa, *Detailed study of quasinormal frequencies of the Kerr black hole*, Phys. Rev. D 55, 3593(1997) 60

[78] G. B. Cook and M. Zalutskiy, *Gravitational perturbations of the Kerr geometry: High-accuracy study*, Phys. Rev. D **90**, no. 12, 124021 (2014), doi:10.1103/PhysRevD.90.124021, arXiv:1410.7698 [gr-qc] 60

[79] S. Chandrasekhar and S. Detweiler, *The quasi-normal modes of the Schwarzschild black hole*, Proc. R. Soc. London, A344, 441 (1975) 60

[80] W. Throwe, *High precision calculation of generic extreme mass ratio inspirals*, `http://hdl.handle.net/1721.1/61270` xiv, 64, 65, 67

[81] John H. Mathews and Kurtis K. Fink , *Numerical Methods Using Matlab*, 4th Edition, Prentice-Hall Inc., New Jersey, USA (2004) 92

Appendix A

Nelder Mead Method

The Nelder-Mead method is designed to minimize a given function $f : \mathbb{R}^n \to \mathbb{R}$ in a way that the knowledge of the derivatives of f is not needed. Our case of interest is the minimization of functions in the complex-frequency plane. This implies that our function is of the kind $f : \mathbb{R}^2 \to \mathbb{R}$. For this reason we focus in the $n = 2$ case.

Let $f(x, y)$ be a function to be minimized. The method starts by choosing three $(n + 1)$ points ($r_1 = (x_1, y_1)$, $r_2 = (x_2, y_2)$ and $r_3 = (x_3, y_3)$) around an input point. The function is evaluated in these three points and their sub-index are re-organized in a way that

$$f(r_1) < f(r_2) < f(r_3). \tag{A.1}$$

This implies that (r_1) is the best point, r_2 is the next best and r_3 is the worst point.

The second step of this method is to choose a fourth point for which $f(r_4) < f(r_3)$. The first attempt to find this fourth point is by performing a "reflection" of the point r_3. By reflection we mean that given the middle point in between r_1 and r_2

$$r_M = \frac{r_1 + r_2}{2} = \frac{1}{2}\left(x_1 + x_2, y_1 + y_2\right). \tag{A.2}$$

There will be a point r_R that the line that connects r_3 and r_R also has r_M as its middle point. This implies that the point r_R is given by

$$r_R = 2r_M - r_3 = r_1 + r_2 - r_3 = (x_1 + x_2 - x_3, y_1 + y_2 - y_3). \tag{A.3}$$

If at the point r_R we have $f(r_R) < f(r_3)$, this implies that we are moving in the correct direction towards the minimum. In order to speed up the code, we can then go further than the point r_R. Then the next choice of point is r_E defined as

$$r_E = 2r_R - r_M = \frac{3}{2}(r_1 + r_2) - 2r_3 = \left(\frac{3}{2}(x_1 + x_2) - 2x_3, \frac{3}{2}(y_1 + y_2) - 2y_3\right). \tag{A.4}$$

If at the point r_R we have $f(r_R) \geq f(r_3)$, we can consider the middle points between the r_3 and r_M (r_{C_1}) and in between r_M and r_R (r_{C_2}). More explicitly:

$$r_{C_1} = \frac{1}{2}(r_3 + r_M) \quad \text{and} \quad r_{C_2} = \frac{1}{2}(r_M + r_R). \tag{A.5}$$

The point to be chosen among r_{C_1} and r_{C_2} is the one which has the smaller value of $f(r)$.

If neither $f(r_{C_i})$ is smaller than $f(r_3)$ it will be needed to change not only one of the three initial points, but two of them. Then we replace r_2 by r_M and r_3 by $r_{M'}$, where $r_{M'}$ is defined by:

$$r_{M'} = \frac{1}{2}(r_1 + r_3). \tag{A.6}$$

After a proper substitution of the point r_3 (as explained above) is made we need to do another comparison and rename the points such that $f(r_1) < f(r_2) < f(r_3)$ and the algorithm should restart. Our code have a internal loop that will only stop when the distance between the three points obtained by the end of an iteration is smaller than a certain precision.

In this appendix we gave a brief review on the Nelder-Mead minimization method. For a more robust explanation of the method we direct the reader to the original paper [75]. Our approach is following the book [81].

Appendix B

Quasi-Normal Modes in the static limit

In this appendix we show the numerical values of the QNM frequencies found for the static limit ($a = 0$). All QNM frequencies were calculated requiring 16 digits of precision in the Nelder-Mead method. The results in this section reproduced data available in [71].

n	$\Re(2M\omega_{lmn})$	$\Im(2M\omega_{lmn})$	n	$\Re(2M\omega_{lmn})$	$\Im(2M\omega_{lmn})$
0	0.4965265283562173	-0.1849754359058844	14	0.1138827216530754	-7.0588242614723885
1	0.4290308391272116	-0.5873352910914572	15	0.1076388804077767	-7.5588298858301907
2	0.3495471352140215	-1.0503751987176475	16	0.1019345654471042	-8.0587165153033316
3	0.2923533988340006	-1.5438178479961673	17	0.0966992437620215	-8.5585032900426174
4	0.2531082919807309	-2.0451005676066696	18	0.0918753100189363	-9.0582062397023968
5	0.2245055815994594	-2.5478512387567702	19	0.0874150860459493	-9.5578388629413776
6	0.2024294110658836	-3.0505326668465852	20	0.0832786401996066	-10.057412586453461
7	0.1846474957013585	-3.5527984667340478	21	0.0794321733827058	-10.556937129275995
8	0.1698699422722535	-4.0546121404360987	22	0.0758468048005483	-11.056420793285824
9	0.1572992817032460	-4.5560176410894342	23	0.0724976449235120	-11.555870696277964
10	0.1464132214186788	-5.0570744262743998	24	0.0693630782316914	-12.055292960281668
11	0.1368531061225688	-5.5578388099154208	25	0.0664242014881736	-12.554692864823763
12	0.1283628845257800	-6.0583593636213461	-	-	-
13	0.1207537642791251	-6.5586766623760287	-	-	-

Table B.1: First 26 QNM frequencies found for the mode $s = 1$,$l = 1$ in the static limit, $a = 0$.

n	$\Re(2M\omega_{lmn})$	$\Im(2M\omega_{lmn})$	n	$\Re(2M\omega_{lmn})$	$\Im(2M\omega_{lmn})$
0	0.7473433688360836	-0.1779246313778713	15	0.1771807742403373	-7.6502104162908118
1	0.6934219937583269	-0.5478297505824693	16	0.1772658049187587	-8.1533291773508900
2	0.6021069092247327	-0.9565539664461436	17	0.1769534131502148	-8.6561004191053505
3	0.5030099243711811	-1.4102964048669906	18	0.1763816962479507	-9.1585939137992660
4	0.4150291596261311	-1.8936897817327030	19	0.1756402482612919	-9.6608594981426344
5	0.3385988061860873	-2.3912161082716935	20	0.1747887765200058	-10.162934199017293
6	0.2665046804903760	-2.8958212523240763	21	0.1738679005724426	-10.664846401122938
7	0.1856446673404019	-3.4076823444122710	22	0.1729056889963510	-11.166618422135411
8	0.0000000000000000	-4.0000000000000000	23	0.1719217573281910	-11.668268178135232
9	0.1265270102512119	-4.6052895303170809	24	0.1709299134350313	-12.169810302837954
10	0.1531069257719723	-5.1216532347630114	25	0.1699399081388461	-12.671256924716690
11	0.1651962892832580	-5.6308847452159755	26	0.1689586186240758	-13.172618221905741
12	0.1714558441266348	-6.1373894878623803	27	0.1679908632304430	-13.673902828129253
13	0.1747885247471989	-6.6424604768651184	28	0.1670399714594522	-14.175118135962898
14	0.1764778815211748	-7.1466413966158448	-	-	-

Table B.2: First 29 QNM frequencies found for the mode $s = 2$,$l = 2$ in the static limit, $a = 0$.

We notice here that the direct comparison between our data on table B.2 and the one available in [71] might lead to the idea that we might be missing some QNMs. A closer look to the data [71] makes clear that there are some QNMs that appear twice, compare overtones 16 with 17 and 19 with 21.

Appendix C

Quasi-Normal Modes in the NEK case

In this appendix we show the numerical values of the QNM frequencies found for the NEK case. All QNM frequencies were calculated requiring 8 digits of precision in the Nelder-Mead method. The results found here should be compared with results in [18, 20, 71].

n	$\Re(2M\omega_{lmn})$	$\Im(2M\omega_{lmn})$
0	1.9713470966806632	-0.0069373462544075
1	1.9713468597857080	-0.0208124415349988
2	1.9713453797831881	-0.0346882478043017
3	1.9713419240436814	-0.0485634659910419
4	1.9713375953012363	-0.0624367815760039
5	1.9713340856818211	-0.0763083934382931
6	1.9713323376196595	-0.0901795811028893
7	1.9713322647878837	-0.1040517402296938
8	1.9713331557214282	-0.1179258510123462
9	1.9713340429536808	-0.1318023505608337
10	1.9713340509847605	-0.1456812351061738
11	1.9713324642294122	-0.1595622208298687
12	1.9713287805720145	-0.1734448743562819
13	1.9713227134222075	-0.1873287089462004

Table C.1: First 14 QNM frequencies found for the mode $s = -2$, $l = 2$, $m = 2$ for $a = 0.9999M$. All modes found are DMs.

n	$\Re(2M\omega_{lmn})$	$\Im(2M\omega_{lmn})$
0*	1.1595905916950376	-0.0801552055206187
1	1.0128246189985108	-0.1548386076219234
2	1.0191995567920022	-0.2218210493975133
3*	1.0812342857353620	-0.2414640438496770
4	1.0189114942447858	-0.2907420089883552
5	1.0165014213372467	-0.3523120790458688
6	1.0152559976961604	-0.4099635096644475
7	1.0133930804868406	-0.4654490258922171
8	1.0101405717137750	-0.5207860324030136
9	1.0064307022327026	-0.5770692853983539
10	1.003030985193748	-0.6340464951810719
11	1.0000364943762467	-0.6912846069656605
12	0.9973003500319220	-0.7485746306385128

Table C.2: First 13 QNM frequencies found for the mode $s = -2$, $l = 2$, $m = 1$ for $a = 0.998M$. DMs are marked with an asterisk next to the overtone number.

n	$\Re(2M\omega_{lmn})$	$\Im(2M\omega_{lmn})$
0*	0.8497014162982315	-0.1439808166999697
1	4.2813025356148538E-13	-0.1908029268511687
2	1.6133932944734374E-11	-0.2549128389211351
3	2.0861339309548894E-10	-0.3192664571585073
4	1.4112152221038231E-9	-0.3838535854911746
5*	0.805266192017904	-0.4375466474032832
6	5.9299537933605541E-9	-0.4486623210969351
7	1.6626013373652602E-8	-0.5136796393498069
8	3.1053668497217304E-8	-0.5788919278698033
9	3.4191619687710365E-8	-0.6442854493903880
10	1.135840168381935E-8	-0.7098467272001575
11*	0.717215586136940	-0.7500069519697677
12	1.239371642637061E-8	-0.7755628272018890
13	2.5688570536685546E-7	-0.8414214727090431
14	1.1658747683348692E-6	-0.9074109471227567
15	3.1301060891667473E-6	-0.9735198957853128
16	5.9597142325921566E-6	-1.0397373761203023
17*	0.5925271414495406	-1.0992299852258983
18	8.3810929082231399E-6	-1.1060535457874829
19	8.3665510313142873E-6	-1.1724609020505298
20	4.8894220654935239E-6	-1.2389550811797087
21	5.0788435566747307E-7	-1.3055336623942467
22	2.5123372245788627E-6	-1.3721922443226842
23	0.0000198044053804	-1.438919648701022
24*	0.4529296319723091	-1.500426838753440
25	0.0000551203790710	-1.505697005013715

Table C.3: First 26 QNMs frequencies found for the mode $s = -2$, $l = 2$, $m = 0$ for $a = 0.998M$. DMs are marked with an asterisk next to the overtone number.

n	$\Re(2M\omega_{lmn})$	$\Im(2M\omega_{lmn})$
26	0.0000975254149259	-1.5725050132612980
27	0.0001234595986826	-1.6393374354593325
28	0.0001104770648556	-1.7062113315348556
29	0.0000585954332592	-1.7731632324870182
30	6.1339246638969148E-6	-1.8402256504334241
31	0.0000206921152345	-1.9073896415811154
32*	0.3274322055589949	-1.9488165448516351
33	0.0001514930143687	-1.9745827207085047
34	0.0003711727149325	-2.0417034399558274
35	0.0005725575563100	-2.1086999011906039
36	0.0006318957562721	-2.1756201952904564
37	0.0004859045755673	-2.2426043847662110
38	0.0001981613243805	-2.3098335098277969
39	2.0476288845307958E-6	-2.3774113055092371
40*	0.2294865036189526	-2.4246081362511984
41	0.0001934703484596	-2.4451760977052985
42	0.0008001211397212	-2.5127268306227174
43	0.0014923338376196	-2.5798143056745361
44	0.0018970031723576	-2.6465234821341333
45	0.0017932766991870	-2.7131419586219955
46	0.0011481121506923	-2.7800774910218619
47	0.0002707506872494	-2.8478249659172592
48*	0.1573845140134125	-2.9128345054153782
49	0.0000858389157906	-2.9164924819378490
50	0.0012258578041372	-2.9849577618968206

Table C.4: Some QNMs frequencies (n from 26 to 50) found for the mode $s = -2$, $l = 2$, $m = 0$ for $a = 0.998M$. DMs are marked with an asterisk next to the overtone number.

Appendix D

Quasi-Normal Modes in the extremal limit

In this appendix we show the numerical values of the QNM frequencies found for the extremal limit ($a = M$). It is worth remembering that for the mode $s = -2, l = 2, m = 2$ no QNM's were found in the analyzed region. The values to be compared with the ones found in [11] are only for the $n = 0$ overtones, here we also present more highly excited overtones. All QNM frequencies were calculated requiring 8 digits of precision in the Nelder-Mead method.

n	$\Re(2M\omega_{lmn})$	$\Im(2M\omega_{lmn})$
0	2.1431894440820635	-0.0644759702177074
1	2.0656356129857118	-0.1936077596772604

Table D.1: QNM frequencies found for the mode $s = 0$, $l = 3$, $m = 2$ in the extremal limit, $a = M$. Only 2 QNM's were found in the analyzed region.

n	$\Re(2M\omega_{lmn})$	$\Im(2M\omega_{lmn})$
0	0.8502902157903121	-0.1436123677901097
1	0.8054871811610688	-0.4365659774477609
2	0.7168565323913904	-0.7487455643472152
3	0.5916519753042957	-1.0980779772217546
4	0.4518396148398792	-1.4995932736046661
5	0.3264000593090661	-1.9482445063583910
6	0.2286126573618755	-2.4241702137821273

Table D.2: First 7 QNM frequencies found for the mode $s = -2$, $l = 2$, $m = 0$ in the extremal limit, $a = M$.

n	$\Re(2M\omega_{lmn})$	$\Im(2M\omega_{lmn})$
0	1.1628664034525474	-0.0765109111482389
1	1.0777093249806252	-0.2372558086108238

Table D.3: QNM frequencies found for the mode $s = -2$, $l = 2$, $m = 1$ in the extremal limit, $a = M$.